ISSP

ACTIVITY REPORT OF SYNCHROTRON RADIATION LABORATORY

2022

Activity Report 2022
TABLE OF CONTENTS

10) **ELECTRONIC STRUCTURE ANALYSIS OF OXYFLUORIDE CATHODE OF ALL-SOLID-STATE FLUORIDE BATTERY USING RESONANT INELASTIC X-RAY SCATTERING**

Kentaro Yamamoto, Datong Zhang, Hisao Kiuchi, Yoshihisa Harada, and Yoshiharu Uchimoto

11) **STUDY OF SOFT X-RAY EMISSION ANGULAR ANISOTROPY OF GAS PHASE**

Naoya Kurahashi, Jun Miyawaki, Kosuke Yamazoe, Hisao Kiuchi, Wenxiong Zhang, Ugalino Ralph, and Yoshihisa Harada

12) **ELECTRONIC STATE ANALYSIS OF EARTH-ABUNDANT Fe–Al–Si THERMOELECTRIC(FAST)MATERIALS USING SCANNING PHOTOELECTRON MICROSCOPY(II)**

Yoshiki Takagiwa, Shunsuke Tsuda,, Naoka Nagamura, Asako Yoshinari, Shingo Takezawa, Kenta Oishi, Kentaro Fuku, and Wenxiong Zhang

13) **ANALYSIS OF ELECTRONIC CONFIGURATION FOR A WATER MOLECULE ENCAPSULATED INSIDE A FULLERENE**

Yoshifumi Hashikawa, Hisao Kiuchi, and Yoshihisa Harada

14) **ELECTROLYTE DEPENDENCE OF THE Mn 3d ELECTRONIC STRUCTURE OF LiMn2O4 CATHODE STUDIED BY SOFT X-RAY EMISSION SPECTROSOPY**

Daisuke Asakura, Yusuke Nanba, Eiji Hosono, Hideharu Niwa, Hisao Kiuchi, Jun Miyawaki, and Yoshihisa Harada

15) **SOFT X-RAY STRUCTURAL ANALYSIS OF CONSTRAINED WATER MOLECULES ON NICKEL-COMPLEX ANION SALT AGGREGATES**

Tomoko Fujino

16) **AMBIENT PRESSURE X-RAY PHOTOELECTRON SPECTROSCOPY STUDY OF THE ELECTRONIC STATES OF THE MoS_2 BASAL PLANE DURING ANNEALING IN HYDROGEN**

Fumihiko Ozaki, YoungHyun Choi, Wataru Osada, Yoshiko Sakaguchi, Shunsuke Tanaka, Kozo Mukai, Masafumi Horio, Iwao Matsuda, and Jun Yoshinobu

17) **BAND BENDING AT (001) AND (101) INTERFACES OF ANATASE PARTICLE REVEALED BY MICROSCOPIC X-RAY PHOTOELECTRON SPECTROSCOPY**

Wenxiong Zhang, Mustafa Al Samarai, Hisao Kiuchi, Daobin Liu , Haochong Zhao, Fangyi Yao, Qi Feng, and Yoshihisa Harada

18) **INFLUENCE OF SURFACE CHARGE INDUCED BY ULTRAFINE WATER ON TRANS- EPIDERMAL WATER RETENTION OF STRATUM CORNEUM LIPIDS EXPLORED BY O K-EDGE SPECTROSCOPY**

Mustafa al Samarai, Wenxiong Zhang, Hisao Kiuchi, Shinsuke Inoue, Yuki Tabata, Hirota Kato, and Yoshihisa Harada

19) **2p3d RESONANT INELASTIC X-RAY SCATTERING PROBING LIGAND FIELD PERTURBATIONS IN Fe-MODIFIED Co SPINELS**

Minmin Chen, Marcos Sepulcre, Dimitrios Manganas, Steven Angel, Eko Budiyanto, Derek Rice, Harun Tüysüz, Hartmut Wiggers, Naoya Kurahashi, Yoshihisa Harada, Olaf Rüdiger, and Serena DeBeer

High Harmonic Laser Experiments (E-Labo)

1) **STUDY ON PHOTO-INDUCED DYNAMICS IN TOPOLOGICAL INSULATOR Bi2Te3 THIN FILMS**

Kaishu Kawaguchi, Ryo Mori, Shinichiro Hatta, Yuto Fukushima, Hiroaki Tanaka, Ayumi Harasawa, Tetsuya Aruga, and Takeshi Kondo

2) **FERMI SURFACE MAPPING OF TOPOLOGICAL INSULATOR Pb(Bi0.3Sb0.7)2Te4**

Koichiro Yaji, Yuya Hattori, Shunske Yoshizawa, Shunsuke Tsuda, Youhei Yamaji, Yuto Fukushima, Kaishu Kawaguchi, Takeshi Kondo, Yuki Tokumoto, Keiichi Edagawa, and Taichi Terashima

3) **DIRECT OBSERVATION OF QUANTUM WELL STATES INDUCED BY THE HYDROGEN-BONDED ORGANIC FRAMEWORKS FORMED ON METAL SURFACE**

Kaname Kanai, Rena Moue, Hiroto Yamazaki, Kaishu Kawaguchi, Ryo Mori, Yuto Fukushima, Ayumi Harasawa, Shik Shin, and Takeshi Kondo

4) **SPIN-AND ANGLE-RESOLVED PHOTOEMISSION STUDY OF MAX PHASE COMPOUND Zr3SnC2**

Takahiro Ito, Manaya Mita, Kiyohisa Tanaka, Masashi Nakatake, Yuto Fukushima, Kaishu Kawaguchi, Takeshi Kondo, Laurent Jouffret, Hanna Pazniak, Serge Quessada, and Thierry Quisse

5) **HIGH-RESOLUTION TEMPERATURE DEPENDENT SPIN-RESOLVED PHOTOEMISSION SPECTROSCOPY OF HALF-METALLIC FERROMAGNET La1-xSrxMnO3**

Takayoshi Yokoya, Noriyuki Kataoka, Takanori Wakita, , Hirokazu Fujiwara, Yuto Fukushima, Kaishu Kawaguchi, Hiroaki Tanaka, Ryo Mori, Ayumi Harasawa, Takeshi Kondo, Hiroshi Kumigashira, and Yuji Muraoka

6) **LIGHT POLARIZATION DEPENDENCE OF LOW-ENERGY ANGLE-RESOLVED PHOTOEMISSION SPECTROSCOPY OF A TRANSITION METAL DICHALCOGENIDE**

Hiroaki Tanaka

7) **SURFACE STATE SPIN POLARIZATION MEASUREMENT OF Co DOPED LaFeAsO**

Soonsang Huh, Yuto Fukushima, Kaishu Kawaguchi, Ayumi Harasawa, Felix Anger, Wurmehl Sabine, Bernd Büchner, and Takeshi Kondo

8) **THICKNESS DEPENDENCE OF SPIN-POLARISED BAND STRUCTURE IN TOPOLOGICAL INSULATOR Bi2Te3 THIN FILMS**

Kaishu Kawaguchi, Ryo Mori, Yuto Fukushima, Hiroaki Tanaka, Shinichiro Hatta, Ayumi Harasawa, Tetsuya Aruga, and Takeshi Kondo

9) **QUANTUM CONFINED SURFACE STATES FORMED IN A HEXAGONAL CORRAL IN SELF-ASSEMBLED HYDROGEN-BONDED ORGANIC FRAMEWORKS**

Kaname Kanai, Rena Moue, Hiroto Yamazaki, Kozo Mukai, Kaishu Kawaguchi, Yuto Fukushima, Fumihiko Ozaki, Ryo Mori, Takeshi Kondo, Ayumi Harasawa, Shik Shin, and Jun Yoshinobu

10) **STUDY ON SPIN STRUCTURE OF THE SURFACE STATE IN TYPE-Ⅱ WEYL SEMIMETAL NbIrTe4**

Soonsang Huh, Soohyun Cho, Wei Xia, Yuto Fukushima, Ayumi Harasawa, Takeshi Kondo, Yanfeng Guo, and Dawei Shen

5 **Staff**

6 **Publication List**

Preface

The Synchrotron Radiation Laboratory (SRL) of the Institute for Solid State Physics (ISSP) advances novel materials research by developing soft X-ray spectroscopic techniques using the high-brilliance synchrotron radiation source and soft X-ray lasers at three locations in Harima, Sendai, and Kashiwa.

In the Harima office, the world's highest performance fast polarization-switching soft X-ray undulator beamline was used for the joint-research use until August 3, 2022, and then transferred to RIKEN, where R&D of a soft X-ray spectroscopic imaging station has started in collaboration with RIKEN SPring-8 from the end of 2022. At the X-ray free electron laser facility, SACLA, nonlinear soft X-ray spectroscopy was developed, exploring its science and technology as a new spectroscopy method.

To advance measurement techniques in the soft X-ray region, the Sendai Office opened next to the new 3GeV X-ray source facility “NanoTerasu” which is under construction on Tohoku University's Aobayama new campus in November 2022. The ambient-pressure photoelectron spectroscopy station, high-resolution soft X-ray emission spectroscopy station, and the three-dimensional nanoESCA station were relocated from SPring-8 to the NanoTerasu. We will continue to strive for higher performance than our prior targets, including high pressure (up to 100 mbar), high spatial resolution (up to 70 nm), and high energy resolution ($E/\Delta E \approx 10{,}000$), and planning to begin operations in April 2024.

In addition to the cutting-edge activities using synchrotron radiation and SACLA, the SRL has promoted the scientific use of laser-based high-harmonic generation in the vacuum ultraviolet and soft X-ray regions at the E-building of the Kashiwa campus, in collaboration with Kobayashi and Itatani laboratories at the LASOR laser group. Since 2015, the SRL has operated a joint research program using the high-resolution laser spin- and angle-resolved photoelectron spectroscopy (SARPES) system, which is designed to provide high-energy (1.7 meV) and -angular resolutions with high-efficiency spin detectors for various types of solids, such as spin-orbit coupled materials and ferromagnetic materials. We also developed a two-dimensional angle- and time-resolved photoemission spectrometer and made it available for joint-research use since 2022.

Our goal is to provide users with a platform that uses both synchrotron radiation and high-harmonic laser generation through strong collaboration with other LASOR group members.

June 30, 2023
Yoshihisa Harada
Director of SRL-ISSP

1. Status of Beamline BL07LSU at SPring-8

As described in the Preface, the University-of-Tokyo high-brilliance synchrotron soft X-ray outstation beamline BL07LSU at SPring-8 was maintained until the first half of 2022 by the permanent staff members with adjuncts for user operations for the purpose of promoting advanced spectroscopy of solid and soft (including bio-) materials, and various joint-research experiments were conducted by both staff and users in the G-type (general), S-type (special), and P-type (priority) applications. Here, the activities at the ambient pressure X-ray photoemission spectroscopy, soft X-ray spectroscopic imaging, 3D-scanning photoelectron microscope (3D nano-ESCA) and high-resolution soft X-ray emission spectroscopy (HORNET) stations until the first half of 2022, and development of soft X-ray spectroscopic imaging station through collaboration with RIKEN from the second half of 2022, are briefly described below.

(1) Ambient-pressure X-ray photoelectron spectroscopy (AP-XPS)

AP-XPS station is aimed for *operando* chemical analysis during catalytic reactions at the gas/solid interface to unveil the reaction mechanism. The AP-XPS system is equipped with a differentially pumped electron analyzer (SPECS, PHOIBOS 150 NAP) and an ambient pressure gas cell. XPS measurements can be performed both under ultrahigh vacuum and in gas pressure up to 100 mbar. Reactant and product molecules of a catalytic reaction are monitored by mass spectroscopy and, simultaneously, chemical states of the reaction intermediates at a surface are directly examined by AP-XPS.

A variety of research projects has been conducted at the AP-XPS station. In 2022, issues at the atomic sheet were focused and the functionalities, such as sensing and reaction, were investigated.

(2) Soft X-ray imaging

We developed a new soft X-ray microscopy system named CARROT (Coherent Achromatic Rotational Reflective Optics for pTychography) in 2021. CARROT can realize high-resolution and high-sensitivity soft X-ray imaging by utilizing the coherent property of BL07LSU. The CARROT system with a total reflection Wolter mirror achieved a resolution of about 50 nm in a test chart evaluation. We have also shown that it is possible to visualize the magnetic domain structures of an ultrathin metal film using X-ray magnetic circular dichroism.

We also demonstrate the potential of applying CARROT to cell biology by measuring drug-treated mammalian cells. Various changes in the cell body were observed using soft X-ray imaging at 50 nm resolution.

(3) 3D-scanning photoelectron microscope (3D-nanoESCA)

3D-nanoESCA can be used for sub-100 nm range microscopic 2D mapping and depth profile of the chemical structure of functional materials and devices. In 2022, two significant experiments were performed. 2D electronic mappings of P-type and N-type alloyed thermoelectric materials (FAST) composed of safe, durable, and inexpensive Fe, Al, and Si elements developed by Dr. Takagiwa were obtained and compared and the p-type sample showed a peak shift to the lower binding energy for both Fe 2p, Al 2p, and Si 2p, and the shift of the chemical potential was quantitatively determined. The shape difference was also detected in the valence spectra, suggesting that the intra-gap position has an effect. Dr. Zhang obtained Ti 2p 2D photoelectron images of TiO_2 (anatase) particles with different facet surfaces, showing the existence of a space-charge layer of about 40 nm between the interfaces of the two facets. Photogenerated electrons and holes are expected to accumulate in the (101) and (001) facets, respectively, enhancing the photocatalytic activity.

(4) Ultra high-resolution soft X-ray emission spectroscopy (HORNET)

The station is dedicated for soft X-ray emission (or resonant inelastic X-ray scattering: RIXS) spectroscopy measurements with high-resolution ($E/\Delta E > 10{,}000$) and under various environmental conditions (gas, liquid, and solid). In 2022, 11 studies were performed. Among them, the studies by Profs. Y. Higaki and S. Horiuchi, and Dr. Y. Hashikawa were performed under the Grant-in-Aid for Scientific Research New Science Project and targeted water at various interfaces; in concentrated polymer, within porous crystals, and encapsulated in fullerenes. Other works include secondary battery electrodes and catalysts for water electrolysis, aiming for the improved performance of them. Dr. Fujino et al. explored d/π-conjugated molecules in water and detected changes in the Ni 3d electronic states due to altered intermolecular interactions in film states upon heating. All these studies are quite advanced for operando RIXS measurements, and they will collectively advance our technique and suggest the possibility of practical applications in the future experiments at NanoTerasu.

2． Status of SARPES

Spin and angle-resolved photoemission spectroscopy (SARPES) stands as a powerful experimental technique that reveals various information about the occupied electronic states in solids, including their energy, momentum, and spin. In recent years, the surge in interest around Rashba surface states and topological materials with spin-polarized electronic structures derived from strong spin-orbit interactions has elevated the significance of spin-resolved measurements. These spin-resolved experiments require high energy resolution and enough photoelectron yield rates to effectively detect the small energy scales of about several meV orders. Following these criteria, we have successfully developed a high-energy resolution SARPES setup utilizing a vacuum-ultraviolet (6.994-eV) laser and spin detectors with the very-low-energy-electron-diffraction (VLEED) at the Laser and Synchrotron Research Center (LASOR) in the Institute for Solid State Physics (ISSP) [1]. Since our initiative of developing the laser-SARPES in FY2014 and the facility commencement for collaborative research in FY2015, our SARPES station has been used to obtain precise spin-resolved electronic structures in proximity to the Fermi level in solids.

Our laser-SARPES setup consists of an analysis chamber, a carousel sample-bank chamber connected to a load-lock chamber, and a molecular beam epitaxy (MBE) chamber. All of these chambers are connected via UHV gate valves. The hemispherical electron analyzer is a custom-made ScientaOmicron DA30-L adapted to incorporate VLEED-type spin detector. The avairable photon sources to excite electrons in materials are the 6.994-eV laser, generated by the 6th harmonic of a high-power Nd:YVO4 quasi-continuous wave laser, and a helium discharge lamp (VG Scienta, VUV5000). In the MBE chamber, the surface evaluating and preparing instruments, such as evaporators, low energy electron diffraction, sputter-gun, and quartz microbalance, can be installed, and samples can be heated by direct current heating or electron bombardment. The carousel chamber offers strage for 16 samples within the UHV environment. Spin-polarized states were investigated in both the bulk and surface of various topological materials, including magnetic and superconducting ones, atomic layers, and ferromagnetic compounds.

Beginning in FY2018, we initiated an upgrade of our laser-SAPRES apparatus by integrating a pulsed laser to develop a pump-probe measurement setup. The newly installed pulsed 10.7-eV laser system [2,3] is ytterbium fiber-based, achieving a 270-fs, 1-MHz repetition rate, and high power by a chirped pulse amplification technique, developed by the Kobayashi group at LASOR in ISSP[4]. This newly developed system, as shown in Fig. 1, enables us to measure optically excited electron populations in the unoccupied bands in energy and momentum space and track the pump-induced ultrafast dynamics of both charge and spin. In addition to a great capability of the time-resolved measurements, the 10.7-eV laser system provides wider momentum information than that is possible with low photon energy sources such as 6.994-eV and gives better momentum resolution and polarization controls than the

helium discharge lamp. In the developed system, while the light polarization of 10.7-eV probe laser, obtained as the third harmonic generation in Xe gas, can be selectively controlled by MgF_2 half-wave plate, pump photon is selectable from 1.19-eV or 2.38-eV for a wide variety of band-gap materials. The original 6.994-eV light source is still available by switching some mirrors and lens in the vacuum beamline.

Currently, we have been working on upgrading the 10.7-eV laser system aimed at stabilizing the pulsed light and installing an optical parametric amplifier (OPA). In addition to the development of an autocorrelation measurement setup, we have assembled laser evaluation systems such as Frequency-resolved optical gating (FROG) to improve the stability of the light. A new amplifier (rod fiber) has been introduced to the system, making higher output light available. These upgrades will enable us to combine our system with the OPA, where the wavelength (photon energy) of the pump light can be selectively tuned between 1350 nm (~0.92-eV) and 4200 nm (~0.3-eV). By leveraging such tunable low-energy pump lights, we will be able to access various exotic light-induced states in quantum materials, such as Floquet states with spin resolution.

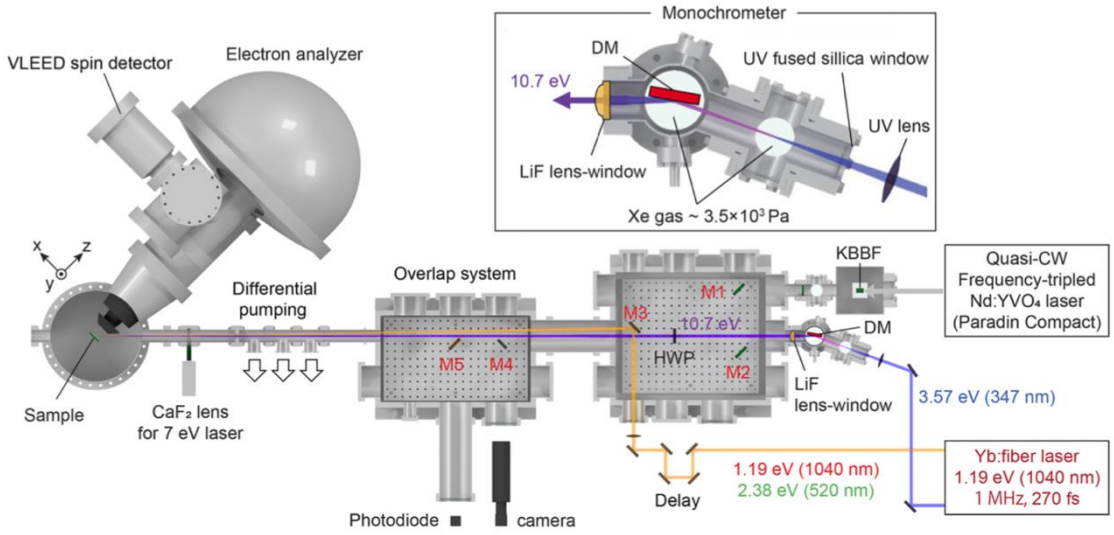

Fig. 1 Scaled layout of the 10.7-eV pulse laser beamline for tr-SARPES[4].

References:

[1] K. Yaji, A. Harasawa, K. Kuroda, S. Toyohisa, M. Nakayama, Y. Ishida, A. Fukushima, S. Watanabe, C.-T. Chen, F. Komori and S. Shin, Rev. Sci. Instrum. 87, 053111 (2016).

[2] Z. Zhao and Y. Kobayashi, Opt. Exp. 25, 13517 (2017).

[3] Z. Zhao, K. Kuroda, A. Harasawa, T. Kondo, S. Shin and Y. Kobayashi, Chin. Opt. Lett. 17, 051406 (2019).

[4] K. Kawaguchi, K. Kuroda, Z. Zhao, S. Tani, A. Harasawa, Y. Fukushima, H. Tanaka, R. Noguchi, T. Iimori, K. Yaji, M. Fujisawa, S. Shin, F. Komori, Y. Kobayashi, and T. Kondo, Rev. Sci. Instrum. 94, 083902 (2023)

Seminar

(LASOR Seminar)

Date: May 23, 2022

Title: Electronic structures of a confined water molecule inside a fullerene revealed by soft X-ray emission spectroscopy

Speaker: Dr. Hisao Kiuchi (ISSP, The University of Tokyo)

Date: May 23, 2022

Title: Development of Soft X-ray Spectromicroscopy using Microfabrication Techniques

Speaker: Dr. Yoko Takeo (ISSP, The University of Tokyo)

Upgrade of ambient pressure X-ray photoelectron spectroscopy system at SPring-8 BL07LSU

Susumu Yamamoto[1,2], Takanori Koitaya[3], Iwao Matsuda[4], and Jun Yoshinobu[4]

[1] *International Center for Synchrotron Radiation Innovation Smart (SRIS), Tohoku University*

[2] *Institute of Multidisciplinary Research for Advanced Materials (IMRAM), Tohoku University*

[3] *Department of Chemistry, Graduate school of Science, Kyoto University*

[4] *The Institute for Solid State Physics, The University of Tokyo*

Introduction

Operando spectroscopy allows direct observation of materials and devices under actual operation conditions to find a correlation between structure and function in materials. As *Operando* spectroscopy in the soft X-ray region, we developed ambient pressure X-ray photoelectron spectroscopy (AP-XPS) system at the high-brilliance soft X-ray beamline BL07LSU of SPring-8 [1, 2]. We have been promoting research on *operando* observation of catalytic reactions. The limitations of the AP-XPS system were revealed by our past experiments: 1) low maximum gas pressure, and 2) low temporal resolution. As for 1) low maximum gas pressure, the maximum gas pressure in the AP-XPS measurements was limited to about 20 mbar for bulk samples. The low maximum gas pressure leads to low reactivity and selectivity in catalytic reactions. Regarding 2) low temporal resolution, the temporal resolution of the present AP-XPS system was limited to sec~min.

Therefore, in our long-term project, we set two goals to upgrade the AP-XPS system at SPring-8 BL07LSU: 1) Increase the maximum gas pressure, and 2) development of picosecond time-resolved AP-XPS system.

Results and discussion

1) Increase the maximum gas pressure in AP-XPS

The XPS signal attenuation in a gas phase is proportional to $\exp(-z\sigma p)$, where z is the distance between the sample and the entrance nozzle of an electron spectrometer, σ scattering cross section of photoelectrons, p gas pressure. In order to mitigate the XPS signal attenuation, one effective approach is to keep z small. When the distance z is small, however, the local gas pressure on the sample surface is decreased due to the differential pumping through the entrance nozzle. To avoid the decrease of local gas pressure, the opening of the entrance nozzle needs to be decreased.

In the past AP-XPS system, the diameter of the nozzle opening was 300 μm, and the distance z was set at ~300 μm. We developed a new nozzle with the opening diameter of 50 μm. The nozzle body was manufactured by an electroforming technique at Institute for Molecular

Science. The opening hole was made by a focused ion beam. The distance z was set at ~100 μm. Using the new 50 μm nozzle, we have succeeded in measuring Au 4f XPS spectra in the presence of 100 mbar N_2 gas. Therefore, the maximum gas pressure of the AP-XPS system was improved from 20 mbar to 100 mbar. After the improvement of the maximum gas pressure, the AP-XPS system was used to study various systems such as H_2 absorption process in Pd alloys, partial oxidation of CH_4, and CO_2 hydrogenation reactions on catalyst surfaces.

2) Development of picosecond time-resolved AP-XPS system

We have developed the picosecond time-resolved AP-XPS system that combined AP-XPS with femtosecond optical laser. To match the repetition rate of soft X-ray with that of optical laser, the soft X-ray chopper was installed at the beamline. The photodiode mounted on an XYZ stage was newly introduced to an analysis chamber to determine time zero in a pump-probe delay time. On a p-type Si(100) substrate covered with natural oxide (SiO_2/p-Si(100)), temporal variation of Si 2p XPS peak energy due to surface photovoltage effect was observed both in ultrahigh vacuum and in CO_2 gas atmosphere. Furthermore, we succeeded in observing the photoexcitation dynamics on α-Fe_2O_3(0001) surface in a water vapor gas atmosphere.

REFERENCES

[1] S. Yamamoto *et al.*, *Synchrotron Radiat. News* **35**, 19-25 (2022).

[2] S. Yamamoto *et al.*, *Journal of the Japanese Society for Synchrotron Radiation Research* **35**, 182-190 (2022). (in Japanese)

DEVELOPMENT OF SOFT X-RAY MICROSCOPY SYSTEM AND ITS APPLICATION TO MEASUREMENT OF MAMMALIAN CELLS

Yoko TAKEO,[1,2] Kai SAKURAI,[3] Noboru FURUYA,[3] Kyota YOSHINAGA,[3] Takenori SHIMAMURA,[4] Satoru EGAWA,[4] Hisao KIUCHI,[1] Hidekazu MIMURA,[4] Haruhiko OHASHI,[2] Yoshihisa HARADA,[1] Mari SHIMURA,[5,6] and Takashi KIMURA[1]

[1]*The Institute for Solid State Physics, The University of Tokyo*

[2]*Japan Synchrotron Radiation Research Institute*

[3]*Department of Applied Physics, School of Engineering, The University of Tokyo*

[4]*Department of Precision Engineering, School of Engineering, The University of Tokyo*

[5]*RIKEN, SPring-8 Center*

[6]*Research Institute, National Center for Global Health and Medicine*

X-ray microscopy has a wide range of applications in science due to its high spatial resolution and variety of analytical techniques. Ptychography provides a particularly high spatial resolution by reconstructing the sample image using phase recovery calculations[1, 2]. The combination of ptychography and spectroscopy in the soft X-ray region is promising for investigating samples with light-element-rich heterogeneous structures. For example, in the combination of soft X-ray ptychography with X-ray absorption spectroscopy, mapping the chemical state of magnetic nanoparticles in bacteria[3] and the visualization of the cathode degradation mechanism of the lithium-ion batteries[4] have been demonstrated.

Ptychography, a lensless imaging technique, has rapidly developed over the past decade. By reconstructing sample images from multiple coherent diffraction patterns using iterative phase retrieval algorithms, it is possible to obtain high spatial resolution images that are not affected by the performance of X-ray optics, such as fabrication accuracy. In addition, the phase retrieval of coherent diffraction patterns allows the acquisition of both conventional absorption images and phase images, which is a significant advantage when measuring samples with high X-ray transmittance, such as biological cells.

Combining ptychography-based imaging with X-ray fluorescence analysis allows for investigating the correlation between microstructure and element distribution. In the soft X-ray region, ptychography and X-ray fluorescence microscopy systems have been developed using zone plates as illumination optics. Previous results have demonstrated their usefulness, such as the visualization of the chemical state of lithium-ion battery materials and the internal microstructures of magneto bacteria and mammalian cells. Although zone-plate-based optical systems offer the advantages of simplicity and small focus size, they also suffer from problems such as chromatic aberration and short working distances. Illumination optics using total reflection X-ray mirrors have excellent features, such as long working distances, suitable for developing instruments combined with detectors for X-ray photography and X-ray fluorescence analysis. In addition, total reflection mirrors are achromatic, so changing the X-ray wavelength does not affect the focusing properties and are thus well-suited for wavelength scans without the need to readjust the optical system.

In this study, we developed a new soft X-ray microscopic imaging system that combines soft X-ray ptychography and an X-ray fluorescence microscope, using an optical illumination system based on a total reflection Wolter mirror[7]. Figure 1 shows the Shematic illustration of the system called CARROT (Coherent Achromatic Rotational Reflective Optics for pTychography.).We measured mammalian cells as samples and visualized the internal structure with soft X-rays by the absorption and phase shift. We successfully captured sub-micrometer-scale subtle changes in cellular structure due to drug administration by taking advantage of the high-resolution images provided by ptychography (Figure 2). Furthermore,

we demonstrated that it is possible to map the elemental distribution inside the cells using X-ray fluorescence by seamlessly changing the irradiation wavelength from the ptychography measurement. We find a correlation between the internal structure and the elemental distribution inside the cells.

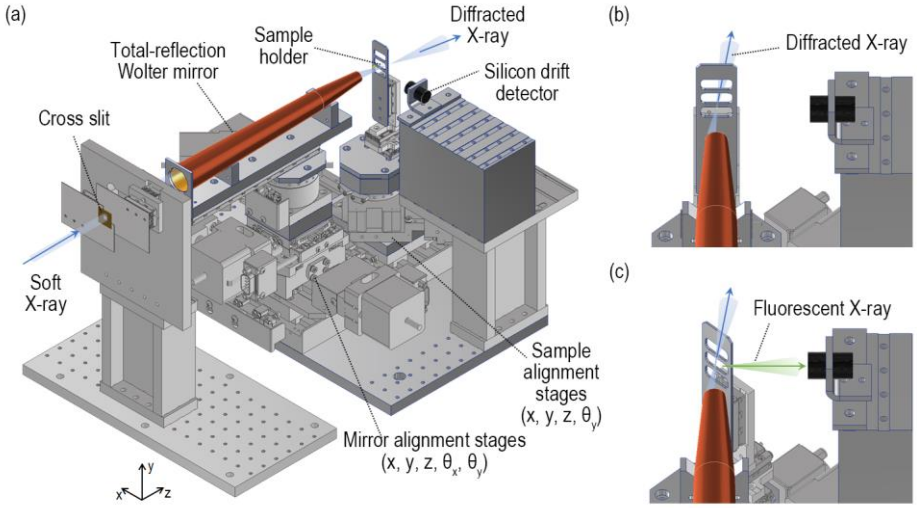

Figure 1 Schematic illustration of the CARROT system. (a) The overall structure inside the vacuum chamber. (b) Ptychography measurement mode. (c) X-ray fluorescence imaging mode.

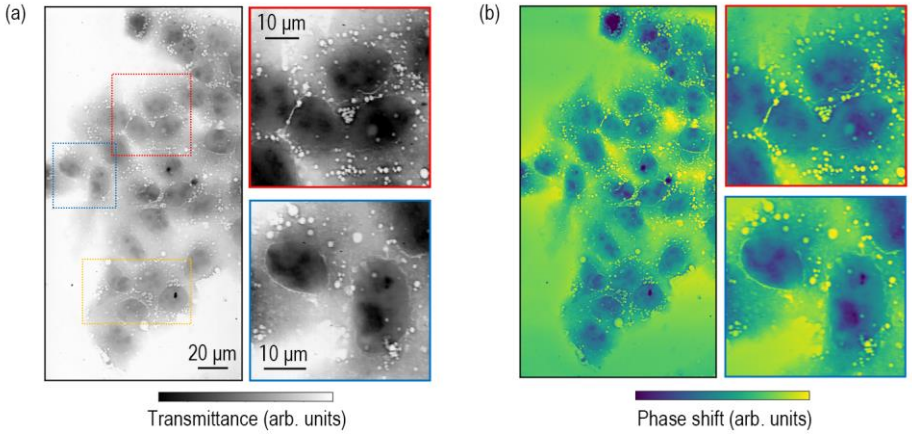

Figure 2 Soft X-ray ptychography measurement of HepG2 cells (DMSO treated). Reconstructed absorption (a) and phase shift (b) images. The magnified images shown in the right panels corresponding to the dotted colored rectangles shown in (a).

REFERENCES

[1] A. M. Maiden, J. M. Rodenburg, Ultramicroscopy, 109 (10), 1256 (2009).
[2] P. Thibault, et al., Science, 321, 379 (2008).
[3] X. Zhu, et al. Proc. Natl. Acad. Sci. , 113 (51) E8219 (2016).
[4] T. Sun, et al., ACS Nano, 15, 1475 (2021).
[5] Y. Takeo, et al., Appl. Phys. Lett. 117, 151104 (2020)
[6] T. Kimura, et al., Opt. Express, 30(15), 26220 (2022).
[7] Y. Takeo, et al., J. Electron Spectrosc. Relat. Phenom., accepted.

CHANGES OF INTRACELLULAR STRUCTURES BY SOFT X-RAY MICROSCOPY SYSTEM OF CT-PTYCHOGRAPHY

Mari Shimura,[1,2] Yoko Takeo,[3,4] Kai Sakurai,[5]
Haruhiko OHASHI,[4,1] Hidekazu Mimura,[6] and Takashi Kimura,[3]

[1]RIKEN, SPring-8 Center
[2]National Center for Global Health and Medicine
[3]The Institute for Solid State Physics, The University of Tokyo,
[4]Japan Synchrotron Radiation Research Institute
[5]Department of Applied Physics, School of Engineering, The University of Tokyo
[6]Department of Precision Engineering, School of Engineering, The University of Tokyo

We had been applied biological samples such as culture cells and medical samples using synchrotron hard x-ray by establishing a scanning x-ray fluorescence microscopy (SXFM) since more than 15 years ago and figured out much evidence that synchrotron x-ray has a potential ability that we have never seen with visible light and electron microscopies [1, 2]. Imaging proteins has been well developed and established in biological and medical fields by visible light microscopies with a labelling technology such as fluorescence; however, synchrotron x-ray microscopy reminds us of a different point of view that proteins are just a part of the cellular contents. In these days, we could obtain an opportunity to apply soft x-ray microscopy system of ptychography with x-ray absorption spectroscopy established at BL07LSU to biological samples [3].

In this study, we prepared a common SiN basement which is available for both SXFM at BL29XU and CARROT at BL07LSU [3]. So that we could observe the same biological samples with hard and soft x-ray fluorescence and ptychography with X-ray absorption spectroscopy in near future. We prepared HepG2 cells, a cell line derived from human hepatoma, treated with or without a newly developed antiretroviral drug, GRL-142 [4]. GRL-142 is a HIV protease inhibitor, which often showed a severe side effect of hyperlipidaemia. Therefore, we expected lipid droplets in cells treated with a high dose of GRL-142. Cells were chemically fixed with 2% paraformaldehyde in PBS and air-dried. In fact, we found increased size and number of lipid droplet-like structures in cytoplasm of the cells with GRL-142, comparing to untreated control cells, which we could hardly see the droplets by visible light microscopies without staining. Notably, we found increase the gap between nucleus and cytoplasm, and higher contrast at nucleus of the cells treated with GRL-142, which we have never seen with visible light microscopies. Higher contrast at nucleus suggested the possibility of increased the width of nucleus and/or the contents due to a stress response with a drug. It is known that cells change the width and hardness depending on the cell cycle, and chromosomes become compact against irradiation to protect them. On the other hand, we have no idea about an increased gap between nucleus and cytoplasm, although this gap may be also related to stress response by the drug. It is quite essential to figure out the molecular mechanisms of these cellular changes in near future. These changes we observed by ptychography were submitted to the article [5].

REFERENCES

[1] A. Fukunaka, et al., Scientific Report. 2023; doi: 10.1038/s41598-023-30498-y. [2] S. Matsuyama, et al., JAAS 35, 1279, 2020: doi.org/10.1039/D0JA00128G. [3] T. Kimura, et al., Opt. Express, Optics Express 30, 2022: doi: 10.1364/OE.462190. [4] H. Bulut, et al,. Scientific Report 10, 10664, 2020. [5] Y. Takeo, et al., JESRP, *under revision*.

ORBITAL CONVERSION IN COFE/CU/OXIDE

Junyeon KIM
Center for Emergent Matter Science, RIKEN

Introduction

Orbital angular moment (OAM) transport opens an emerging mechanism for the spin manipulation. Particularly, a recent experimental report presents the OAM-induced spin manipulation in CoFe/Cu/Al_2O_3 stacks is much more efficient than that by conventional mechanisms [1]. In the CoFe/Cu/Al_2O_3 stacks, nonzero OAM is polarized at the Cu/Al_2O_3 interface (Fig. 1(a)), and exerts torque when OAM is transferred to the CoFe layer. This talk is called orbital torque (Fig. 1(b)). Nowadays, the orbital torque greatly draws interest for the spin accumulation since there is no clear restrictions on materials for the nonzero OAM generation. It is apparently contrast to the spin angular momentum generation which is mainly shown in material systems consisted of heavy elements.

A recent theoretical study reports that the orbital hybridization between the *p*-orbital of oxygen atom and the *d*-orbital atom serves the formation of a chiral orbital texture by orbital Rashba effect (Fig. 1(a)) [2]. Indeed, we recently observed very large orbital torque even if we replace Al_2O_3 to other oxides such as MgO, SiO_2 and TiO_2 [3]. Particularly, orbital torque is maximum when the Oxide is SiO_2, and minium when the Oxide is Al_2O_3. For further understand on the nonzero OAM generation at the Cu/Oxide interface, we require detailed material characterization. Also observation of a modulation of the energy spectrum by a generation of nonzero OAM is also desired.

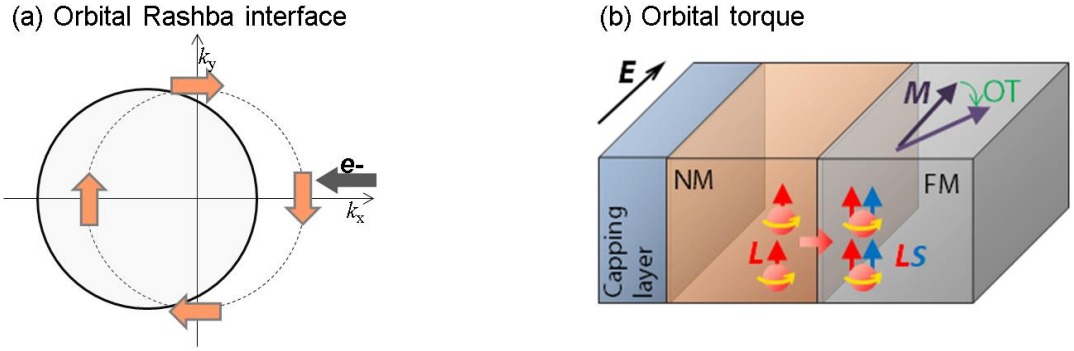

Fig. 1(a)Excess OAM generation at a chiral orbital texture. Here the chiral orbital texture is formed by orbital Rashba effect. (b) Orbital torque in FM/Cu/Oxide system.

Experimental method

For the observation of the Cu/Oxide interface, L-edge X-ray absorption spectroscopy (XAS) and X-ray magnetic circular dichroism (XMCD) was utilized. Nominally, the 3*d* orbital state of Cu is known to be fully occupied. However Grioni et al. claimed that there is still unoccupied 3*d* orbital state for Cu due to a hybridization between *s* state and *d* states [4]. And the number of unoccupied 3*d* orbital state can be promoted by formations of compounds such as CuOx. Thus we could expect the L2, 3 edge X-ray absorption.

As a first, we attempt to obtain the energy spectrum nearby the Cu/Oxide interface. Next, we also attempt to obtain a clue of the nonzero OAM generation by turning on/off the charge current.

The observation was performed in superconducting magnet magneto-optical observation system in the free board. The CoFe/Cu/Oxide stacks are electronically connected by the silver paste. And the observation was carried out by high speed switching of the circularly polarized

light and total electron yield (TEY) technique. To optimize the sample condition, 2, 5, 7, 10 nm of Al_2O_3 was tested considering with the detection length of the TEY technique (~10 nm).

Experimental results and discussion

Figure 2 displays the XAS spectra for the Al_2O_3, SiO_2, and TiO_2 samples. The XAS spectrum for the Al_2O_3 sample confirms the presence of only metallic Cu at the Cu/Al_2O_3 interface (Fig. 2(a)). On the other hand, we observe the formation of Cu oxide (CuO or Cu_2O) at the Cu/Oxide interface in the XAS spectrum for the SiO_2 (Fig. 2(b)), and TiO_2 sample (Fig. 2(c)). We speculate that the released oxygen atoms could form Cu oxides among the larger pool of released oxygen atoms. Considering the orbital torque is large in order of SiO_2, TiO_2, and Al_2O_3 capped sample, the XAS spectra support the interatomic interaction between Cu and oxygen atoms promotes the OAM polarization at the Cu/Oxide interface.

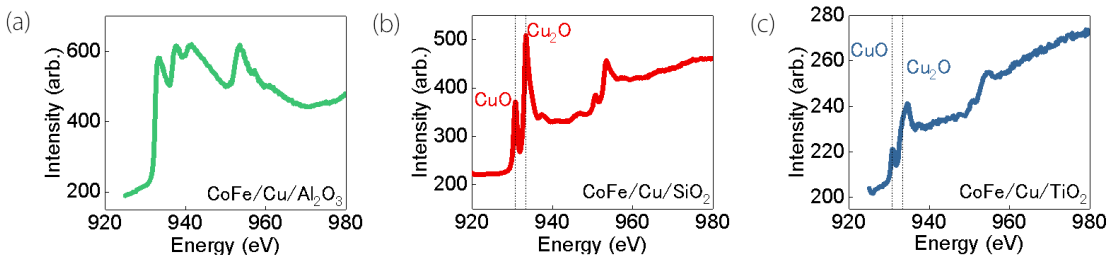

Fig. 2 (a), (b), (c) XAS spectrum for the Al_2O_3 sample (a), SiO_2 (b), and TiO_2 (c) samples. Guide lines for (b) and (c) represents the position of peak for CuO (left) and Cu_2O (right).

REFERENCES

[1] J. Kim *et al*. Phys. Rev. B **103**, L020407 (2021).
[2] D. Go *et al*., Phys. Rev. B **103**, L121113 (2021).
[3] J. Kim *et al*. Submitted to Phys. Rev. Mat.
[4]M. Grioni *et al*., Phys. Rev. B **39**, 1541 (1989).

OPERANDO X-RAY CIRCULAR DICHROISM MEASUREMENT FOR DETECTION OF ORBITAL EDELSTEIN EFFECT

Masafumi Horio[1], Tomoaki Senoo[1], Junyeon Kim[1], Yoshichika Otani[1], Iwao Matsuda[1]
[1]*The Institute for Solid State Physics, The University of Tokyo*

In order to meet the demands of the information society in recent years, increasing the performance of computing devices has become an important issue. Spintronics is a state-of-the-art technology that exploits the spin of electrons, and advances have been made in this field through research that enables high-performance manipulation of magnetism. Among these, research on spin-orbit torque (SOT) [1-3] has attracted much attention due to its scientific interest and technological applications. This technique utilizes spin transport phenomena, such as the spin Hall effect (SHE) and the Edelstein effect (EE), to inject spin into magnetic materials. These phenomena occur in systems with strong spin-orbit interaction and require heavy elements, which are rare and typically expensive. However, recent studies have reported torque generation in systems without heavy elements [4,5]. It was claimed that the experimental results can be explained by a recently proposed interfacial transport phenomenon called the orbital Edelstein effect [OEE, Fig. 1(a)]. This discovery opened the way to new techniques and increased interest in the study of spin transport phenomena at interfaces. However, no direct experimental evidence of OEE has been obtained. This is because experimental information about electronic states at interfaces has not yet been provided.

In the present study, we focused on the interface between Cu and SiO_2 where accumulation of orbital angular momentum (OAM) due to the OEE is expected [5]. We performed x-ray circular dichroism (XCD) measurements at SPring-8 BL07LSU under electric current. In order to detect accumulation of OAM, electric current was applied perpendicularly to the incident x-rays. The measurements were conducted at room temperature in the partial electron yield mode. Detailed sample structure and experimental condition are illustrated in Figs. 1(b) and 1(c), respectively.

Figure 2(a) shows Cu *L*-edge spectra under various current values. While there appear significant changes in the spectral line shape, the influence of electric current cannot be separated from gradual temporal changes confirmed by performing measurements repeatedly in the same condition [Fig. 2(b)]. The "contamination" from this temporal change by x-ray irradiation is inevitable if one makes a full energy scan across the Cu *L*-edge, which takes ~30 minutes. In order to extract genuine effects of current application, we fixed the photon energy at 934.5 eV and monitored absorption intensity for a short time (~several minutes) while repeatedly turning on and off electric current. Figures 2(c) and 2(d) show the results of such measurements performed with left and right circular polarization (LCP and RCP). In both measurements, decrease of absorption intensity was observed due to the generation of

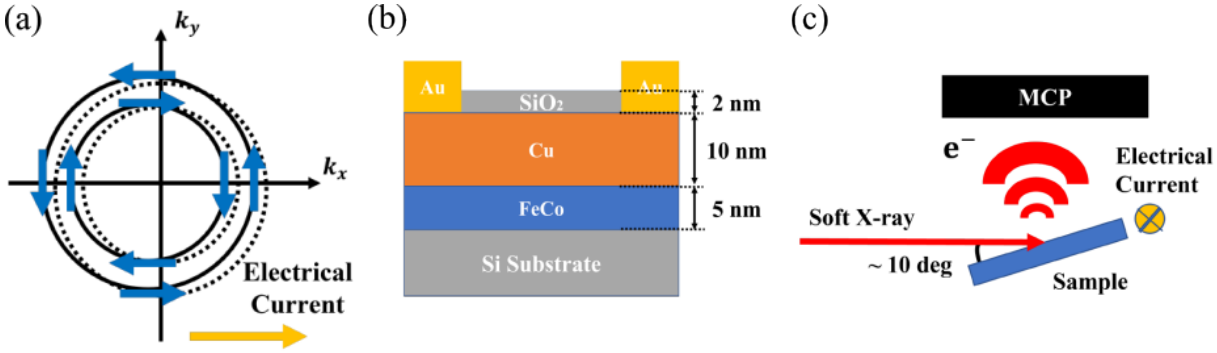

Fig. 1: Experimental setups. (a) Schematic illustration of OEE. (b) Sample structure. (c) Geometry of XCD measurements.

magnetic field that traps electrons and moves them back to the sample. Comparing the magnitude of the intensity decrease between the measurements conducted with right and left circular polarization, we found larger decrease for RCP. According to the sum rule of x-ray magnetic circular dichroism, this is consistent with expectation from OEE shown in Fig. 1(a) Utilization of fast polarization switching that has been developed at SPring-8 BL07LSU [6] may pave the way for further clarifying the effect of electric current and eventually proving the occurrence of OEE.

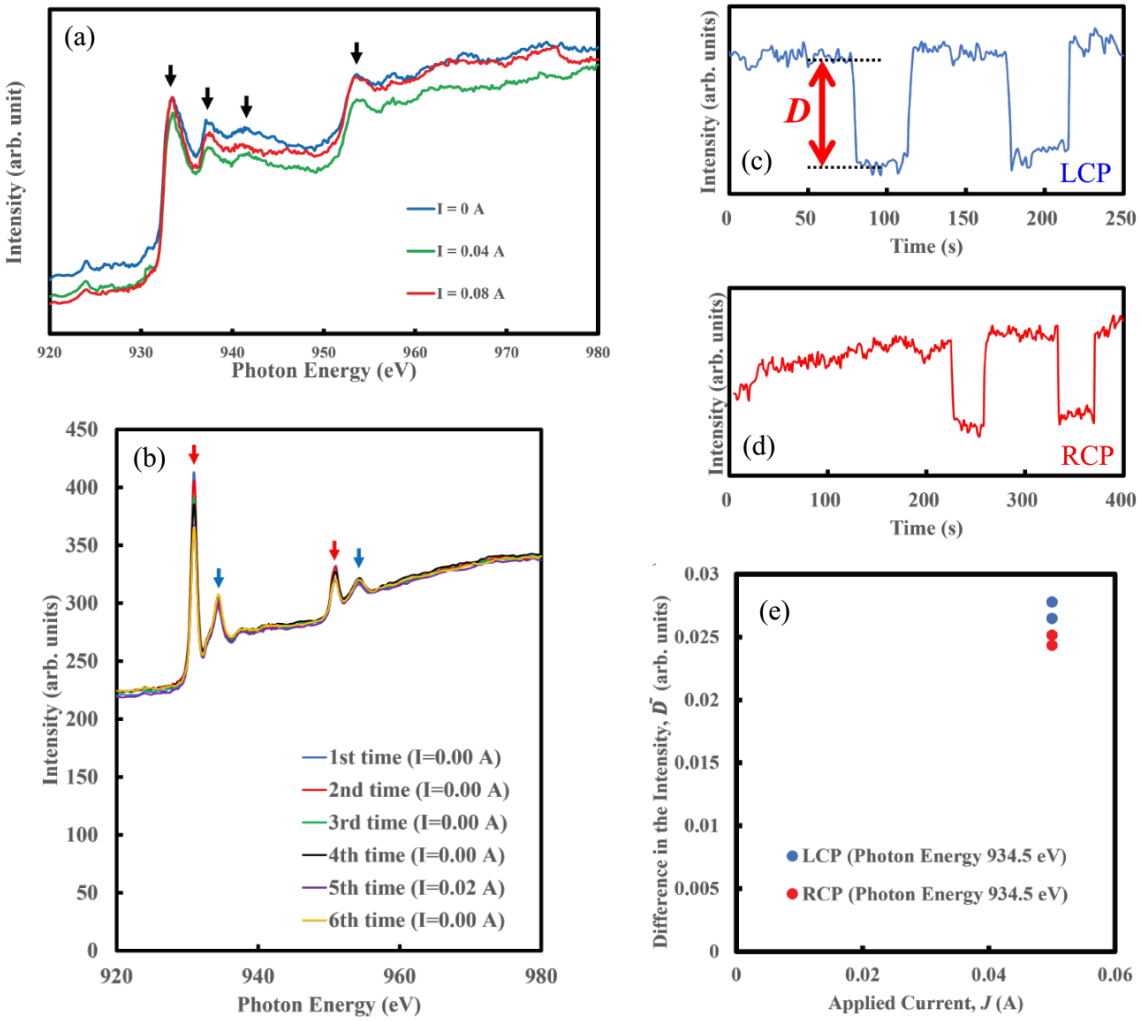

Fig. 2: XCD results on the Cu/SiO_2 sample. (a) Cu *L*-edge spectra measured under electric current as indicated. (b) Cu *L*-edge spectra measured repeatedly. (c),(d) Absorption intensity as a function of time measured at the photon energy of 934.5 eV with LCP and RCP. Sharp decrease is observed upon application of electric current. (e) Magnitude of intensity decrease for LCP and RCP.

REFERENCES

[1] I. M. Miron *et al*., Nature **476**, 189 (2011).
[2] L. Liu *et al*., Science **336**, 555 (2012).
[3] A. Manchon *et al*., Rev. Mod. Phys. **91**, 035004 (2019).
[4] H. An *et al*., Nat. Commun. **7**, 13069 (2016).
[5] J. Kim *et al*., Phys. Rev. B **103**, L020407 (2021).
[6] J. Miyawaki *et al*., AAPPS Bulletin **31**, 1-24 (2021).

XPS ANALYSES OF THE NOVEL SURFACE PHASES, GROWN BY BORON DEPOSITION ON A COPPER CRYSTAL SURFACE

Yuki Tsujikawa, Xiaoni Zhang, Masafumi Horio, Tetsuya Wada, Masashige Miyamoto, Toshihide Sumi, Fumio Komori, Iwao Matsuda
Institute for Solid State Physics, The University of Tokyo

Takahiro Kondo
Department of Materials Science and Tsukuba Research Center for Energy Materials Science, Faculty of Pure and Applied Sciences and R&D Center for Zero CO_2 Emission with Functional Materials, University of Tsukuba

In a history of surface science, a numerous number of the ordered phases were observed at various crystal surfaces, depending on adsorbate elements, coverages, or growth conditions. Recently, there have been growing interests in chemistry and physics of boron polymorphs or metal borides on surfaces due to unique multi-center bonding between boron atoms [1]. On the well-known Cu(111) substrate, the 2D ordered phase, $\sqrt{73}\times\sqrt{39}$, is prepared by boron deposition [2]. Structure analysis by the diffraction method unveiled that a 2D Cu-B compound, Cu boride is formed at the surface [3]. On the other hand, by the boron deposition on Cu(110), we discovered a 1D anisotropic ordered phase, 3×1, as a pattern of electron diffraction [4]. These novel B/Cu surface phases are intriguing playgrounds to explore the electronic or chemical states of these elements at the interface. In the present research, we conducted experiments of high-resolution X-ray photoelectron spectroscopy to confirm the electronic structure of these B/Cu .

The XPS measurement was made at the soft X-ray beamline BL07LSU of the synchrotron radiation facility SPring-8 with the electron analyzer (Phoibos-150 NAP, Specs Co.). All the data were obtained at room temperature. A sample was prepared on the surface of commercial crystals of Cu(110) and Cu(111). The surface phases was prepared by boron deposition on a clean surface of Cu(110) or Cu(111). The ordered structures were examined by observations of low energy electron diffraction (LEED), while the chemical states were investigated by XPS. As shown in Fig.1, only signals of B and Cu were observed, confirming no detectable impurity.

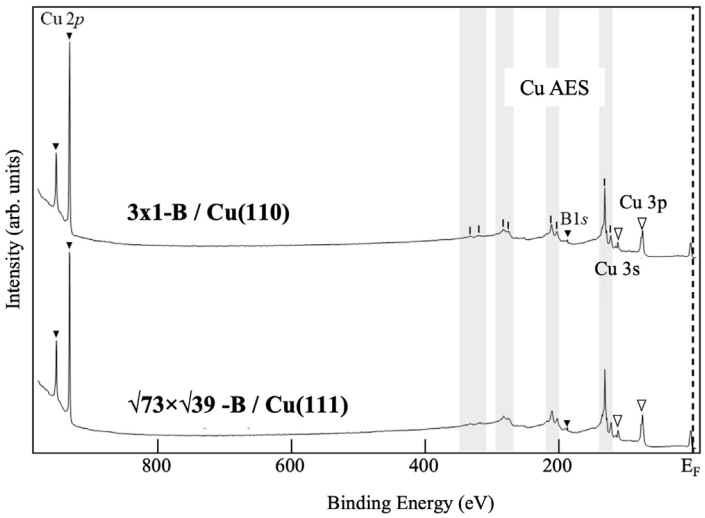

Figure 1 XPS spectra of the ordered surface phases of B/Cu(110) and B/Cu(111), taken at photon energy of hν = 1050 eV. Peaks of the B and Cu core-levels are indicated with black and white arrows, respectively. Signals of Auger electron spectroscopy (AES) are shown for Cu by gray bars.

Figure 2 shows XPS spectra of the Cu $2p_{3/2}$ and B 1s core level of the $\sqrt{73}\times\sqrt{39}$-B/Cu(111) surface. The sample has two Cu components of the surface layer (L) and in the bulk (Bu), while a clean Cu(111) surface is composed of a single component besides the negligible defect remanent. The (L) component can be identify as the surface Cu atom in Cu boride. In contrast, the B 1s spectrum of the $\sqrt{73}\times\sqrt{39}$-B/Cu(111) surface has a single component. The binding energy of 187.8 eV, determined from curve fitting, indicates that the boron atoms are

negatively charged [3]. It is likely that electrons were transferred to the boron atoms from the surrounding copper.

The surface phase of the 3×1-B/Cu(110) was discovered by us at the SPring-8 beamline, BL07LSU, by LEED [4]. The XPS spectrum of the Cu $2p_{3/2}$ core-level, as measured *in situ*, is curve-fitted with two components, as shown in Fig.3. In addition to the peak (Bu), ascribed to the clean Cu(110) surface, a new component, labelled (L), can be found. Since the Cu atom in the bulk crystal (Bu) has neutral charge, the peak position of the L component at the higher binding energy indicates that the Cu atoms in the 2D phase are positively charged. On the other hand, the B 1*s* core-level spectrum can be curve-fitted by two components, labelled I and II. The major component (I) is naturally assigned to the 3 × 1-B/Cu(110) surface, while the minor component (II) can be ascribed to either a part of the surface phase or the other contributions, such as surface impurities. By a comparison with Fig.2, binding energy of the component (I) at 187.4 eV indicates that the boron atoms in the 3 × 1-B phase are also negatively charged. The similarity with √73×√39-B/Cu(111) result suggest that the 3 × 1-B/Cu(110) phase are also a 2D Cu-B compound.

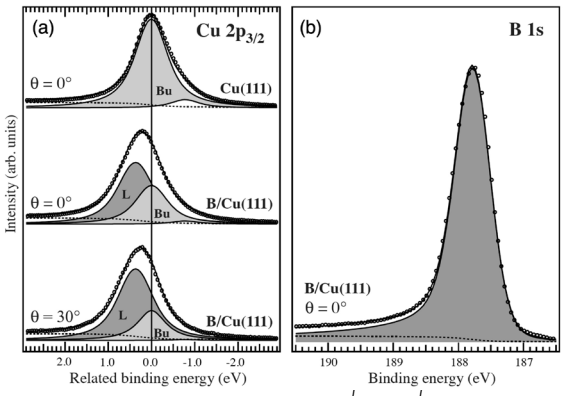

Fig.2 XPS spectra of the √73×√39-B surface phase on Cu(111): (a) Cu $2p_{3/2}$ and (b) B 1*s* core-level. Photon energies were (a) hν = 1050 eV and (b) hν = 285 eV. For a reference, a spectrum of the clean Cu(111) surface is shown. The peak components are obtained by the curve-fits and labeled with different symbols.

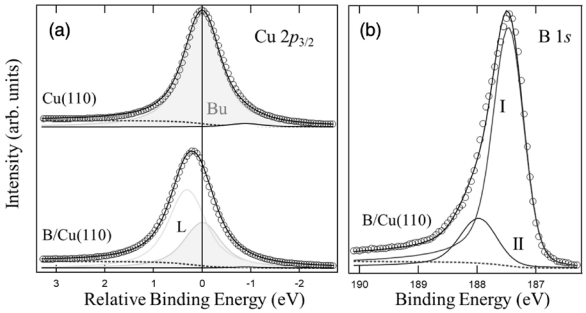

Fig.3 XPS spectra of the 3×1-B surface phase on Cu(110): (a) Cu $2p_{3/2}$ and (b) B 1*s* core-level. Photon energies were (a) hν = 1050 eV and (b) hν = 285 eV. For a reference, a spectrum of the clean Cu(110) surface is shown. The peak components are obtained by the curve-fits and labeled with different symbols.

In conclusion, we found that the boron atoms were negatively charged in the surface phases of √73×√39-B/Cu(111) and 3×1-B/Cu(110). The unique electronic property has also been known in the previous research of 2D boron or borophene [1]. The layer itself is unstable in the free-standing form but stable on a 2D metal substrate after electron doping. These microscopic findings indicate that low-dimensional boron structures on surfaces likely have the universal electrophilic property.

REFERENCES

[1] I. Matsuda, K. Wu ed., 2D Boron: Boraphene,Borophene, Boronene (Springer, 2021).
[2] R. Wu, I. K. Drozdov, S. Eltinge, P. Zahl, S. Ismall-Belgl, I. Božović, and A. Gozar, Nat. Nanotech. **14**, 44 (2019).
[3] Y. Tsujikawa, M. Horio, X. Zhang, T. Senoo, T. Nakashima, Y. Ando, T. Ozaki, I. Mochizuki, K. Wada, T. Hyodo, T. Iimori, F. Komori, T. Kondo, I. Matsuda, Phys. Rev. B **106**, 205406 (2022).
[4] Y. Tsujikawa, X. Zhang, M. Horio, T. Wada, M. Miyamoto, T. Sumi, F. Komori, T. Kondo, I. Matsuda, Surf. Sci. **732**, 122282 (2023).

ELECTRONIC STRUCTURE OF WATER CONFINED IN AQUEOUS MICROPHASE TWO-PHASE SYSTEMS

Yuji Higaki, Takumi Masuda
Faculty of Science and Technology, Oita University

Introduction

A large number of studies for the irregular structure and dynamics of water confined in nanometer scale molecular assembly including reverse micelles, and recently, metal-organic frameworks, carbon nanotubes, and polymer brushes.[1,2] Water molecules involved in hydration of ions experience constraints which prevent the formation of the preferred tetrahedral configurations characteristic of bulk water to cause hydrogen-bonding distortion. The hydrogen-bonding state of water has been studied by spectroscopic methods such as infrared spectroscopy, sum frequency generation spectroscopy, and solid-state NMR measurements. Soft X-ray absorption (XAS) and soft X-ray emission (XES) spectroscopies have recently attracted attention for their ability to show the detailed hydrogen bonding configurations from the electronic structures of the oxygen responsible for the hydrogen bonds.[3]

We developed a new class aqueous phase separation system of double hydrophilic block copolymers.[4] Double hydrophilic block copolymers comprising two kinds of zwitterionic polymers, poly(carboxybetaine methacrylate) (PCB2) and poly(sulfobetaine methacrylate) (PSB4), exhibits microphase separation in the highly concentrated aqueous solution to produce a highly ordered periodic lattice structure with nanometre scale compartments, and the morphology transforms in response to the polymer concentration (**Figure 1**). This morphology transition is manifested by selective water partitioning to the PCB2 phase owing to the poor water capacity of PSB4 phase. The double hydrophilic microphase-separated structure involving hydration water could be a good prototype for investigating the structure and dynamics of water confined in the fields with crowded charged polymers.

In this study, hydrogen bonding configurations of waters confined in the microphase separated zwitterionic mesophases were investigated by meas of XAS and XES spectroscopies. Systematic experiments were conducted by adjusting the polymer concentration in the microphase-separated structure to address the impact of microphase separation at the electronic structure level and to elucidate detailed information on the hydrogen bonding form and its role in microphase separation.

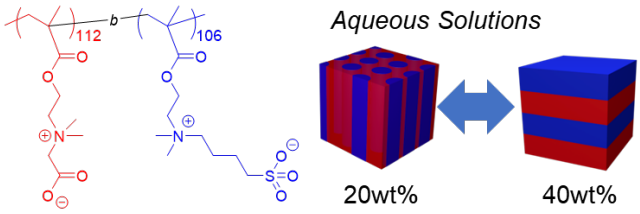

Figure 1. Chemical structure of the PCB2$_{112}$-*b*-PSB4$_{106}$ block copolymer and the schematic of morphologies.

Experiment

PCB2$_{112}$ (M_n = 24400, M_w/M_n = 1.12), PSB4$_{102}$ (M_n = 30200, M_w/M_n = 1.10), and the diblock copolymer PCB2$_{112}$-*b*-PSB4$_{106}$ (M_n = 54000, M_w/M_n = 1.19, , volume fraction of PCB2 = 0.41) were synthesized by reversible addition fragmentation chain transfer polymerization. The molecular mass and molecular mass distribution were well-controlled. The PCB2$_{112}$-*b*-PSB4$_{106}$ diblock copolymer aqueous solution produces microphase separated structure with lamellar morphology, where the long period was 46.2 nm and the PCB2 lamellar thickness was 28.0 nm, at polymer concentration (ϕ) = 40wt%, while the morphology transforms to columnar morphology with hexagonally packed cylindrical domains, where the cylinder radius is 13.2 nm and the cylinder center distance is 52 nm at ϕ = 20wt%.

XES and XAS measurements were conducted at the BL07LSU HORNET station at Spring-8 employing home-made liquid cell (**Figure 2**). The aqueous solution of PCB2-*b*-PSB4 diblock

copolymers were put onto the SiC membrane separating vacuum chamber, and the cell was sealed with a screw cap. Milli-Q water (Millipore Inc., Billerica, MA) with a resistance of >18 MΩ cm was used as the water source. The excitation energy was 550 eV, which is well above the ionization threshold. Each XES spectrum was normalized with the integration of the intensity between 515 and 530 eV to compare the spectrum shape.

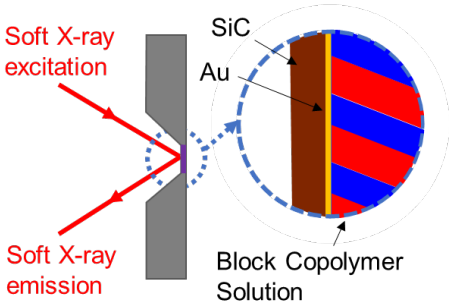

Figure 2. Schematic representation of the experimental setup for the XES spectroscopy of water confined in the microphase separated PCB2$_{112}$-*b*-PSB4$_{106}$ aqueous solutions.

Results and Discussion

The hydrogen-bonding structure configurations of water confined in microphases were investigated by O 1s XES spectroscopy. XES spectra of the PCB2$_{112}$-*b*-PSB4$_{106}$ aqueous solutions exhibited two peaks at 525.8 eV and 526.7 eV, which have been assigned to the oxygen of water with distorted and tetrahedral hydrogen bonding configurations, respectively (**Figure 3(a)**).[4] In comparison with the XES spectrum of bulk water, the 1b$_1$" peak intensity was pronounced with respect to 1b$_1$' peak, indicating the significant hydrogen-bonding distortion in the water confined in the zwitterionic polymer mesophase. Meanwhile, the XES spectrum shape was independent of the ϕ. This result suggests that the hydrogen bonding distortion remains identical with decreasing the zwitterionic PCB2$_{112}$-*b*-PSB4$_{106}$ concentrations. Since the PSB4 phase has water capacity limit at approximately 50wt%, the PCB2 phase contains relatively more water and its polymer concentration can be estimated to 32.2, 20.2, and 11.6wt% when the block copolymer concentrations are 40, 30, 20wt%, respectively. Thus, the hydrogen-bonding state of water in the mesoscopic phase-separated structures of lamellar structure with 50wt% PSB4 and 32.2wt% PCB2 phases, and the columnar structure with 50wt% PSB4 cylindrical domains and 11.6wt% PCB2 matrix were identically distorted.

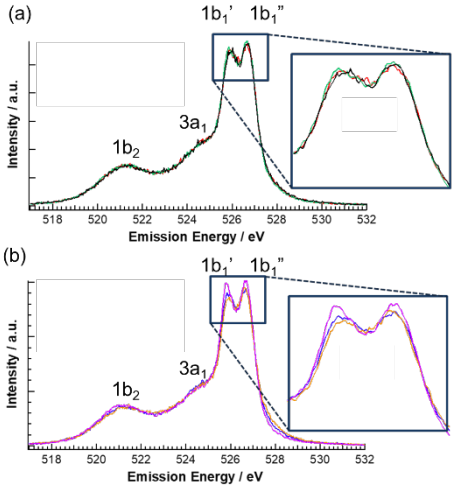

Figure 3. XES spectrum of (a) PCB2$_{112}$-*b*-PSB4$_{106}$ aqueous solutions with ϕ = 40wt% (black), 30wt% (red), and 20wt% (blue), and (b) PCB2$_{112}$ aqueous solutions with ϕ = 40wt% (yellow) and 10wt% (purple), and a PSB4$_{102}$ aqueous solution with ϕ = 40wt% (blue). The additional panels show magnified data at 1b$_1$' and 1b$_1$" peaks.

We then verified the hydrogen bonding configuration of water in PCB2 and PSB4 solutions (**Figure 3(b)**). The 40wt% PCB2 and 40wt% PSB4 aqueous solutions showed the XES spectra comparable to PCB2$_{112}$-*b*-PSB4$_{106}$ solutions. On the other hand, the 10wt% PCB2 solutions showed a slight increase in the intensity of 1b' peak relative to the 1b", while the spectrum is identical to that of bulk water. Thus, the water molecules in the PCB2 phase of the microphase separated 20wt% PCB2$_{112}$-*b*-PSB4$_{106}$ solution are perturbed relative to those in PCB2 solutions, probably because of the obstruction of hydrogen bonding network due to the phase boundary.

REFERENCES

[1] M. A. Wells, *Biochemistry* **1974**, *13*, 4937–4942.

[2] K. Yamazoe, Y. Higaki, Y. Inutsuka, J. Miyawaki, A. Takahara, Y. Harada, *Langmuir* **2022**, *38*, 3076.

[3] T. Tokushima, Y. Harada, O. Takahashi, Y. Senba, H. Ohashi, L. G. M. Pettersson, A. Nilsson, S. Shin, *Chem. Phys. Lett.* **2008**, *460*, 387.

[4] Y. Higaki, M. Takahashi, T. Masuda, *Macromol. Chem. Phys.* **2022**, *224*, 2200416.

SOFT X-RAY EMISSION SPECTROSCOPIC ANALYSIS OF 1D WATER CHANNEL WITHIN A NONCOVALENT POROUS CRYSTAL

Shinnosuke HORIUCHI,[1,2] Shota OGURA,[1] Yuka IKEMOTO,[3] Hisao KIUCHI,[4] Kazuo TATSUTA,[4] Yusuke TOMIYORI,[4] Yoshihisa HARADA[4]

[1]*Division of Chemistry and Materials Science, Graduate School of Engineering, Nagasaki University*

[2]*Department of Basic Science, Graduate School of Arts and Sciences, The University of Tokyo*

[3]*Spectroscopy Division, Japan Synchrotron Radiation Research Institute*

[4]*Synchrotron Radiation Laboratory, The Institute for Solid State Physics, The University of Tokyo*

Water molecules on material interfaces play crucial roles in abundant natural phenomena and material sciences [1,2]. Although the importance of interfacial water has been recognized, it is still challenging to elucidate a three-dimensional alignment of water clusters and the hydrogen-bonding network on a non-flat material surface in an atomic resolution. Recently, X-ray diffraction studies using crystalline porous materials can visualize not only the absolute configuration of small molecules but clustering motifs of the guests on the pore surface [3–5]. In addition, X-ray emission spectroscopy (XES) is one of the useful techniques to probe electronic transitions between core and valence orbitals of oxygen atoms, which can provide useful information reflected from the hydrogen-bonding states of water molecules, because the time scale of the excitation process and the O1s core-hole lifetime in femtoseconds are much shorter than that related to rearrangements of the hydrogen-bonding network [6]. Thus, the combination of these techniques will provide a clear relationship between a structure and its character of a water cluster formed on the pore surface of the crystalline material.

We have recently synthesized a supramolecular crystal composed of coordination complex salts and macrocyclic organic hosts (Figure 1). The supramolecular crystal contained one-dimensional (1D) water channels in the crystal lattice, where the molecular alignments of the water molecules can be determined by the single crystal X-ray diffraction analysis. In particular, the large water cluster and its temperature-dependent dynamic character were observed in the X-ray analysis. This result suggests that this supramolecular crystal containing 1D water channels is a suitable material for elucidating the inhomogeneous nature of interfacial water molecules. Thus, for unveiling the electronic structure of the water molecules in the 1D pore, we performed the soft X-ray emission spectroscopic analysis of the 1D water channels within the supramolecular crystal.

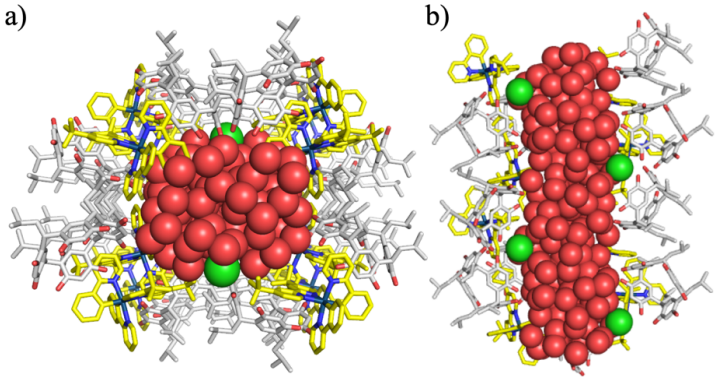

Figure 1. Crystal structures of the supramolecular crystal viewed from a) the top and b) the side of the 1D water channels. Red spheres represent oxygen atoms of the water molecules in the pore.

The supramolecular crystal contains hydroxy (–OH) groups in the framework. Thus, the dehydration process of the crystal was investigated by the O1s XES measurement to eliminate the effect of the framework. The XES measurement was performed using the SPring-8 BL07LSU ultra-high resolution soft X-ray emission spectrometer HORNET. During the measurement, a steam-nitrogen gas mixture flowed over the sample, enabling precise control of humidity around the sample and the dehydration rate. The intensities of the XES spectra during the dehydration process were summarized in Figure 2a. The intensity of the spectra

gradually decreased and was mostly constant after 400 min. This result indicates that the dehydration process was completed at 400 min and the spectra after 400 min are derived from the hydroxy groups in the framework. Thus, the XES spectra of the water molecules in the 1D pore of the supramolecular crystal were obtained from the difference spectra using the averaged spectra recorded from 600 to 745 min as a background spectrum. As a result, the difference spectrum showed characteristic features of water molecules, which involved four peaks assigned to $1b_1$", $1b_1$', $3a_1$, and $1b_2$, respectively (Figure 2b). In general, the XES spectrum of bulk liquid water consists of the four peaks corresponding to oxygen 2p orbitals of water, which are obtained by the emitted X-ray associated with the electronic transition from the valence state to the core level. These spectral features can be associated with two distinct structural motifs in liquid water, where the $1b_1$' peak at 525.8 eV and the $1b_1$" peak at 526.7 eV correspond to fourfold icelike hydrogen-bonds and less than fourfold highly distorted hydrogen-bonds, respectively (Figure 2c). The relative intensities of the two $1b_1$ peaks are dependent on the measurement conditions, which will provide spectroscopic aspects for the hydrogen bonding of water molecules in the 1D pore. Intriguingly, the intensity of $1b_1$" at 526.7 eV was higher than that of $1b_1$' at 525.8 eV. This result strongly suggests that the structure of water molecules in the 1D pore is mainly less than fourfold highly distorted hydrogen-bonds even at ambient conditions, rather than fourfold icelike hydrogen-bonds. Variable-temperature X-ray diffraction studies revealed that the water molecules in the 1D pore showed temperature-sensitive and dynamic characteristics. Thus, these XES results clearly explained the flexible character of the hydrogen-bonding network of the water molecules in the supramolecular crystal.

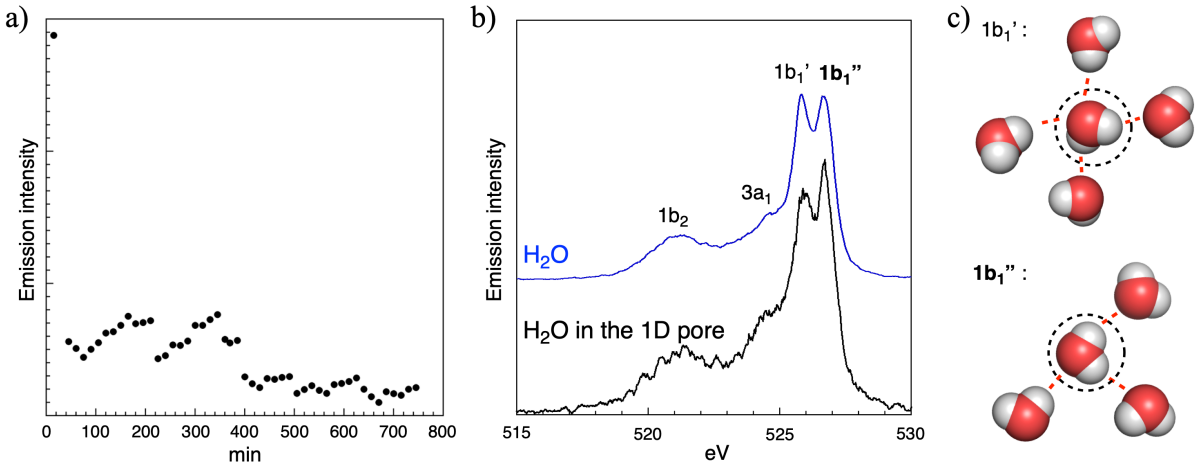

Figure 2. a) Emission intensities of the XES spectra. b) The O1s X-ray emission spectra of bulk liquid water (blue line) and H_2O molecules in the 1D pore (black line). c) Molecular structures of fourfold icelike hydrogen-bonds (upper) and less than fourfold highly distorted hydrogen-bonds (bottom) of water molecules.

In summary, O1s XES spectra of water molecules in the supramolecular crystal were obtained by following the dehydration process of the crystal. The XES spectra indicated that the crystal contained weakly hydrogen-bonded waters in the 1D channel, which is well-reflected with the dynamic character of water molecules observed in the X-ray crystallographic study. This combination study provides a clear relationship between the hydrogen-bonded structure and temperature-sensitive and dynamic characteristics of the interfacial water molecules.

REFERENCES

[1] Björneholm, O. et al. *Chem. Rev.* **116**, 7698 (2016).
[2] Brini, E. et al. *Chem. Rev.* **117**, 12385 (2017).
[3] Inokuma, Y. et al. *Nature* **495**, 461 (2013).
[4] R. Kubota, *Nat. Chem* **6**, 913 (2014).
[5] Hanikel, N. et al. *Science* **374**, 454 (2021).
[6] Fransson, T. et al. *Chem. Rev.* **116**, 7551 (2016).

Electronic states analysis of oxygen evolution reaction catalyst for alkaline water electrolysis by Operando soft X-ray absorption/emission spectroscopy

Kazuo Tatsuta[a*], Jun Kikuma[b], Shinya Matsuno[b], Shin Kawashima[b], Hisao Kiuchi[a], and Yoshihisa Harada[a]
[a]The Institute for Solid State Physics, the University of Tokyo, [b]Asahi Kasei Corporation
*Current affiliation: Asahi Kasei Corporation

In improving the efficiency of hydrogen generation by water electrolysis, there are two important factors: one is to reduce the voltage above the theoretical electrolysis voltage that must be applied for the electrolytic reaction (overvoltage), and the other is to suppress the increase in overvoltage due to catalyst degradation. Various electrocatalysts have been developed to solve these problems. Perovskite-type oxides acting as anode catalysts have a wide range of elemental choices, among them, $LaNiO_3$ is particularly promising in the next-generation alkaline water electrolysis system because of its high electrical conductivity and stable oxygen evolution reaction (OER) in the alkaline electrolyte. Our previous studies have confirmed that the addition of a small amount of transition metal elements to $LaNiO_3$ can suppress catalyst degradation for a long time, however little difference was found by hard X-ray absorption spectroscopy (XAS) of Ni, and the correlation between durability during operation and the chemical stability of Ni could not be found. On the other hand, the use of soft X-ray emission spectroscopy (XES), which can directly observe the strength of orbital hybridization and charge transfer energy expected to clarify the correlation between durability and the chemical state of Ni. Therefore, in this study, we worked on the development of a technique to perform Ni-L edge XES measurements of $LaNiO_3$ under alkaline water electrolysis operando conditions, with the aim of providing feedback for further anode material optimization.

The cell for Operando measurement was based on the liquid cell developed by Tokushima et al.[1], and was modified to enable water electrolysis in a three-electrode system by inserting contact probes for the reference electrode (RE), counter electrode (CE), and working electrode (WE). A screw-in Ag/AgCl RE was screwed directly into the cell. A 0.5 mm diameter Pt wire was used as CE, inserted into the electrolyte channel in the cell, and the insertion opening was sealed with epoxy resin. The membrane with 150 nm thick Si_3N_4 window with $LaNiO_3$ and Au/Ti layers was used as WE. The cell was fabricated with acrylic resin using a 3D printer. A 20% KOH solution was used as the electrolyte, and the flow rate was 10 ml/min during Operand measurement.

All measurements described below were performed on the beamline BL07LSU at SPring-8. Before Operando measurement, ex-situ Ni-L edge XAS and XES measurements were carried out on $LaNiO_3$ surface. The samples for Operando measurement were previously energized at 0.55 V, which is the OER potential, for 6 hours to confirm that the OER activity was enhanced. Before XES measurements, XAS measurements were performed. For Operando Ni-L edge XAS measurements, applied potentials were 0.35 V (before OER), 0.57 V (during OER), and the open circuit potential, and performed at several different points on the Si_3N_4 window to prevent damage to the window by X-rays. For Operando Ni-L edge XES measurements, the excitation energies were set to 853.2 eV. To prevent damage to the Si_3N_4 window caused by X-ray irradiation, the irradiation positions were changed every 2 min, and the data were obtained by integrating the spectra from all measurement positions. The applied potentials were 0.35 V and 0.57 V.

The obtained XAS spectra were normalized to the peak intensity at 853 eV for the operando measurement results, and the spectra obtained at multiple measurement positions were

arranged by measurement potential and are shown in Figure 1 together with the ex-situ measurement results. The peak at 850.6 eV is an absorption peak of La-M_4. The spectral shape obtained by ex-situ measurement was similar to that of $LaNiO_3$ deposited by laser deposition[2]. On the other hand, most of the spectral shapes obtained by the operando measurement were significantly different from those by the ex-situ measurement, and the shapes differed depending on the measurement positions. The spectral shapes obtained from the operando measurements, characterized by a peak on the high energy side (~855eV) of Ni-L_3 that is significantly lower than the peak on the low energy side (~853eV), suggest that the catalyst layer exists as a compound with predominantly Ni^{2+} components[3]. This result suggests that the catalyst layer has already changed to a chemical state different from that of $LaNiO_3$ during pre-energization. The large variations in spectral shape from position to position did not allow us to determine the spectral change with potential.

The obtained XES spectra are shown in Figure 2 together with the results of ex-situ measurement, normalized by the intensity of the main peak, where the abscissa axis is represented as energy transfer. The Operando measurements were integrated for about 5 hours, but because the noise was very high in all cases, no characteristic structures other than the main peak around 1 eV could be identified, and the structural differences between the spectra were also unclear, making it impossible to clarify changes due to electric potential.

In order to elucidate the cause of the variation of XAS spectra by measurement positions and the large noise in XES spectra, cross-sectional SEM and TEM observations of the catalyst layer on the Si_3N_4 window of the samples used for operando measurements were performed and thickness variation of about 5 nm to 300 nm was observed. It is suggested that the variation in thickness correlates with the variation in the chemical state of the catalyst layer and is the cause of the variation in the shape of the XAS spectra. In addition, there are many thin regions, which may have resulted in insufficient intensity and increased noise in XES spectra, in which the emission intensity was integrated by scanning over the window. These results clearly indicate that improving the thickness uniformity of $LaNiO_3$ on the Si_3N_4 window is a future challenge.

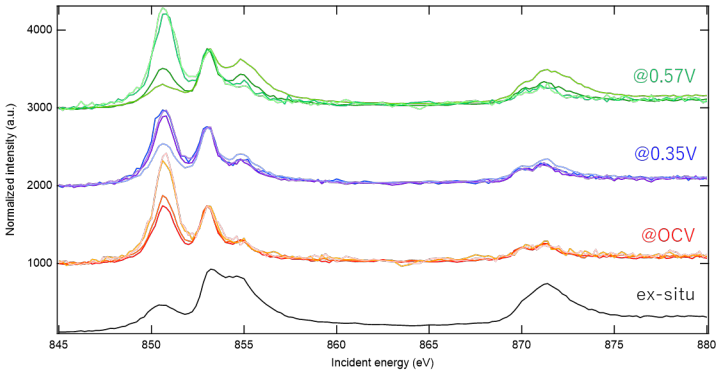

Fig.1 ex-situ and Operando Ni-L edge XAS spectra

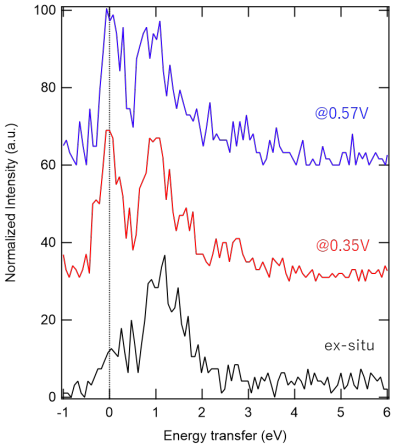

Fig.2 ex-situ and Operando Ni-L_3 edge XES spectra obtained at excitation energy of 853.2 eV

REFERENCES

[1] T. Tokushima, Y. Harada, Y. Horikawa, O. Takahashi, Y. Senba, H. Ohashi, L. G. M. Pettersson, A. Nilsson, S. Shin, *J. Electron Spectrosc. Relat. Phenom.*, 177 (2010) 192.
[2] M. Hepting, D. Li, C. J. Jia, H. Lu, E. Paris, et al., *Nat. Mater.*, 19 (2020) 381.
[3] C. Tian, D. Nordlund, H. L. Xian, Y. Xu, Y. Liu, D. Sokaras, F. Lin, and M. M. Doeff, *J. Electrochem. Soc.*, 3 (2018) A696

ELECTRONIC STRUCTURE ANALYSIS OF OXYFLUORIDE CATHODE OF ALL-SOLID-STATE FLUORIDE BATTERY USING RESONANT INELASTIC X-RAY SCATTERING

Kentaro YAMAMOTO[1,2], Datong ZHANG[1], Hisao KIUCHI[3], Yoshihisa HARADA[3], Yoshiharu UCHIMOTO[1]

[1]*Graduate School of Human and Environmental Studies, Kyoto University*

[2]*Faculty of Engineering, Nara Women's University, Kitauoyanishimachi, Nara, 630-8263*

[3]*Synchrotron Radiation Laboratory, The Institute for Solid State Physics, The University of Tokyo*

All-solid-state fluoride-ion rechargeable batteries are expected to be high-power, high-energy density rechargeable batteries because they can use multi-electron transfer reactions with monovalent fluoride-ions as carriers. Until now, development of cathode materials has focused on simple metal/metal fluoride (M/MFx) systems[1,2]. However, the absence of a diffusion path for F^- during the fluorination and defluorination reactions and the large volume change associated with the fluorination and defluorination reactions of the most densely packed metal cathodes (such as Cu) have made it difficult to achieve the following rate characteristics. In this study, we focused on Cu_3N as a new cathode material to solve this problem, because Cu_3N cathode has many anion vacancy sites in its structure and is expected to show better rate characteristics than metal cathodes. The reaction mechanism was further elucidated by electron spectroscopy.

Cu_3N was synthesized by mixing Cu_2O and $CO(NH_2)_2$ in the ratio of 1:2 mol, annealing at 190°C for 6 h, and washing and drying[3]. A bulk-type electrochemical cell was constructed with $Cu_3N/La_{0.9}Ba_{0.1}F_{2.9}$/Vapor grown carbon fiber (VGCF) as a composite positive electrode, $La_{0.9}Ba_{0.1}F_{2.9}$ as an electrolyte and $Pb/PbF_2/La_{0.9}Ba_{0.1}F_{2.9}$/VGCF as a composite negative electrode. Charge-discharge measurements were performed in the cutoff voltage range of -1.5 to 2.9 V at 140°C. Cu K, *L*-edge XAS and N *K*-edge XAS, RIXS measurements were performed on the samples after charge and discharge.

The charge-discharge curve measurements of the Cu_3N cathode are shown in Figure 1. The Cu_3N cathode exhibits reversible charge-discharge behavior within the Cu^+/Cu^{2+} redox range, while showing a potential flat area at about 0.65 V (vs. Pb/PbF_2) (Figure 1 a). Charge and discharge capacities of 290 mAh g^{-1} and 236 mAh g^{-1} were obtained during initial charge and discharge, respectively. The Cu_3N cathode maintained a charge and discharge capacity of 100 mAh g^{-1} even when the current density was increased to 200 mA g^{-1}, showing higher rate and cycle properties than the Cu cathode. Furthermore, the Cu_3N cathode showed an extremely high capacity of 780 mAh g^{-1} on initial charge and 550 mAh g^{-1} on discharge, exceeding the theoretical capacity (393 mAh g^{-1}) of the Cu^+/Cu^{2+} redox (Figure 1b).

Cu *L*-edge, N *K*-edge XAS and RIXS measurements were performed on Cu_3N during the charging process to clarify the origin of this capacitance that cannot be explained by the Cu^+/Cu^{2+} redox. In the Cu *L*-edge XAS spectra, a peak was observed at about 930.5 eV; toward F=3, this peak shifted to the lower energy side with charging, and the peak position of the sample charged up to F=3 was consistent with that of CuF_2. Subsequently, when the samples were charged from F=3 to F=6, no change in peak position was observed. These results indicate that oxidation of Cu^+ to Cu^{2+} occurred from F=0(pristine) to F=3, but that Cu was not oxidized from F=3 to F=6. In the N *K*-edge XAS spectra (Figure 2a), no noticeable change in spectral shape with charging was observed from F=0(pristine) to F=2. On the other hand, from F=2 to F=6, the peak shape around 401 eV changed and the peak intensity increased dramatically. This dramatically changed peak shape is very similar to that of nitrogen gas[4]. In the N *K*-edge RIXS spectrum at 400.8 eV, vibrations similar to those of N_2 gas in the previous study[5], and the value

of the width of the Cu_3N frequency is consistent with the N_2 gas value (2360 cm^{-1}, 0.292 eV), suggesting the presence of N_2 molecules within Cu_3N. These results indicate that nitrogen redox occurs in the Cu_3N cathode during charging, leading to the high capacity.

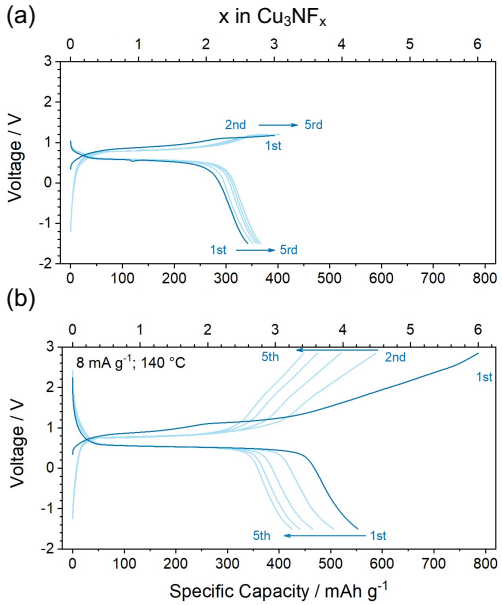

Fig. 1. Electrochemical measurements of Cu_3N cathode material at 140 °C. Charge/discharge profiles under capacity limitation of (a) F=3 and (b) F = 6 at 8 mA g^{-1}.

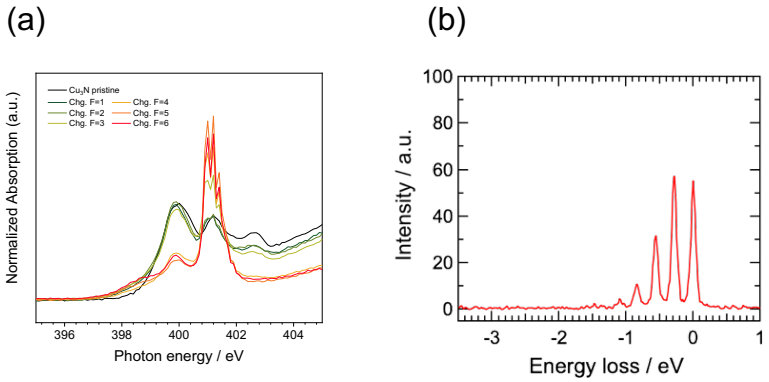

Fig. 2. (a) N *K*-edge XANES spectra of Cu_3N cathode obtained upon charging and (b) N *K*-edge RIXS spectrum of Cu_3N cathode after full charging.

REFERENCES

[1] M. Anji Reddy and M. Fichtner, *J. Mater. Chem.* 2011, **21**, 17059–17062.

[2] D. Zhang, K. Yamamoto, A. Ochi, Y. Wang, T. Yoshinari, K. Nakanishi, H. Nakano, H. Miki, S. Nakanishi, H. Iba, T. Uchiyama, T. Watanabe, Y. Orikasa, K. Amezawa, Y. Uchimoto, *J. Mater. Chem. A*, 2021, **9**, 406–412.

[3] M. D. Reichert, M. A. White, M. J. Thompson, G. J. Miller, and J. Vela, *Inorg. Chem.* 2015, **54**, 6356–6362.

[4] H. J. Song, H. J. Shin, Y. Chung, J. C. Lee, M. K. Lee, *J. Appl. Phys.* 2005, **97**, 113711-7.

[5] L. Kjellsson, V. Ekholm, M. Agåker, C. Såthe, A. Pietzsch, H. O. Karlsson, N. Jaouen, A. Nicolaou, M. Guarise, C. Hague, J. Lüning, S. G. Chiuzbăian, and J.-E. Rubensson, *Phys. Rev. A*, 2021, **103**, 022812-7.

STUDY OF SOFT X-RAY EMISSION ANGULAR ANISOTROPY OF GAS PHASE

Naoya Kurahashi[1], Jun Miyawaki[2], Kosuke Yamazoe[3], Hisao Kiuchi[1], Wenxiong Zhang[1], Ugalino Ralph[1] and Yoshihisa Harada[1]

[1]*Synchrotron Radiation Laboratory, The Institute for Solid State Physics, The University of Tokyo*

[2] *National Institutes for Quantum Science and Technology*

[3]*Japan Synchrotron Radiation Research Institute*

Soft X-ray emission spectroscopy is a powerful technique to observe the electronic state of occupied orbitals, which emits excess energy as light when valence electrons relaxation to inner-holes generated by the excitation light of soft X-rays. The measurement under ambient pressure and measurement of wet samples are possible using the X-ray transmission window. In contrast, photoelectron spectroscopy is another method for directly observing occupied electron orbitals, and it is possible that photoelectron spectroscopy and emission spectroscopy provide complementary information, as exemplified by the results of bulk water measurements. While soft X-ray emission spectroscopy can measure samples in a variety of environments, it tends to have a broad natural width of the spectrum, due to the short lifetime of inner-holes. Because of this, it may not be possible to completely separate the electron orbitals, and a method for assigning electron orbitals other than emission energies is required.

Since photoelectron spectroscopy for atoms and molecular has long been used to study photo-excitation dynamics, there has been a need for a method to understand the electronic excitation states. To solve this problem, a photoelectron velocity mapping method[1] has been developed that enables simultaneous observation of the kinetic energy and emission angle of photoelectrons. In the process of photoelectron emission, the orbital angular momentum of electrons changes by ±1 according to the law of conservation of angular momentum. For example, electrons from the *s*-orbital are emitted in the form of *p*-orbitals, while those in the *p*-orbital are emitted as a superposition of *s*- and *d*-orbitals. As a result, by measuring the kinetic energy and emission angle distributions of photoelectrons, information on the energy levels and angular momenta of the original orbitals can be obtained, which enables precise assignment of electron orbitals.

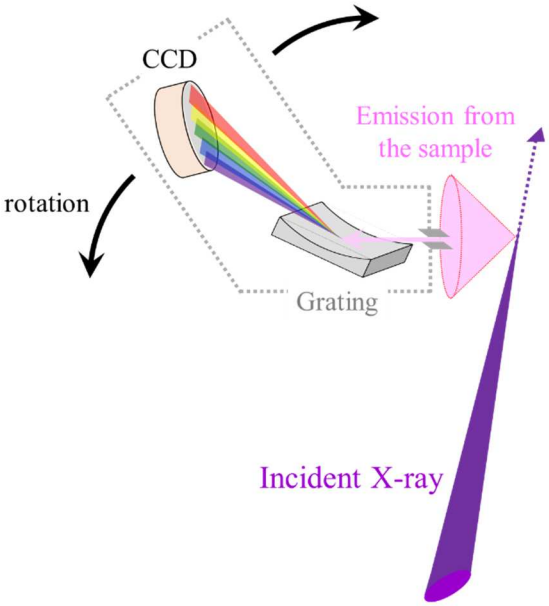

Fig. 1 Schematic of soft X-ray emission angular anisotropy measurement. The incident light and emission points were fixed and the spectrometer was rotated in the horizontal plane.

We have planned a soft X-ray emission angular anisotropy observation experiment on a gas-phase sample, because we thought that the electron orbital information could be obtained from the soft X-ray emission angular distribution in the same way as the photoelectron emission angular distribution has information on the orbital angular momentum (Fig. 1). By using a gas-phase sample, the angular emission anisotropy is considered to depend only on the angle between the molecular axis and the electric field plane of light (polarization) and the symmetry between the core-excited intermediate and final states of the molecule, making it easy to compare with theoretical calculations. In angle-resolved spectroscopy, it is necessary to consider the

lifetime of the intermediate state because the angle information is lost due to molecular rotation. However, in soft X-ray emission spectroscopy, the lifetime of the intermediate state is very short (few femto-seconds), and the positional relationship between the molecule and the light is considered to be conserved. Due to the trade-off between energy resolution and detection efficiency in emission spectroscopy, and the low efficiency of X-ray fluorescence for light elements, soft X-ray emission spectroscopy for gaseous samples has been considered difficult. To solve this problem, we have developed a high-density gaseous sample introduction method. This method enables us to introduce a high-density gas-phase sample into a very small area while maintaining a high vacuum in the measurement chamber.

Using the newly developed sample introduction method, we performed soft X-ray emission angle anisotropy observation of oxygen gas and succeeded in the first soft X-ray emission angle anisotropy measurement of gaseous molecules. The pressure in the vacuum chamber remained at around 10^{-4} Pa even though 100 kPa oxygen gas was introduced, and no influence on the light source or other devices was observed.

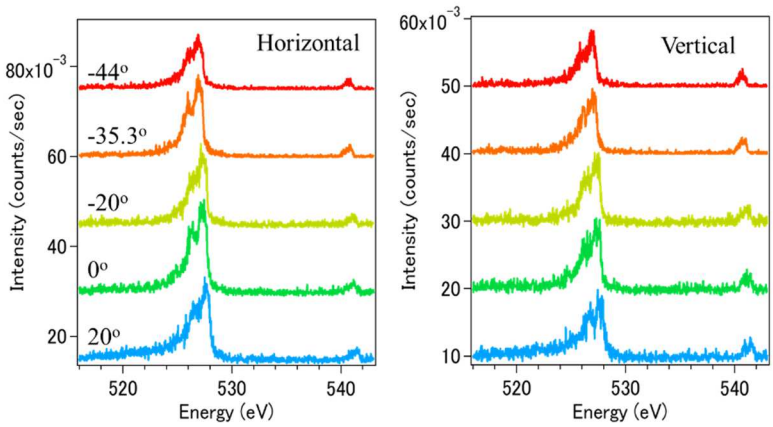

Fig. 2 Soft X-ray emission angle anisotropy measurements of oxygen excited at 541.3eV. The angle in the figure indicates the angle between the electric field plane of the excitation light and the monochromator.

The soft X-ray emission angular anisotropy at excitation energy of 530.8 eV, which is the π* excitation ($^3\Sigma_g^- \rightarrow {}^3\Pi_u$) was re-measured. In the case of horizontal polarization, the anisotropy parameters were -0.62±0.04 for $^3\Sigma_{g^-}$ emission and +0.23±0.15 for $^3\Pi_g$ emission. These values were close to the respective anisotropy parameters of -0.57 and +0.36 obtained from geometric calculations. From this result, it is concluded that the emission process of $^3\Pi_u$ excitation in oxygen gas is a dipole transition, which occurs sufficiently faster than the molecular rotation. Since the lifetime of $^3\Pi_u$ is expected to be highly dependent on the excitation energy, we would like to challenge the excitation energy dependence of $^3\Pi_u$ angular anisotropy in the next beam time. On the other hand, no clear angular anisotropy was observed at 541.3 eV (Fig. 2), which is the Rydberg excitation, and it is possible that the molecular rotation cancels out the angular anisotropy because the excited state lifetime tends to be long due to the hydrogen atom-like electron configuration in the Rydberg excitation. However, no clear conclusion has been reached on the emission lifetime in this region due to a lack of examples of studies, so we would like to compare our results with theoretical calculations.

No angular anisotropy was observed in any of the peaks when the polarization was set to vertical. This indicates that the measurement system maintains cylindrical symmetry in longitudinal polarization. This means that the sample emission occurred at the center of rotation of the spectrometer and that the gas-phase sample measurement setup was successful.

With this study, we have successfully performed windowless experiments of soft X-ray emission spectroscopy of oxygen gas and measured the angular anisotropy of the soft X-ray emission. In the future, we would like to try soft X-ray emission angle anisotropy experiments of vaporized water, which is important for comparison with bulk water.

REFERENCES

[1] T. Suzuki, *Annu. Rev. Phys. Chem.*, 57, 555 (2006).
[2] J.-E. Rubensson *et al.*, *J. Electron Spectros. Relat. Phenomena*, 185, 294 (2012).

ELECTRONIC STATE ANALYSIS OF EARTH-ABUNDANT FE–AL–SI THERMOELECTRIC (FAST) MATERIALS USING SCANNING PHOTOELECTRON MICROSCOPY (II)

Yoshiki TAKAGIWA[1], Shunsuke TSUDA[1], Naoka NAGAMURA[1,2,3], Asako YOSHINARI[1,3], Shingo TAKEZAWA[1,3], Kenta OISHI[1,2,3], Kentaro FUKU[4], Wenxiong ZHANG[5]

[1]*National Institute for Materials Science (NIMS), Tsukuba, Ibaraki, Japan.*
[2]*PRESTO, Japan Science and Technology Agency, Honcho, Saitama, Japan.*
[3]*Tokyo University of Science, Katsushika, Tokyo, Japan*
[4]*Tohoku University, Sendai, Miyagi, Japan*
[5]*The University of Tokyo, Kashiwa, Chiba, Japan*

One of the unsolved global-scale issues is developing technology that effectively uses energy represented by unused waste heat. It is known that exhaust heat below 200°C occupies ~70% of the total. From this perspective, thermoelectric materials that can directly convert heat to electrical energy can be considered clean energy materials. Unfortunately, except for space and remote areas, our society has not yet implemented power generation using thermoelectric materials.

To develop environmentally friendly thermoelectric materials that are non-toxic and low-cost with sufficient power output to drive sensor devices, in particular, at a low-temperature region below 400 K, we developed FAST materials (**Fe**-**Al**-**Si** **T**hermoelectric Materials) composed of τ_1-$Fe_3Al_2Si_3$ phase forms a narrow bandgap of ~0.2 eV near the Fermi level [1]. We demonstrated that the Al/Si ratio fine-tuning could control its conduction type and enhance the power factor without chemical substitutions [2]. Relatively large power factors were obtained for p- and n-type thermoelectric materials below 400 K, which possessed high oxidation resistance and excellent mechanical properties [3]. Recently, we improved the power factor at mid-temperatures using machine-learning-assisted synthesis and evaluation by tuning the compositions [4,5]. Furthermore, we succeeded in the bonding technology to build a small-sized and highly integrated thermoelectric power generation module: the operation of temperature/humidity sensors and wireless transmission was performed [6] (Fig. 1). To better understand the intrinsic thermoelectric characteristics of FAST materials, the electronic structure, including the magnitude of the bandgap and formation of impurity states, needs to be experimentally investigated.

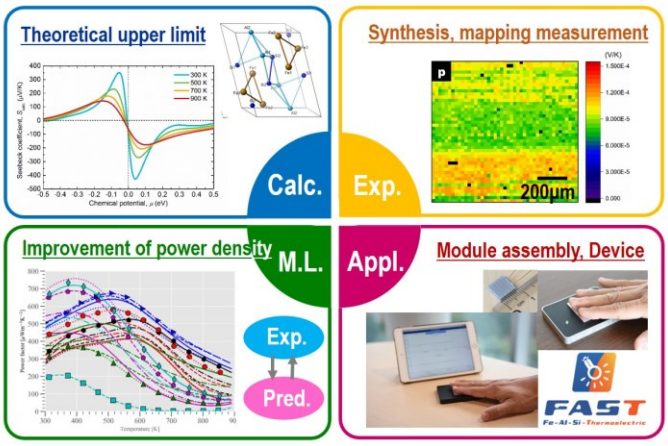

Fig. 1 Materials development, modularization technology, and power generation demonstration tests using experiment, mapping measurement, computational science, and machine learning.

In this work, we investigated the electronic structures of polycrystalline p- and n-type FAST materials by photoemission spectroscopy to obtain deeper insight into controlling the p-n characteristics to enhance the thermoelectric properties of FAST materials [7]. The core-level spectra of the p- and n-FAST materials for Al 2p, Al 2s, Si 2p, and Fe 3p are shown in Fig. 2, respectively. The solid curves are the raw spectra. For clarity, the spectra of the p-FAST material were by 0.15 eV toward the higher binding-energy side.

The photoemission spectra of the valence bands of the p- and n-FAST materials are shown in Fig. 3. Considering the photoemission cross section, these spectra strongly reflect Fe 3d orbitals. The dashed blue curve in Fig. 3 corresponds to the spectrum of the p-FAST material shifted by 0.15 eV toward higher binding energy. From Fig. 3, the energy positions of the highest intensities are almost the same. This indicates a rigid band shift owing to carrier doping by changing the Al/Si ratio.

We found that the photoemission spectra of the p- and n-FAST materials were consistent with the covalent bonding nature and semiconducting behavior. Because the core-level shifts were independent of the elements and orbitals, the observed chemical-potential change should be the dominant factor of the core-level shift of ~0.15 eV, close to the band gap of ~0.18 eV obtained from transport measurements.

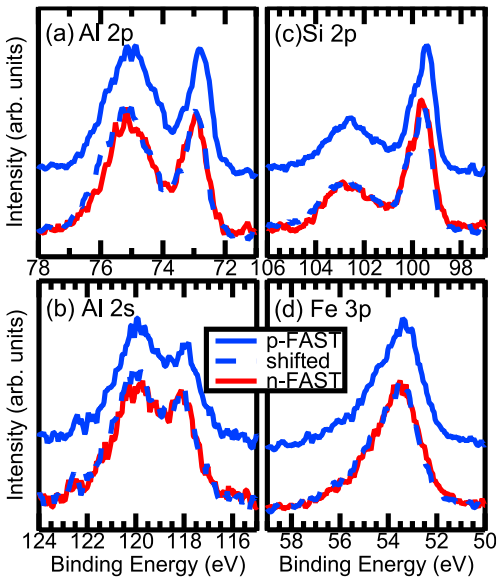

Fig. 2 Photoemission spectra of the (a) Al 2p, (b) Al 2s, (c) Si 2p, and (d) Fe 3p core levels. The blue (red) curves are the spectra of p-FAST (n-FAST) material. The solid curves are the raw spectra, and the dashed curves are the spectra shifted by 0.15 eV toward higher binding energy.

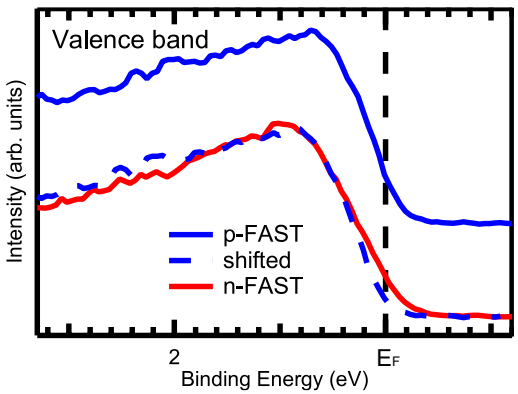

Fig. 3 Valence-band spectra of the p- and n-FAST materials. The blue and red solid curves are the spectra of the p- and n-FAST materials. The dashed blue curve is the spectrum of the p-FAST material shifted by 0.15 eV toward higher binding energy.

REFERENCES

[1] Y. Takagiwa, Y. Isoda, M. Goto, and Y. Shinohara, J. Therm. Anal. Calorim. **131**, 281 (2018).

[2] Y. Takagiwa, Y. Isoda, M. Goto, and Y. Shinohara, J. Phys. Chem. Solids **118**, 95 (2018).

[3] Y. Takagiwa and Y. Shinohara, Scripta Mater. **172**, 98 (2019).

[4] Z. Hou, Y. Takagiwa, Y. Shinohara, Y. Xu, and K. Tsuda, ACS Appl. Mater. Interfaces **11**, 11545 (2019).

[5] Y. Takagiwa, Z. Hou, K. Tsuda, T. Ikeda, and H. Kojima, ACS Appl. Mater. Interfaces **13**, 53346 (2021).

[6] Y. Takagiwa, T. Ikeda, and H. Kojima, ACS Appl. Mater. Interfaces **12**, 48804 (2020).

[7] S. Tsuda, A. Yoshinari, S. Takezawa, K. Ohishi, N. Nagamura, W. Zhang, Y. Iwasaki, and Y. Takagiwa, Mater. Res. Express **10**, 055506 (2023).

ANALYSIS OF ELECTRONIC CONFIGURATION FOR A WATER MOLECULE ENCAPSULATED INSIDE A FULLERENE

Yoshifumi Hashikawa,[1] Hisao Kiuchi,[2] Yoshihisa Harada[2]
[1]*Institute for Chemical Research, Kyoto University*
[2]*Synchrotron Radiation Laboratory, The Institute for Solid State Physics, The University of Tokyo*

Introduction. Water clusters found in hydrophobic subnanospaces such as graphitic interlayers and cavity of carbon nanotubes have been revealed to exhibit distinct properties essentially different from those in a bulk environment. For such water, the induction/expression of their functions and properties is heavily dependent on their physical and electronic structures offered by intermolecular hydrogen-bondings whilst authentic physical nature of water, i.e., a single water molecule without any hydrogen-bonding, has still remained unrevealed. To tackle this issue, in 2011, we have synthesized $H_2O@C_{60}$ where a single water molecule was isolated within a fullerene C_{60} cavity.[1] The X-ray absorption spectroscopy (XAS) and X-ray emission spectroscopy (XES) at O K-edge are powerful approaches to clarify the nature of water. In addition, resonant inelastic X-ray scattering (RIXS) measurement by an emission spectrometer with a high energy resolution could provide a potential energy surface of the molecule of target, thus revealing an effect of the environment surrounding the water molecule. Hence, these measurements are expected to be a crucial clue to probe the interaction between the water molecule and the carbon wall. Herein, we report our preliminary results on the physical nature of a single water molecule inside C_{60}.

Experimental methods. First, a powdery sample of $H_2O@C_{60}$ was moulded in a shape of a φ7 pellet by applying a hydraulic press. The measurements of O K-edge XAS, XES, and RIXS were performed at room temperature (SPring-8 BL07LSU). The XAS spectra were taken with a partial fluorescence yield mode using SDD (silicon drift detector). The XES and RIXS spectra were recorded with scanning the pellet sample for reducing a local sample damage by the irradiation with a small beam spot size of 7 μm × 50 μm.

Results and discussion. Figure 1 shows O 1*s* XAS and XES spectra of $H_2O@C_{60}$ as well as those for water reported previously.[2] In the XAS spectra, the energy shifts of molecular orbitals were observed with vanishing a Rydberg band (Figure 1b). This likely arises from a hybridization of widely distributed molecular orbitals of H_2O with those of C_{60}. Upon seeing the XES spectra, the emission band corresponding to a transition from

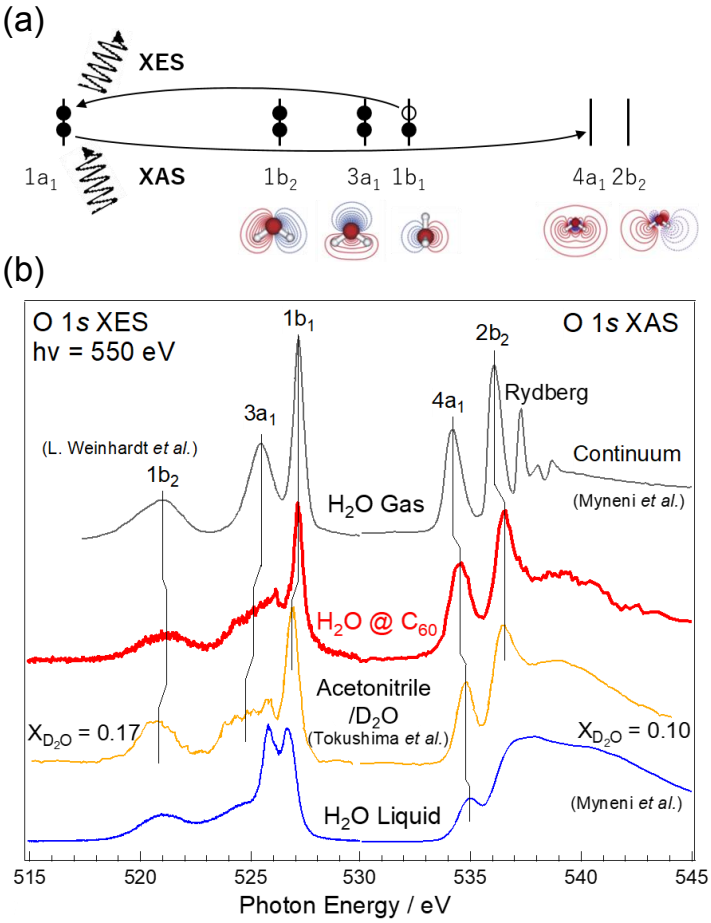

Figure 1. (a) Molecular orbital diagram of water and (b) XAS and XES spectra of $H_2O@C_{60}$ and previous reports.

$3a_1$ where the electron cloud is aligned in an axis of an electric dipole moment was found to be significantly broadened (Figure 1b). This is suggestive of the polarization shielded by the C_{60} cage. To get further insights into this phenomena, the theoretical calculations are currently ongoing.

Figure 2 illustrates RIXS spectra at the $4a_1$ and $2b_2$ resonances of $H_2O@C_{60}$ as well as gaseous water[3] reported previously, both of which showed multiple modes of vibration. Compared with gaseous water, the larger deviation of the peaks were confirmed for $H_2O@C_{60}$ at higher energy loss area. This is demonstrative of the flattening of a potential energy surface at higher energy levels. This is considered to be caused by the attractive interaction present between the single molecule of H_2O with the C_{60} wall, which might promote a water dissociation within the C_{60} cavity.

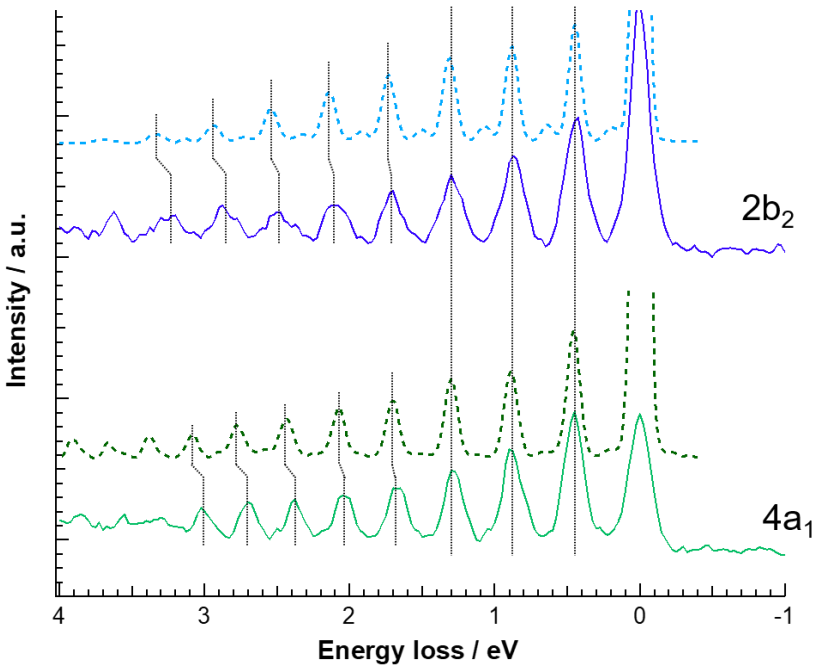

Figure 2. RIXS spectra of $H_2O@C_{60}$ (solid curve) and gaseous H_2O[3] (dashed curve).

Conclusion. We examined the electronic properties of $H_2O@C_{60}$ by XAS, XES, and RIXS measurements at SPring-8 BL07LSU. The XAS spectra showed a band shifts as well as a vanished Rydberg band, implying the presence of an orbital–orbital interaction between H_2O and C_{60}. This interaction was revealed to be attractive by RIXS measurements suggesting the flattening of a potential energy surface at higher energy levels. The additional measurements and theoretical studies are in progress for further understanding the nature of a single molecule of H_2O.

REFERENCES

[1] (a) Kurotobi, K.; Murata, Y. *Science* **2011**, *333*,613–616. (b) Hashikawa, Y.; Kizaki, K. Hirose, T.; Murata, Y. *RSC Adv*. **2020**, *10*, 40406–40410.

[2] (a) Weinhardt, L.; Benkert, A.; Meyer, F.; Blum, M.; Wilks, R. G.; Yang, W.; Bär, M.; Reinert, F.; Heske, C. *J. Chem. Phys*. **2012**, *136*, 144311. (b) Tokushima, T.; Harada, Y.; Takahashi, O.; Senba, Y.; Ohashi, H.; Pettersson, L. G. M.; Nilsson, A.; Shin, S. *Chem. Phys. Lett*. **2008**, *460*, 387–400. (c) Myneni, S.; Luo, Y.; Näslund, L. Å.; Cavalleri, M.; Ojamäe, L.; Ogasawara, H.; Pelmenschikov, A.; Wernet, P.; Väterlein, P.; Heske, C.; Hussain, Z.; Pettersson, L. G. M.; Nilsson, A. *J. Phys. Condens. Matter* **2002**, *14*, L213–L219.

[3] Cruz, V. V. d.; Ertan, E.; Couto, R. C.; Eckert, S.; Fondell, M.; Dantz, M.; Kennedy, B.; Schmitt, T.; Pietzsch, A.; Guimarães, F. F.; Ågren, H.; Gel'mukhanov, F.; Odelius, M.; Föhlisch, A.; Kimberg, V. *Phys. Chem. Chem. Phys*. **2017**, *19*, 19573–19589.

Electrolyte Dependence of the Mn 3*d* Electronic Structure of $LiMn_2O_4$ Cathode Studied by Soft X-ray Emission Spectroscopy

Daisuke Asakura[1,2], Yusuke Nanba[1], Eiji Hosono[2,3], Hideharu Niwa[4], Hisao Kiuchi[4], Jun Miyawaki[4], and Yoshihisa Harada[2,4]

[1]*Research Institute for Energy Conservation, National Institute of Advanced Industrial Science and Technology (AIST)*

[2]*AIST-UTokyo Advanced Operando-Measurement Technology Open Innovation Laboratory, AIST*

[3]*Global Zero Emission Research Center, AIST*

[4]*Synchrotron Radiation Laboratory, The Institute for Solid State Physics, The University of Tokyo*

Li-ion battery (LIB) is one of the key energy-storage devices for CO_2 reduction and realization of sustainable society. To further enhance the performances of LIBs for applications to electric vehicles and large-scale stationary energy storage systems, increasing the charge-discharge capacity of the cathode is highly desired. Electronic-structure analysis using X-ray spectroscopy has been playing an important role on the clarification of the redox mechanism of cathode materials for LIBs, which will lead to increase of the charge-discharge capacity. By clarifying the redox mechanism of typical cathode materials, it is expected to obtain strategies to design novel cathode materials.

We have been studying the electronic structure of several cathode materials using soft X-ray absorption (XAS) and emission spectroscopy (XES). For example, the Mn *L*-edge XAS and XES studies for $LiMn_2O_4$, which is a prototypical cathode material, revealed the redox reaction of $Mn^{3+} \Leftrightarrow Mn^{4+}$ at the Mn^{3+} site in the initial state. The Mn^{4+} state has very strong charge-transfer (CT) effect between the O 2*p* and Mn 3*d* orbitals, resulting in the important role of O 2*p* orbital on the redox reaction.[1,2] These studies have been investigated for the charge-discharge reaction with a conventional organic electrolyte solution, 1-mol$\cdot$ dm^{-3} $LiClO_4$/ethylene carbonate (EC)-diethyl carbonate (DEC).

On the other hand, it is well known that $LiMn_2O_4$ could exhibit charge-discharge reaction with aqueous electrolyte solutions.[3] The usage of aqueous electrolyte solutions is advantageous in terms of safety (non-flammable) and manufacturing cost, while the working voltage is reduced to around 1.0 V (in contrast to ~4.0 V for organic electrolyte solutions) because of the narrow voltage window of H_2O. To investigate the redox reaction of $Mn^{3+} \Leftrightarrow Mn^{4+}$ in the case of aqueous electrolyte solution, we performed Mn *L*-edge XES studies for $LiMn_2O_4$ with 1-mol$\cdot$ dm^{-3} $LiNO_3/H_2O$.[4]

Powdered $LiMn_2O_4$ sample was fabricated by a sol-gel method.[2,4] The *operando* XES measurements with the aqueous electrolyte solution were carried out by HORNET spectrometer at BL07LSU, SPring-8. The setup of *operando* cell and details of the electrochemical measurements for *operando* XES are described in Ref. 4. To analyze the XES spectra, we conducted configuration-interaction full-multiplet (CTM) calculations.[2,4]

Figure 1 shows a comparison of the Mn L_3-edge XES spectra between the cases of the aqueous and organic electrolyte solutions. The line shape for the initial state is identical because the powder samples were fabricated with the same method. As described in Ref. 2, the initial state has been attributed to a mixed state of Mn^{3+} and Mn^{4+}. In contrast, the line shape after the first charge-discharge cycle is considerably different between the cases of aqueous (spectrum A) and organic (spectrum B) electrolyte solutions, indicating that the redox reaction is dependent on electrolyte. For the organic electrolyte solution, spectrum B is similar to the spectrum of the initial state, while the sample after the charge-discharge has

been measured under an *ex situ* condition.[2] This result indicates that the redox reaction with the organic electrolyte solution is relatively reversible for the first cycle. For the aqueous electrolyte solution, the redox reaction for the first cycle is irreversible. However, CTM calculations revealed that spectrum A also consist of Mn^{3+} and Mn^{4+}.[4] The difference from spectrum B is mainly originated from the charge-transfer energy Δ (from O 2*p* to Mn 3*d* orbitals) for each Mn^{3+} and Mn^{4+}.[4]

The *operando* XES results after the second cycle with the aqueous electrolyte solution (not shown here) were similar to those after the first cycle,[4] indicating that the second cycle is reversible. The change from the spectrum of the initial state to spectrum A suggests formation of surface-electrolyte interface (SEI) layer characteristic of the aqueous electrolyte solution, while SEI layer is also formed for the cases of organic electrolyte solutions. Thus, after that the SEI layer is once formed on the first cycle, the reversibility of the redox reaction with the aqueous electrolyte solution should be enhanced.

As above, difference of electrolytes causes different redox reaction. The SEI layer formed by the charge-discharge should strongly affect the electronic structure of cathode materials. We will try to the Mn *L*-edge *operando* XES of $LiMn_2O_4$ with solid-state electrolyte as all-solid-state battery.[5] The $LiMn_2O_4$/solid-state electrolyte interface is expected to be completely different from the $LiMn_2O_4$/liquid electrolyte interfaces. Thus, the redox reaction with solid-state electrolytes should be verified in the future.

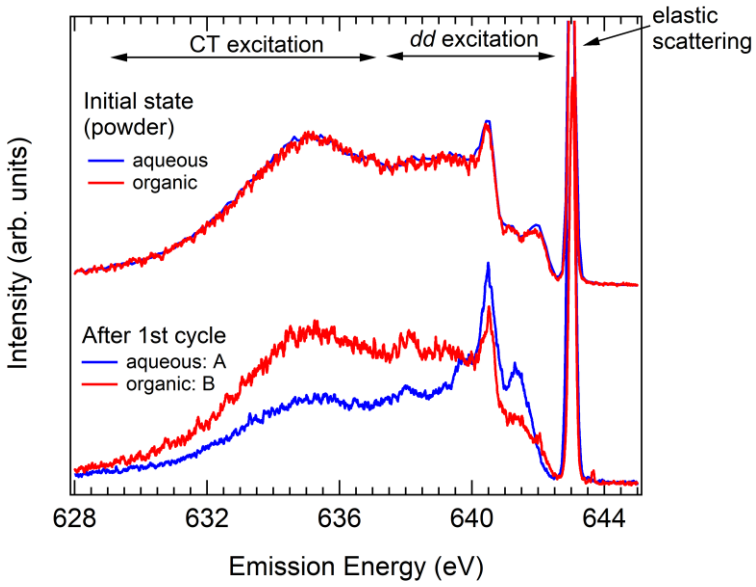

Fig. 1. Mn L_3-edge XES spectra for $LiMn_2O_4$ with the cases of aqueous and organic electrolyte solutions. The initial state corresponds to the powder sample before charge-discharge for both electrolytes. Spectra A and B after the first cycle were measured under *operando* and *ex situ* conditions, respectively.[2,4] The excitation energy was 643.0 eV.

REFERENCES

[1] D. Asakura *et al*., Electrochem. Commun. **50**, 93 (2015).
[2] D. Asakura *et al*., Phys. Chem. Chem. Phys. **21**, 18363 (2019).
[3] For example, W. Pei *et al*., J. Power Sources **63**, 275 (1996) and V. A. Nikitina *et al*., Langmuir **33**, 9378 (2017).
[4] D. Asakura *et al*., Phys. Chem. Chem. Phys. **24**, 19177 (2022).
[5] For example, H. Kitaura *et al*., J. Electrochem. Soc. **157**, A407 (2010).

SOFT X-RAY STRUCTURAL ANALYSIS OF CONSTRAINED WATER MOLECULES ON NICKEL-COMPLEX ANION SALT AGGREGATES

Tomoko Fujino
The Institute for Solid State Physics, The University of Tokyo

Introduction

Open-shell π/d-conjugated complexes have electron-rich structures and diverse electronic functionalities, including optical and magnetic properties. By combining the central metal and ligand, the electronic structure of these complexes can be precisely adjusted. When these complexes are assembled with effective intermolecular interactions such as π–π interactions, they form band structures that exhibit different electronic functionalities from those in the isolated form, including electrical and magnetic conductivities. We focused on assembling electronically charged open-shell complexes, which offer benefits such as hydrophilicity that enhance their fabrication applicability in environmentally friendly electronic devices. These charged complexes also provide structural diversification in assembled structures and functions depending on the variations of counter ions. However, these complexes are still rare even despite several decades of research because electrostatic repulsion between charged molecules severely hampers their assembly, except for charge-transfer complexes in segregated stacks between donors and acceptors. Only a few examples, such as $[M(dmit)_2]^{2-}$ (dmit = 2-thioxo-1,3-dithiol-4,5-dithiolate, M = Ni, Pd, Pt, etc) anion salts, have succeeded in exhibiting a tightly π-stacked form, resulting in properties such as unique magnetic characteristics, near-IR absorption, and superconductivity under high pressures.

We previously developed neutral metal dithiolene complexes with electron-donating substituents on their side chains [1,2]. These complexes displayed conductive properties when assembled in single crystals [1] or thin films [2] demonstrating the unique conductive properties, but not in isolated salt forms. We hypothesized that combining the hydrophilic precursors of the neutral complexes with hydrophobic counter cations that possess long-chain alkyl chains could form amphiphilic open-shell d/π conjugated complex anion salts. Such an amphiphilic structure may form macroscopic assemblies in aqua, exhibiting strong π–π interactions between complex anions. This mobile soft aggregate could demonstrate dynamic macro-sized structural changes responsive to the external environment. Therefore, we synthesized an amphiphilic salt of the d/π-conjugated complex anion with a hydrophobic counter cation possessing double dodecyl chains, which formed a macro-sized assembly where the complex anions showed considerable π–π stackings at room temperature, demonstrating rich conductive properties. The macrostructures exhibited temperature-dependent dynamical structural changes at approximately 65 °C, but the detailed mechanism in the properties remains unclear due to the lack of atomic-level structural information.

In this study, we investigated the origin of these unique electronic functionalities by Ni XAS at BL07LSU, which was developed by Prof. Harada's group. By using Ni XAS, we analyzed the electronic characteristics and temperature dependency of an aqueous solution of the complex anion salts flowing in the system. Our analysis showed that at lower temperatures than the transition temperature, the suspended solution displayed a spectrum with two peaks at the Ni L3 absorption edge, unlike the isolated forms of complex anions, where only a higher-energy peak was observed. We suspect the lower-energy peak may be a result of possible intermolecular Ni–Ni interactions. When the temperature was raised above

the transition temperature of the dynamical change, the lower-energy peak disappeared, but it reappeared when the solution was cooled again. It appears that the interactions between Ni elements disappeared when the assembled form was released. This is likely consistent with the observation of high-temperature small- and wide-angle X-ray scattering that showed macro-sized assembly was released, resulting in the loss of the formed band structures based on the intermolecular π–π stacking. The intramolecular structural details were further addressed with the wide-ranged XAS measurements covering the energy ranges for Ni L3 and L2 absorption edges. At 80 °C, charge-transfer satellite peaks appeared on L3 and L2 absorption edges, but not at low temperatures. This indicates that intramolecular charge transfer occurred from the ligand to the central metal when the assembly was released into the isolated form at high temperatures. These findings confirmed that the release of the macro-sized assembly caused changes in the loss of intermolecular Ni–Ni interactions, altering the intramolecular electronic structure.

This work was supported by Prof. Yoshihisa Harada, Dr. Hisao Kiuchi, and Dr. Naoya Kurahashi (ISSP, The Univ. of Tokyo) for their support on XAS measurements and fruitful discussions. We appreciate their kind and professional suggestions. We also thank Assoc. Prof. Mafumi Hishida (ISSP, The Univ. of Tokyo) for small- and wide-angle X-ray scattering measurements. We appreciate Prof. Hatsumi Mori and Mr. Masatoshi Ito (ISSP, The Univ. of Tokyo) for the synthesis support and considerable discussions. This work was partially supported by JSPS Grants-in-Aid for Scientific Research (JP20H05206, JP21K05018, JP22H04523), JST PRESTO (JPMJPR22Q8), a research grant from Naito Foundation, the Kao Foundation for Arts and Science.

REFERENCES

[1] Yokomori, S.; Dekura, S.*; Fujino, T.; Kawamura, M.; Ozaki, T.; Mori, H.* *J. Mater. Chem. C* **2020**, *8* (42), 14939-14947.

[2] Ito, M.; Fujino, T.*; Zhang, L.; Yokomori, S.; Higashino, T.; Makiura, R.; Takeno, K. J. Ozaki, T.; Mori, H.* *J. Am. Chem. Soc*., **2023**, *145* (4), 2127–2134.

AMBIENT PRESSURE X-RAY PHOTOELECTRON SPECTROSCOPY STUDY OF THE ELECTRONIC STATES OF THE MoS_2 BASAL PLANE DURING ANNEALING IN HYDROGEN

Fumihiko Ozaki, YoungHyun Choi, Wataru Osada, Yoshiko Sakaguchi, Shunsuke Tanaka, Kozo Mukai, Masafumi Horio, Iwao Matsuda and Jun Yoshinobu
The Institute for Solid State Physics, The University of Tokyo

Introduction

Molybdenum disulfide (MoS_2) has attracted attention in various applications such as gas sensors, field-effect transistors, and optoelectronic devices due to its unique optical properties and high carrier mobility. A formation of sulfur vacancies on the MoS_2 surface plays an important role in device performance because the electronic state is affected by sulfur vacancies [1]. In addition to these applications, MoS_2 has also been used as a catalyst for a variety of other applications, including hydrogenated desulfurization (HDS) catalysts. The sulfur vacancies serve as adsorption sites for molecules such as organosulfur compounds [2].

Many studies have been conducted to characterize the properties of sulfur vacancies. In particular, the electronic properties of MoS_2 surfaces with sulfur vacancies have been investigated by X-ray photoelectron spectroscopy (XPS) [3]. The XPS spectra of the core-levels show the chemical components associated with the sulfur vacancies. Quantitative explanations for this chemical shift are lacking, and the electronic state of sulfur vacancies is not fully understood yet.

Annealing in hydrogen is one of the methods of sulfur vacancy formation; adsorbed hydrogen atoms are reacted with and sulfur and desorbed as H_2S above 600 K, leading to the formation of sulfur vacancies [4]. In this study, ambient pressure (AP-) XPS measurements of the MoS_2 basal plane were performed to clarify the electronic state during annealing in hydrogen, and it is found that at the HDS reaction temperature of 600 K, a low-binding energy component appears in both the Mo 3d and S 2p spectra. Furthermore, the intensity ratio of the Mo 3d and S 2p spectra (S 2p/Mo 3d) decreases dramatically at 600K. This indicates the formation of sulfur vacancies on the MoS_2 basal plane.

Experimental

A natural MoS_2 single crystal was used as a sample (ALLIANCE Biosystems; about 50 mm^2, 0.5 mm thick). After mounting the sample on a metal plate, surface layers were peeled off in air using Scotch tape. Within 10 minutes after peeling, the sample was transferred to a load lock chamber and annealed in an ultra-high vacuum chamber at about 550 K for 30 minutes. AP-XPS measurements were performed in a chamber equipped with a hemispherical electron energy analyzer at SPring-8 BL07LSU. High-purity H_2 gas was introduced into the gas cell and the sample was slowly heated in H_2 from 302 K to 750 K for a total of 2.5 hours. All XPS spectra were obtained using a photon energy of 680 eV. The binding energies of the measured XPS spectra were calibrated using the Fermi level of a gold foil attached to the sample holder.

Results and discussion

Initially, 1.5 mbar of hydrogen gas was introduced into the gas cell, and then a sample temperature was increased from 302 K to 750 K. Figure 1 show the AP-XPS spectra of Mo 3d, S 2p, and valence band as a function of sample temperature, respectively. The intensity ratio of the S 2p core level to the Mo 3d core level is also shown in Figure 2. The peak energies of the Mo 3d core-level, the S 2p core-level, and the valence band uniformly shift to a lower binding energy of about 0.2 eV up to 600 K. Judging from this uniform energy shift, it can be

attributed to band bending in the MoS_2 crystal [5]. Furthermore, the S 2p/Mo 3d intensity ratio is almost constant up to 600 K, indicating that the HDS reaction does not occur.

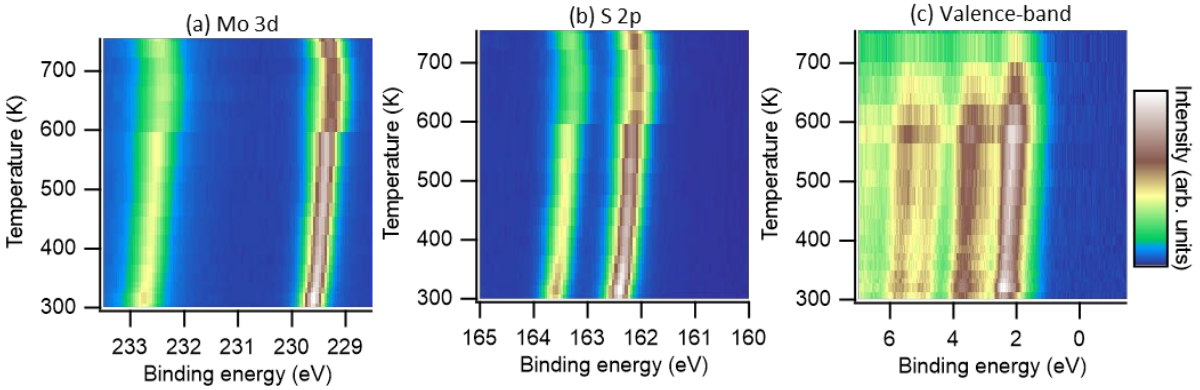

Figure 1. (a) Mo 3d, (b) S 2p, (c) Valence-band AP-XPS spectra of the MoS_2 basal plane as a function of the sample temperature in H_2 gas of ~1.5 mbar. The sample temperature increased from 302 K up to 750 K.

After 600 K heating, the peaks shift to lower binding energy and their widths become significantly broadened. This indicates the appearance of a new component in the Mo 3d and S 2p spectra. Furthermore, the S 2p/Mo 3d intensity ratio decreases markedly above 600 K, indicating that the HDS reaction takes place as indicated by the previous studies [6]. Hence, the new component observed in the Mo 3d and S 2p spectra may be related to the formation of sulfur vacancies.

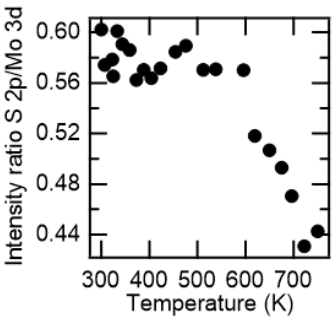

Figure 2. Plot of the S 2p/Mo 3d intensity ratio.

To clarify the spectral changes with new components, a comparison of the XPS spectra at 538 K and 619 K shows a decrease in intensity around 229.38 eV (162.21 eV) and an increase around 229.13 eV (161.88 eV) for Mo 3d (S 2p). Such a lower binding energy shift implies an increase in electron density at the Mo and S atoms. The electrons left on the MoS_2 surface by the desorption of sulfur as H_2S would be redistributed to the surrounding atoms. This interpretation has been supported by our recent first-principles calculations including the estimation of absolute binding energies based on the several defect models as well as AP-XPS data [7].

Acknowledgments

The AP-XPS measurements using synchrotron radiation were performed at SPring-8 BL07LSU as joint research between the Synchrotron Radiation Research Organization and The Institute for Solid State Physics, The University of Tokyo (Proposal No. 2022A7449, 2021B7432).

REFERENCES

[1] M. D. Siao *et al*., Nat. Commun. **9**, 1442 (2018).
[2] R. V. Mom *et al*., Nat. Commun. **10**, 2546 (2019).
[3] S. W. Han *et al*., Phys. Chem. Chem. Phys. **21**, 15302 (2019).
[4] X. S. Li *et al*., J. Catal. **137**, 385 (1992).
[5] F. Ozaki *et al*., Appl. Surf. Sci. **593**, 15 (2022).
[6] A. Bruix *et al*., ACS Nano **9**, 9322 (2015).
[7] F. Ozaki et al., submitted (2023).

BAND BENDING AT (001) AND (101) INTERFACES OF ANATASE PARTICLE REVEALED BY MICROSCOPIC X-RAY PHOTOELECTRON SPECTROSCOPY

Wenxiong Zhang[1], Mustafa Al Samarai[1], Hisao Kiuchi[1], Daobin Liu[1], Haochong Zhao[1], Fangyi Yao[2], Qi Feng[2], Yoshihisa Harada[1]

[1] *The Institute for Solid State Physics, The University of Tokyo*

[2] *Department of Advanced Materials Science, Kagawa University*

Titanium dioxide (TiO_2) has been used in many technological areas, including photocatalysis, solar cells, gas sensors, etc. Among different polymorphs (brookite, anatase, and rutile), anatase TiO_2 is considered a superior photocatalysis due to its higher electron mobility and longer carrier lifetime. It was reported that the (001) and (101) facets co-exposed anatase particles showed highly improved photocatalytic properties.[1] Theoretical calculation and experimental results on the (001) and (101) facets-exposed thin films have demonstrated that a surface heterojunction would be formed between two facets due to their difference in the Fermi levels.[2,3] As a result, photogenerated electrons and holes could accumulate on the interface of the (101) and (001) facets, therefore exhibiting different photocatalytic properties on these facets. For a deeper understanding of the charge separation mechanism of anatase TiO_2, a microscopic X-ray photoelectron spectroscopy (XPS) with spatial resolution better than 100 nm is employed to elucidate the facet-dependent electronic structure of micron-sized anatase TiO_2 particle.

Figure 1a shows the Ti 2*p* photoelectron intensity mapping image of the anatase TiO_2 particle. The particle exhibits a truncated octahedral bipyramid morphology, which is consisted of eight {101} facets on the sides and two {001} facets on the top and bottom. The geometrical relationships between the photoelectron analyzer and the incident beam spot on the sample caused the intensity difference in the mapping image.[4] Figures 1b and 1c show the pinpoint O 1*s* and Ti 2*p* XPS spectra shown in the enlarged area of the orange square (Fig. 1a) respectively. The consecutive 4 spots (~100 nm^2 each) cover the (101) and (001) facets of the anatase particle, as well as the interface between them. It is noted that the O 1*s* and Ti 2*p* XPS spectra of anatase TiO_2 continuously shift to the low binding energy from the (101) facet to the (001) facet. Figure 1d shows that the valence band maximum exhibits the same tendency as O 1*s* and Ti 2*p* XPS spectra, suggesting a smaller binding energy of the valence band maximum for the (001) facet. As a result, the interface areas for both (101) and (001) facets were calculated to be ~50 and ~80 nm respectively according to the dotted fitting spectra results (Fig. 1d). It can be concluded that a band bending (space charge layer of 130 nm) between (001) and (101) facets could be formed due to the difference of the valence band maximum between the (101) and (001) facets, hence, the photogenerated electrons and holes could accumulate on the interface, thereby exhibiting enhanced photocatalytic activities. For the strategy of morphology control to improve the photocatalysis performance of TiO_2, microspectroscopy using synchrotron soft X-ray is an important technique.

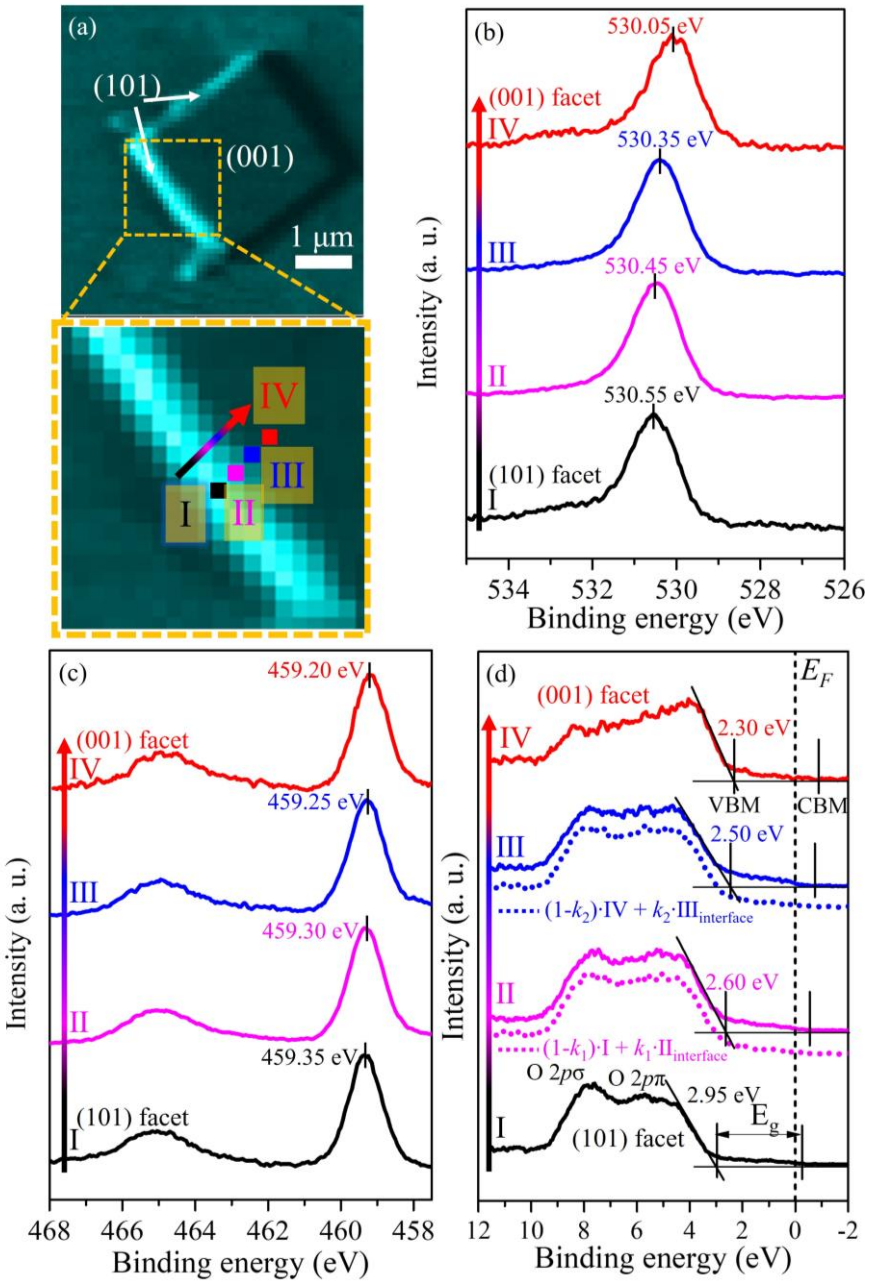

Figure 1. (a) Ti 2*p* photoelectron intensity mapping image of anatase TiO_2 particle and its enlarged area of the orange square. Pinpoint (b) O 1*s*, (c) Ti 2*p*, and (d) valence band XPS spectra of TiO_2 particle from consecutive 4 spots shown in Fig. 1a. CBM: conduction band minimum. VBM: valence band maximum. E_g: band gap energy. Norm.: normalization. *CBM is only speculation according to E_g = 3.2 eV. k_1 = 0.5 (0.5 x 100 nm = 50 nm, interface at area II). k_2 = 0.8 (0.8 x 100 nm = 80 nm, interface at area III).

REFERENCES

[1] H. G. Yang et al., *Nature*, 453 (2008) 638-642
[2] J. Yu et al., *J. Am. Chem. Soc.*, 136 (2014) 8839-8842
[3] S. Kashiwaya et al., *Adv. Energy Mater.*, 8 (2018) 1802195
[4] W. Zhang et al., *CrystEngComm.*, 25 (2023) 183-188

Influence of surface charge induced by ultrafine water on trans-epidermal water retention of stratum corneum lipids explored by O *K*-edge spectroscopy

Mustafa al Samarai[1], Wenxiong Zhang[1], Hisao Kiuchi[1], Shinsuke Inoue[2], Yuki Tabata[2], Hiroto Kato[2], and Yoshihisa Harada[1]

[1]*Synchrotron Radiation Laboratory, The Institute for Solid State Physics, The University of Tokyo*
[2]*Innovation center, Aisin Corporation.*

In recent years, nanosized water clusters called ultrafine water (UFW), which have several nanometers or less diameter, have attracted attention for their wide range of functions such as humidification, moisture retention, deodorization, air cleaning and sterilization, and static electricity removal. However, little is known about the mechanism of their functions. For example, in moisturizing, penetration into the subcutaneous tissue is considered because the UFW is smaller than the intercellular space on the skin surface. However, this alone cannot account for the long-lasting moisturizing effect [1]. Therefore, it is necessary to clarify the physicochemical properties of UFW to understand those macroscopic functions. In this study, a mixed-lipid bilayer model (artificial skin) of stratum corneum film (consisting of ceramide, cholesterol, and palmitic acid in a 1:1:1 molar ratio and approx.12.5 nm thick) was prepared on Au-coated 150 nm thick SiC membrane. We investigated the electronic structure of absorbed UFW vs. water by regular humidification at 60% relative humidity (RH) on the artificial skin using O *K*-edge XAS and XES to obtain detailed information on the hydrogen-bonded configuration of water on those surfaces, and to discuss the relationship between the chemical state and the function of UFW. XAS/XES will represent unoccupied/occupied valence electronic structures of water, which is quite sensitive to various hydrogen-bonded configurations in water [2].

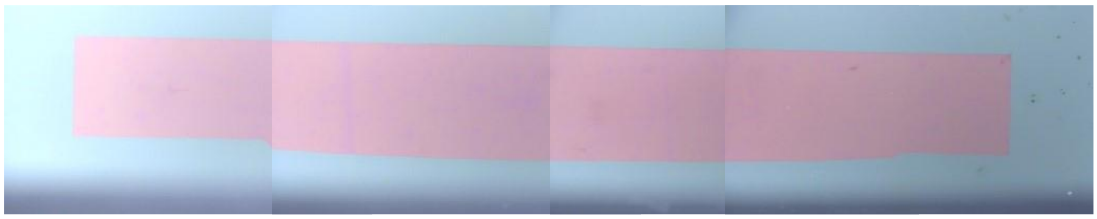

Figure 1: Photo image of the artificial skin prepared on a 150 nm thick SiC membrane (purple area); it was a key to make an uniform layer on the Au-coated membrane at 12.5 nm thickness where interference fringes were completely invisible.

The summary of the XAS/XES data for humidification by either UFW or 60%RH is shown in Fig. 2. Based on the combination of the obtained data, an obvious extraordinary increase of hydration in the artificial skin by flowing UFW was confirmed compared to regular

humidification at 60%RH. For both identical samples the O *K*-edge XAS and XES for the dry state were measured (black curves in Fig. 2) followed by the humification either by UFW vs. 60%RH. Finally, the samples were redried to investigate the nature of the trapped water within or on the artificial skin samples.

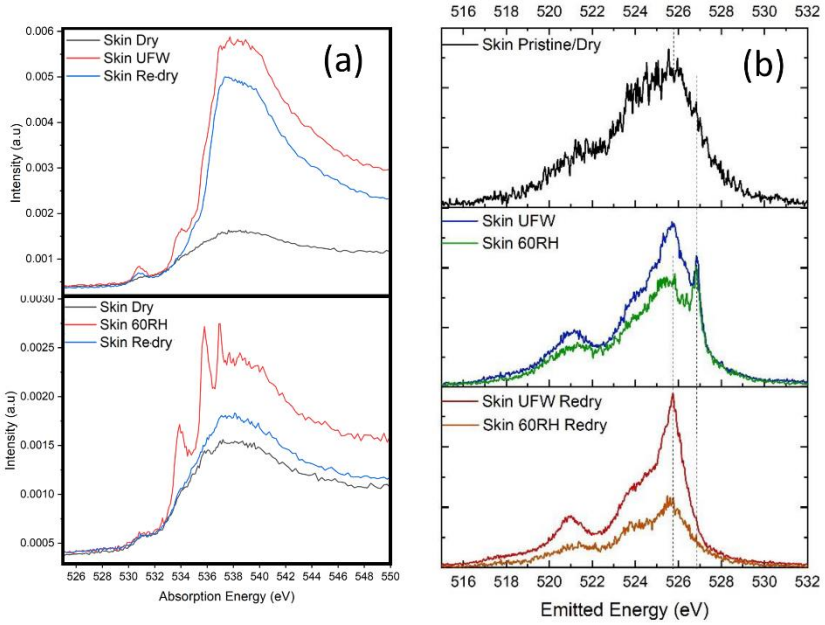

Figure 2. O K-edge (a) XAS and (b) XES for Dry artificial skin (black) under humidification by UFW vs regular humidification at 60%RH. Retention of hydration is reflected in the Redry data.

The surface to volume ratio in the smaller UFW water clusters (~ 1nm) is four orders of magnitude higher than the water mist (~ 10μm in diameter) found in the regular humidified gas flows. Therefore we expected different water absorption behavior and amount for the UFW humidification. For both the humidification pathways there are dominantly two water species, the gas phase water (at ~534 eV and ~526.9 eV in Figs. 2a and 2b) and trapped water (at ~538 eV and ~525.8 eV in Figs. 2a and 2b). Hereby, first the gas phase water is dominant especially in the 60%RH case, followed by the gradual isotropic equilibrium shift towards precipitation of additional water from the vapor to the already present water domains on the surface of artificial skin and trapped within the lipid bilayer. Interestingly we see a higher water /humidification absorption for the UFW-treated sample. Furthermore, following the redrying process a considerably higher amount of water was retained for the UFW treated sample relative to the regularly humidified (60%RH) sample.

This experimental evidence suggests that initial humidification with UFW produces water adsorption sites on the hydrophobic skin surface. In the future, by accumulating data under more specific conditions, we can identify the coordination of various water layers and the involved chemical bonds, which will help design the function of novel UFW.

REFERENCES

[1] N. Nishimura *et al*., Skin Res. Technol. **25**, 294 (2019).
[2] T. Tokushima *et al.*, Chem. Phys. Lett. **460**, 387 (2008).

2p3d Resonant Inelastic X-ray scattering Probing Ligand Field Perturbations in Fe-modified Co spinels

Minmin Chen,[1] Marcos Sepulcre,[1] Dimitrios Manganas,[2] Steven Angel,[3] Eko Budiyanto,[2] Derek Rice,[1] Harun Tüysüz,[2] Hartmut Wiggers,[3] Naoya Kurahashi,[4] Yoshihisa Harada,[4,5] Olaf Rüdiger,[1] Serena DeBeer[1]

[1] Max Planck Institute for Chemical Energy Conversion, 45470 Mülheim an der Ruhr, Germany

[2] Max-Planck-Institut für Kohlenforschung, 45470 Mülheim an der Ruhr, Germany

[3] University of Duisburg-Essen, 47057 Duisburg, Germany

[4] Institute for Solid State Physics, The University of Tokyo, Kashiwa, Chiba 277-8581, Japan

[5] Synchrotron Radiation Research Organization, The University of Tokyo, Sayo, Sayo-gun, Hyogo 679-5148, Japan

Spinels are an essential class of minerals which serve as fundamental structural models for advanced functional materials. Fe loading into spinels can significantly alter the physical-chemical properties of the parent spinel.[1] BET, XRD, APT, HRTEM, SAED, EELS, Raman spectroscopy and Mössbauer spectroscopy have been widely used to explore the role of Fe role in modulating morphology, crystal structure, oxidation state, and geometric structure. Recently, 2p3d RIXS has been used as a site-selective technique to probe the mixed-valence pure Co spinel.[2] Here we used 2p3d RIXS to directly probe the geometric and electronic environment surrounding a Co center in Fe-loaded Co-based spinels. $CoFe_2O_4$ (containing only $Co^{2+}(O_h)$), $CoAl_2O_4$ (containing only $Co^{2+}(T_d)$), and $ZnCo_2O_4$ (containing only $Co^{3+}(O_h)$) were chosen as references to study the spectral signatures of the different sites. Ligand-field multiplet calculations were used to reproduce the L-edge XAS and 2p3d RIXS of the references.[3] The calculated Tanabe-Sugano diagrams allow for the ligand field modulations of the low-lying excited states to be visualized. These electronic structure changes can then be correlated with the differences in Fe-induced electrocatalytic performance.

Figure 1 shows both L-edge XAS and 2p3d RIXS can distinguish Co^{2+} with different site symmetries (T_d vs. O_h), but 2p3d RIXS exhibits higher resolution and it is more sensitive to modulations in the ligand field splitting. Co^{2+} is excited primarily at lower incident energies (<780eV) than the Co^{3+} ions. Visually assigning characteristic inelastic features is a challenge. Herein, we utilize ligand-field-theory calculations within the ORCA code in order to reproduce experimental spectra of the references (Figure 2). In addition, the contributions from different multiplets can be deconvoluted based on the calculated spectra.

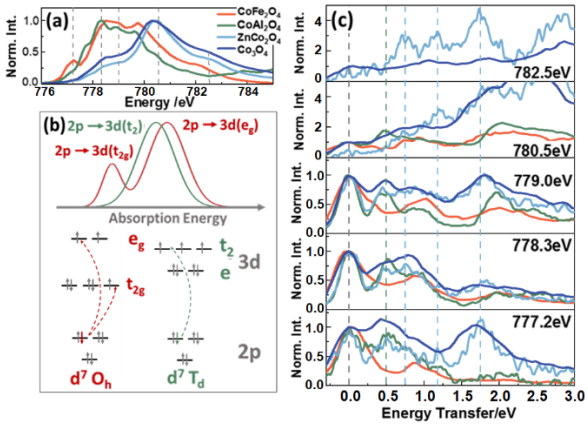

Fig. 1 Experimental cobalt (a) L_3-edge XAS and (c) 2p3d RIXS of $CoFe_2O_4$, $CoAl_2O_4$, $ZnCo_2O_4$ and Co_3O_4 at different incident energy (c) Schematic L_3-edge XAS of free ion with d^7 in O_h and T_d symmetry.

The combination of experimental and calculated spectra, shows that the transition at 0.5 eV energy transfer (at 779 eV incident energy) corresponds primarily to the $Co^{2+}(T_d)$ site. Figure 3 shows that the electronic structure of the $Co^{2+}(T_d)$ is sensitive to the amount of Fe loading. The sample with the lowest Fe loading, $Co_{2.95}Fe_{0.05}O_4$, exhibits an increase in the energy transfer, compared to the pristine Co sample, while Co_2FeO_4 with higher Fe incorporation shows a shift towards lower ET. This observation suggests a higher crystal field splitting for the sample with less Fe-loading, which interestingly correlates with a lower potential for the oxidation of the $Co^{2+}(T_d)$ site observed in cyclic voltammetry measurements. The opposite effect is observed for the Co_2FeO_4, indicating that this feature can be used to provide an electronic explanation for Fe-induced changes observed in electrocatalytic measurements, where the samples with the lowest Fe-loading showed enhanced electrocatalytic water oxidation performance.

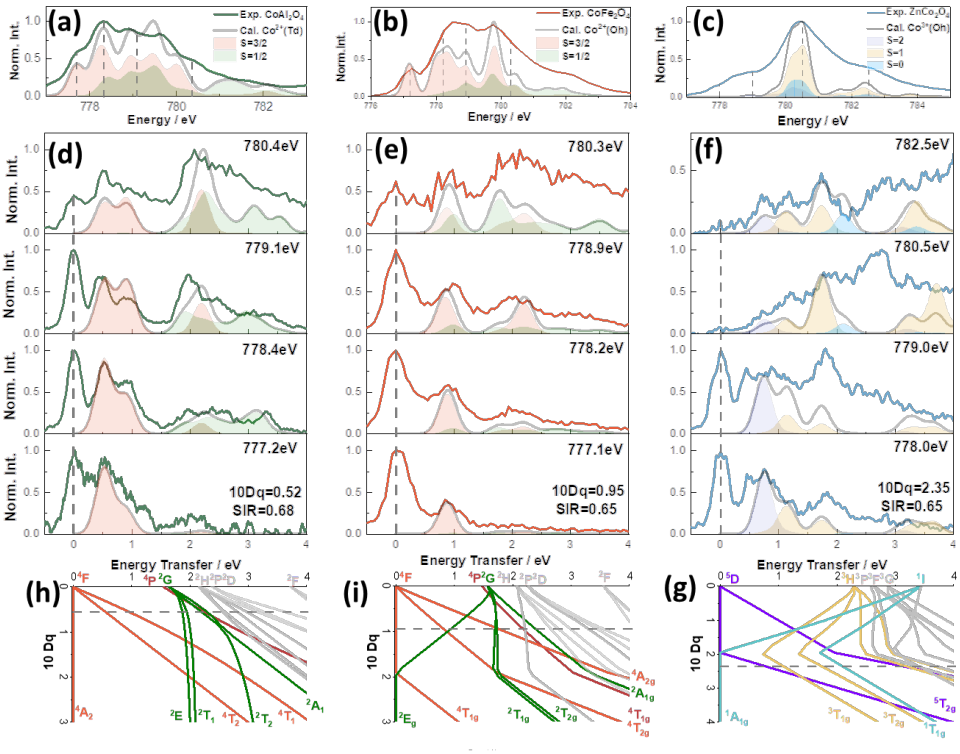

Fig.2 Experimental and ligand-field multiplet calculated L_3-edge XAS and 2p3d RIXS, as well as calculated Tanabe-Sugano diagrams of (a, d, g) $CoAl_2O_4$, (b, e, h.) $CoFe_2O_4$, and (c, f, i) $ZnCo_2O_4$.

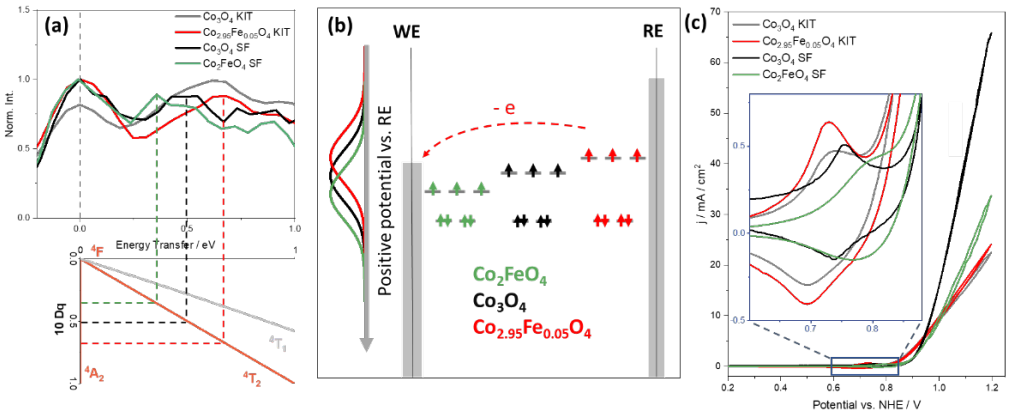

Fig. 3 (a) 2p3d RIXS show ligand field splitting of $Co^{2+}(T_d)$ affected by Fe loading. (b) Schematic diagram of relationship between 10Dq and oxidation potential. (c) Comparison of OER performance and the corresponding enlarged pre-catalytic redox couple of Co_3O_4 $Co_{2.95}Fe_{0.05}O_4$ and Co_2FeO_4.

References

[1] X. Deng, H. Tüysüz, et al, Chem. Mater., 2017, 29, 40−52.
[2] R. P. Wang, F. de Groot, J. Phys. Chem. C 2022, 126, 8752−8759.
[3] F. Neese, WIREs Computational Molecular Science 2011, 2, 73-78.

STUDY ON PHOTO-INDUCED DYNAMICS IN TOPOLOGICAL INSULATOR Bi_2Te_3 THIN FILMS

Kaishu Kawaguchi[1], Ryo Mori[1], Shinichiro Hatta[2], Yuto Fukushima[1], Hiroaki Tanaka[1], Ayumi Harasawa[1], Tetsuya Aruga[2], Takeshi Kondo[1]

[1]*ISSP, The University of Tokyo*

[2]*Graduate School of Science, Kyoto University*

INTRODUCTION

Spin-orbit interaction, where the orbital and spin components of electrons strongly intertwine, gives rise to distinctive electronic properties. Notably, due to their intimate relationship with topology, a variety of materials and functionalities in topological insulators have been actively researched in recent years. These materials, represented by Bi_2Se_3, Bi_2Te_3, and others, have the interesting feature of having unique spin-polarized conduction electrons on their surfaces, even though their bulk is completely insulating [1]. Such novel materials have expected to be a highly promising foundation for the design of new electronic devices, such as quantum computing, spintronics, and so on. Angle-Resolved Photoemission Spectroscopy (ARPES) serves as a powerful experimental method to directly observe the electronic structure of these topological insulators, allowing us to analyze the behavior of electrons. Furthermore, with the incorporation of time-resolved techniques, ARPES opens the possibility to observe the dynamics of topological insulators in ultrafast time scales [2]. Time-resolved ARPES can observe how the electronic structure of materials changes by light pulses, thereby presenting a new way to control quantum properties.

In this study, we apply these advanced methods to thin films of topological insulators. By thinning these materials, interference effects can occur between surface and interface states, and potential modulation originating from the substrate becomes feasible. This will allow us to introduce novel perturbation effects to the properties of topological insulators from substrates. We anticipate that deepening our understanding of the dynamics and light-induced transitions in topological insulator thin films from a band picture will pave new horizons in opt-spintronics.

METHODS

We carried out experiments using a thin film of the topological insulator Bi_2Te_3, fabricated on a *p*-type Si(111) substrate [3]. The research was measured by 10.7 eV pulse laser as a probe light source to the ARPES apparatus [4]. The optical energy of the pump pulse is set at 2.57 eV.

RESULTS AND DISCUSSION

Figure 1 presents the results from time-resolved ARPES measurements of Bi_2Te_3 thin films at 2 QL (quintuple layer). A photo-induced potential shift, namely surface photovoltage [5], were clearly observed. The maximum energy shift is approximately 0.3 eV, indicating a considerably large surface photovoltage in comparison with prior studies about single crystal of Bi_2Te_3 [6]. The energy shift occurs on sub-nano seconds scale (Fig. 2), suggesting that this phenomenon originates from charge transfer near the surface or interface; Bi_2Te_3 thin film is unlikely to induce sufficient charge transfer within thickness of 2 nm in this case, therefore the 0.3 eV energy shift is likely to be due to photoexcitation of band bends originating from the *p*-type Si(111) substrate as the mechanism. Based on these results, utilizing a highly doped substrate can be considered an effective method to induce a photoelectric field in thin films. In the future, the doping dependence of the substrate and the thickness dependence of the thin film will be studied to investigate the possibility of controlling the electronic state by surface photovoltages.

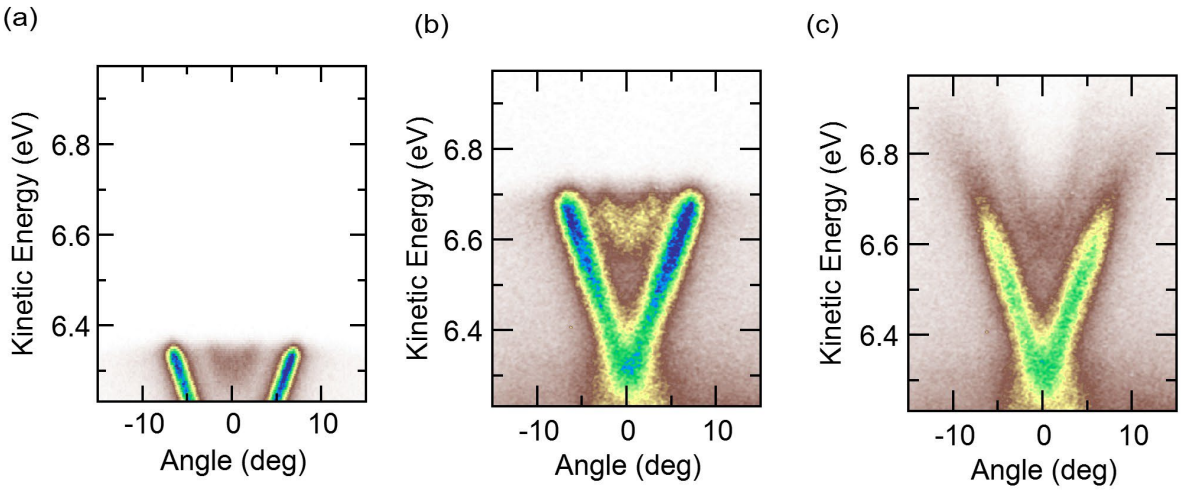

Fig. 1 : Time-resolved ARPES results of Bi_2Te_3 thin film at 2 QL thickness. (a) is the ground state without the pump pulse. (b) and (c) are the results at delay times of -1 ps (before arriving the pump pulse) and 0 ps (after arriving the pump pulse), respectively.

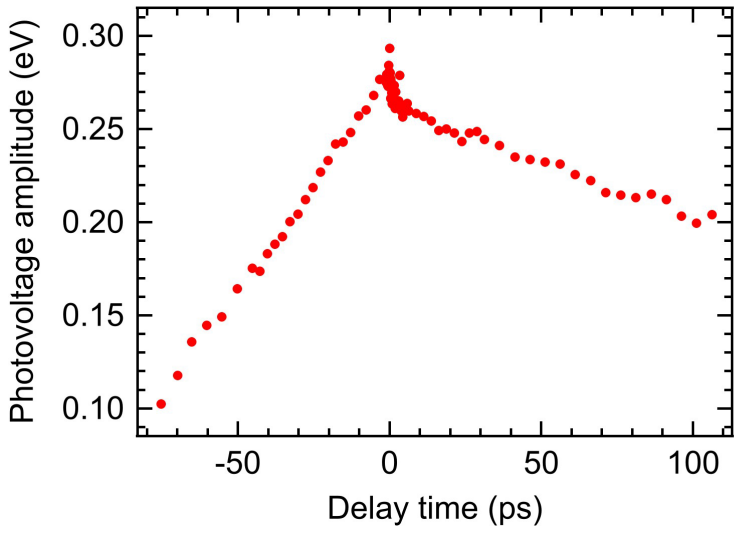

Fig. 2 : Time evolution of surface photovoltage amplitude estimated from the peak position of the band dispersion, where delay time is the time difference between the pump and probe pulse.

REFERENCES

[1] H. Zhang *et al.*, Nat. Phys. **5**, 438 (2009).
[2] J. A. Sobota *et al.*, Phys. Rev. Lett. **108**, 117403 (2012).
[3] S. Hatta *et al.*, Sci. Rep. **11**, 5742 (2021).
[4] K. Kawaguchi *et al.*, arXiv:2303.16466 (2023).
[5] D. K. Schroder, Meas. Sci. Technol. **12**, R16 (2001).
[6] S. Ciocys *et al.,* npj Quantum Materials. **5**, 1–7 (2020).

FERMI SURFACE MAPPING OF TOPOLOGICAL INSULATOR $PB(BI_{0.3}SB_{0.7})_2TE_4$

Koichiro YAJI[1], Yuya HATTORI[2], Shunsuke YOSHIZAWA[1], Shunsuke TSUDA[1], Youhei YAMAJI[3], Yuto FUKUSHIMA[4], Kaishu KAWAGUCHI[4], Takeshi KONDO[4], Yuki TOKUMOTO[5], Keiichi EDAGAWA[5], and Taichi TERASHIMA[2]

[1]*Research Center for Advanced Measurement and Characterization, NIMS*

[2]*International Center for Materials Nanoarchitectonics, NIMS*

[3]*Center for Green Research on Energy and Environmental Materials, NIMS*

[4]*Institute for Solid State Physics, The University of Tokyo*

[5] *Institute of Industrial Science, The University of Tokyo*

Topological materials are placed at a central research field in solid-state physics and materials science. Topological surface states (TSSs) are formed through a phase transition from a trivial insulator to a topological insulator, the so-called topological phase transition. The topological phase transition has been experimentally demonstrated in several systems, where the bulk band inversion is artificially controlled by changing the composition and modulating the lattice constant, etc. In contrast, experimental studies on the topological phase transition in pristine topological materials have not been established so far, even though examining it helps us understand the fundamental electronic properties of the topological materials. In the present study, we have performed the Fermi surface mapping of $Pb(Bi_{0.3}Sb_{0.7})_2Te_4$ to elucidate the electronic band structure. Here, the Pb-based ternary compounds, $Pb(Bi_{1-x}Sb_x)_2Te_4$, is known as a strong topological insulator, which have been confirmed by angle-resolved photoemission spectroscopy [1–3]. This work is part of a project to elucidate topological phase transitions in pristine materials.

Laser-ARPES measurements have been performed at the Institute for Solid State Physics, The University of Tokyo [4]. The samples were cleaved with scotch tape in an ultra-high vacuum chamber. The photoelectrons were excited by lasers with photon energies of 6.994 eV [5] and 10.7 eV [6]. We used a p-polarized light. The sample temperature was kept at 30 K during the measurements.

Figures 1(a) and (b) show the ARPES intensity map along ΓM and constant energy contours of. Figure 1(b) shows constant energy contours $Pb(Bi_{0.3}Sb_{0.7})_2Te_4$ with an excitation energy (hν) of 6.994 eV. Above the Dirac point (DP), the constant energy contours gradually change from circular to hexagonal shapes: the constant energy contour at E_B = 110 meV is circular, at E_B = 70 meV hexagonal, and at E_B = 30 meV the conduction band appears at Γ. In contrast, a strong warping effect appear in the constant energy contours below the DP. The constant energy contours at E_B = 330 meV is elongated in ΓM.

Photoexcitation with a 10.7 eV laser allows us to investigate a wider wavenumber range [Fig. 1(c)]. The photoelectron intensity distribution of the constant energy contours with hν = 10.7 eV is different from hν = 6.994 eV, resulting from the final state effect in photoemission. In the contours at EB = 190 meV, corresponding to the DP, and EB = 260 meV, a sole surface state (or surface resonance) is observed around Γ in each image, meaning that the valence band maximum (VBM) for x = 0.70 is located at Γ. At EB = 330 meV, a steeply elongated surface resonance is observed in Γ. Therefore, the energy dispersions of the surface resonances are moderate along Γ while they are steep away from ΓM.

The previous theoretical calculations suggest that the VBM for x = 0.0 is located at k = ±0.3 $Å^{-1}$ in Γ with the energy position comparable to the DP, while the VBM for $PbSb_2Te_4$ (i.e. x =

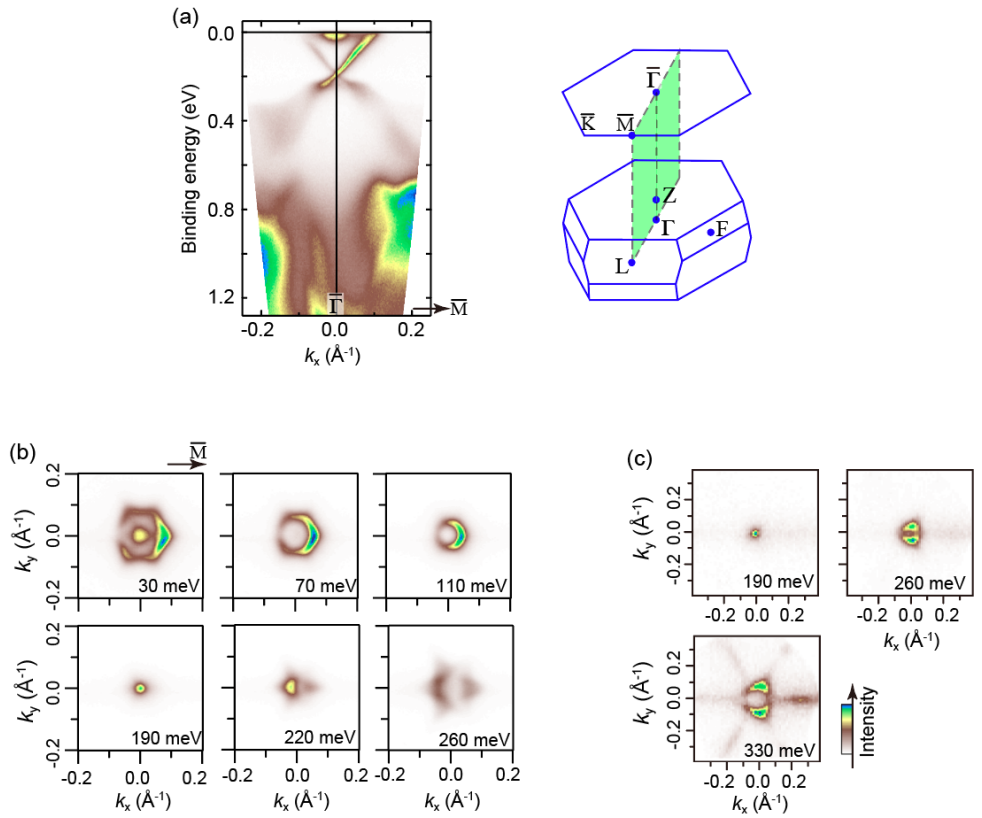

Fig. 1 (a) ARPES intensity images recorded along ΓM for $Pb(Bi_{0.3}Sb_{0.7})_2Te_4$. [7] (B,C) Constant energy contours of the ARPES intensity taken with hν = 6.994 eV [7] and 10.7 eV photons, respectively.

1.0) is located at Γ with the energy 200 meV lower than the DP [1]. In the previous ARPES study for x = 0.0, the band at k = ±0.3 Å^{-1} in Γ is located at 20 meV lower energy than the DP, which is assigned as the VBM [3]. The present study reveals that in the case of x = 0.70, the band at k = ±0.3 Å^{-1} in Γ is found in a deeper binding energy side by 100 meV than the energy of the DP. Our ARPES suggests that the band energy at k = 0.3 Å^{-1} in Γ can be tunable by the replacement of Bi with Sb.

REFERENCES

[1] T. V. Menshchikova, S. V. Eremeev, E. V. Chulkov, Applied Surface Science **267**, 1 (2013).

[2] S. Souma, K. Eto, M. Nomura, K. Nakayama, T. Sato, T. Takahashi, K. Segawa, and Y. Ando, Phys. Rev. Lett. **108**, 116801 (2012).

[3] K. Kuroda, H.Miyahara, M. Ye, S. V. Eremeev, Y.M. Koroteev, E. E. Krasovskii, E. V. Chulkov, S. Hiramoto, C. Moriyoshi, Y. Kuroiwa, K. Miyamoto, T. Okuda, M. Arita, K. Shimada, H. Namatame, M. Taniguchi, Y. Ueda, and A. Kimura, Phys. Rev. Lett. **108**, 206803 (2012).

[4] K. Yaji, A. Harasawa, K. Kuroda, S. Toyohisa, M. Nakayama, Y. Ishida, A. Fukushima, S. Watababe, C.-T. Chen, F. Komori, and S. Shin, Rev. Sci. Instrum. **87**, 053111 (2016).

[5] T. Shimojima, K. Okazaki, and S. Shin S. J. Phys. Soc. Jpn. **84**, 072001 (2015).

[6] K. Kawaguchi, K. Kuroda, Z. Zhao, S. Tani, A. Harasawa, Y. Fukushima, H. Tanaka, R. Noguchi, T. Iimori, K. Yaji, M. Fujisawa, S. Shin, F. Komori, Y. Kobayashi, and Takeshi Kondo, *submitted*.

[7] K. Yaji, Y. Hattori, S. Yoshizawa, S. Tsuda, F. Komori, Y. Yamaji, Y. Fukushima, K. Kawaguchi, T. Kondo, Y. Tokumoto, K. Edagawa, T. Terashima, *submitted*.

DIRECT OBSERVATION OF QUANTUM WELL STATES INDUCED BY THE HYDROGEN-BONDED ORGANIC FRAMEWORKS FORMED ON METAL SURFACE

Kaname Kanai[1], Rena Moue[1], Hiroto Yamazaki[1], Kaishu Kawaguchi[2], Ryo Mori[2], Yuto Fukushima[2], Ayumi Harasawa[2], Shik Shin[2], Takeshi Kondo[2]

Faculty of Science and Technology Tokyo University of Science[1], The Institute for Solid State Physics, The University of Tokyo[2]

The capability to control the electronic properties of the material surface is essential for the development and optimization of applications involving interfacial electron transfer, such as optoelectronic devices and photovoltaic devices. Therefore, noble metal (111) surfaces are of particular interest due to their unique susceptibility to the presence of adsorbates due to their electronic structure. In fact, the two-dimensional free electron-like Shockley state (SS) localized at the Γ point of the noble metal (111) surfaces is easily modulated by periodic potentials formed by regularly adsorbed atoms and molecules[1-3]. This change in SS at the noble metal surface can be revealed by observing the change in its energy band dispersion. For example, it is known to appear as a change in Rashba effect. The effect is an effect in which spin-orbit interactions due to spatial inversion symmetry breaking at the noble metal surface causes spin splitting in the SS. The magnitude of the effect is highly dependent on its surface states. It is also known that the formation of a molecular layer with corrals on the noble metal can form quantum confinement by confining SS, that is, the surface free electrons, in the corrals. Recently, in order to investigate the latter, the focus has been on observing the effects of self-organized ordered layers with large corrals on the surface electronic structure[3, 4]. This is potentially problematic because the properties of the electronic states are inherently sensitive to defects in the self-assembled molecular layer. Another approach to compensate for the imperfections in self-assembly is to use a ring of molecules such that each individual molecule acts as a corral to confine electrons. This allows each molecule to form nearly identical confinement potential, forming a long-range defect-free quantum confined surface states (QCSS)[5].

In this study, we investigated the effect of a self-assembled film of [8]cycloparaphenylene ([8]CPP) (figure 1a), which has a ring-shaped molecular structure, on the SS of Au(111). The adsorption structure of [8]CPP was determined by low-energy electron diffraction (LEED) and the energy band dispersion was directly observed by angle-resolved photoemission spectroscopy (ARPES).

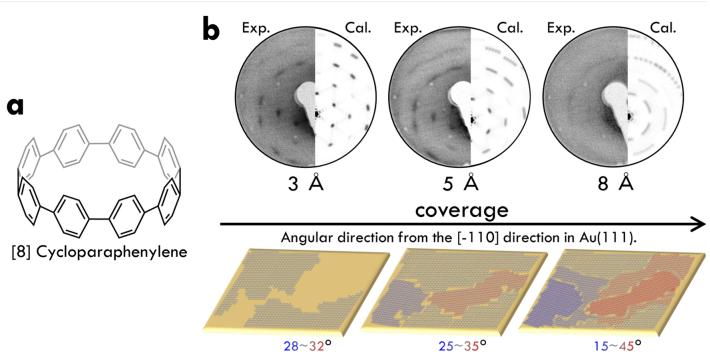

Figure 1. a) Molecular structures of [8]CPP. b) Experimental and simulated LEED results for [8]CPP/Au(111) and schematic of the [8]CPP growth process on Au(111).The right half of the circle shows the LEED pattern observed at the primary energy of E_p=25 eV (exp.). The left half of the circle shows the LEED pattern simulated by calculation (cal.). The bottom row of b) shows a schematic of the growth process of the [8]CPP monolayer on Au(111) obtained from the LEED results shown in the top row. When [8]CPP coverage is 3, 5, and 8 Å, the adsorption structure is formed along the angular direction of 28~32°, 25~35° and 15~45°) from the [-110] direction in Au(111).

Figure 1b shows the experimental (exp.) and calculation (cal.) results of LEED with stepwise increasing coverage of [8]CPP monolayers on Au(111). Furthermore, the adsorption structures of [8]CPP with different coverage were determined from the LEED results. From left to right, the results correspond to about 3, 5, and

8 Å coverage of [8]CPP, respectively, and it was confirmed that [8]CPP forms an adsorption structure as if flatly adsorbed on the Au(111) surface, a result similar to previous studies[5]. In addition, we confirmed that the growth direction of the adsorption structure diffused as the coverage increased. In short, this study revealed for the first time that the adsorbed structures gradually become multi-domain as the coverage increases.

The changes in SS observed by ARPES in accordance with the changes in the adsorption structure of the revealed [8]CPP are shown in figure 2. Figures 2a, c, e, and g are band mappings by ARPES, and figures 2b, d, f, and h are second-order derivative (SOD) results to clarify the features. Figures 2a and b show the SS of Au(111), where the spin splitting (Rashba splitting) due to the Rashba effect is clearly visible. In [8]CPP(3 Å)/Au(111), where few multi-domains are observed, the bottom of the energy band dispersion representing the SS is flattened (figures 2c, d). In [8]CPP (5 Å)/Au(111), where the multi-domains were clearly observed, the flattened energy band dispersion (flat band) was obscured, but the Rashba splitting was again confirmed with a shift of about 0.1 eV to the low binding side (figures 2e, f). In addition, the Brillouin zone was modulated by the super-periodic structure formed by [8]CPP, and a new energy band dispersion was also observed due to the folding of the Au(111) *sp* band. In [8]CPP(8 Å)/Au(111), where multi-domains dominate, the flat band disappear and the energy band dispersion indicative of Rashba splitting and folding are obscured (figures 2g, h). The analysis revealed that the magnitude of Rashba splitting is about 18% when [8]CPP was adsorbed at about 5 Å. The flat band observed at 3 and 5 Å adsorption suggest quantum confinement caused by the confinement of surface electrons in the corral. However, the flat band are weakly dispersive because the confinement by organic molecules is incomplete and the electrons trapped in the corrals interact with each other to form a dispersion.

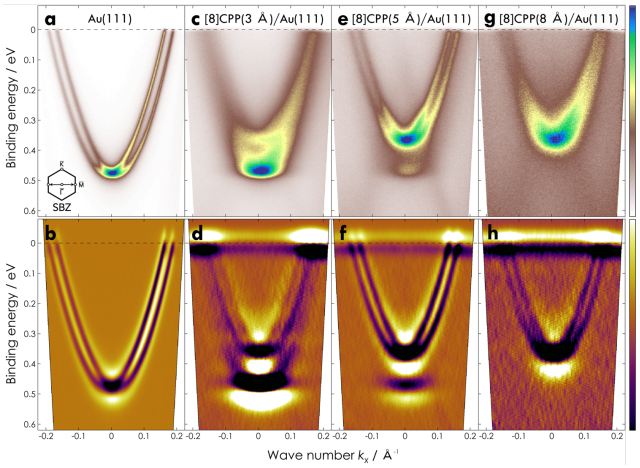

Figure 2. Band mapping around the Γ point of a) clean Au(111) by AEPES. The lower left corner of the figure shows the measured orientation in the *k*-space in the schematic of the surface Brillouin zone (SBZ). b) SOD of the band mapping by ARPES of clean Au(111) versus energy. The black areas on the SOD represent the electronic states. Band mapping around the Γ point of c) [8]CPP(3 Å)/Au(111), b) [8]CPP(5 Å)/Au(111) and b) [8]CPP(8 Å)/Au(111) by ARPES. Band mapping based on the SODs of the corresponding ARPES results, d), f), h).

In this study, we observed the formation of [8]CPP on Au(111). As a result, we revealed for the first time the formation of multi-domains with increasing coverage. In addition, the surface electronic states in each were observed by ARPES, which affected the Rashba effect on the Au(111) surface and suggested the formation of quantum confinement.

REFERENCES

[1] C. R. Ast *et al., Phys. Rev. Lett.,* **98**, 186807 (2007).
[2] J. Zroff *et al., Surface Scienece,* **603**, 354-358 (2009).
[3] I. Piquero-Zulaica *et al., Nat. Commun.,* **8**, 787 (2017).
[4] J. Zhang *et al., Chem. Commun.*, **50**, 12289-12292 (2014).
[5] B. N. Taber *et al., J. Phys. Chem. Lett.* **7**, 3073-3077 (2016).

SPIN- AND ANGLE-RESOLVED PHOTOEMISSION STUDY OF MAX PHASE COMPOUND ZR_3SNC_2

Takahiro Ito[1,2], Manaya Mita[2], Kiyohisa Tanaka[3], Masashi Nakatake[4], Yuto Fukushima[5], Kaishu Kawaguchi[5], Takeshi Kondo[5], Laurent Jouffret[6], Hanna Pazniak[7], Serge Quessada[7] and Thierry Ouisse[7]

[1]*Synchrotron radiation Research center (NUSR), Nagoya University, Nagoya 464-8603, Japan*

[2]*Graduate School of Engineering, Nagoya University, Furo-cho, Chikusa, Nagoya 464-8603, Japan*

[3]*Institute for Molecular Science, Okazaki 444-8585, Japan*

[4]*Aichi Synchrotron Radiation Center, Seto, 489-0965, Japan*

[5]*Institute for Solid State Physics, Th University of Tokyo, Kashiwa 277-8581, Japan*

[6]*Université Clermont Auvergne, CNRS, ICCF, F-63000 Clermont–Ferrand, France*

[7]*Univ. Grenoble Alpes, CNRS, Grenoble INP, LMGP, F-38000 Grenoble, France*

MAX phases ($M_{n+1}AX_n$, where M is an early transition metal, A belongs to groups 13-15 and X is either C or N, n = 1 - 3) have recently attracted much attention due to their possible application to the production of a new class of two-dimensional (2D) systems called MXenes [1]. However, the bulk electronic structure of MAX phases has been studied mostly through *ab initio*, DFT calculations, mainly due to a lack of single crystalline samples. We have performed angle-resolved photoemission spectroscopy (ARPES) on several MAX phase single crystals to directly investigate the electronic structure of these systems [2-5]. Among the MAX phases, Zr_3SnC_2 is characterized by relatively higher two-dimensionality than 211 phase due to the thicker MX layer. In addition, the strong spin-orbit coupling effect due to the 4d transition metal Zr is expected. We have performed SARPES study on Zr_3SnC_2 to eucidate the electronic and spin structures with using He I light source, which is available for the spin mapping at the wide momentum space.

Figures 1(a(b)) and (c) show the band structure (which compared with DFT calculation along ΓM line of the Sn-terminated surface) and the constant energy ARPES image at 3.1

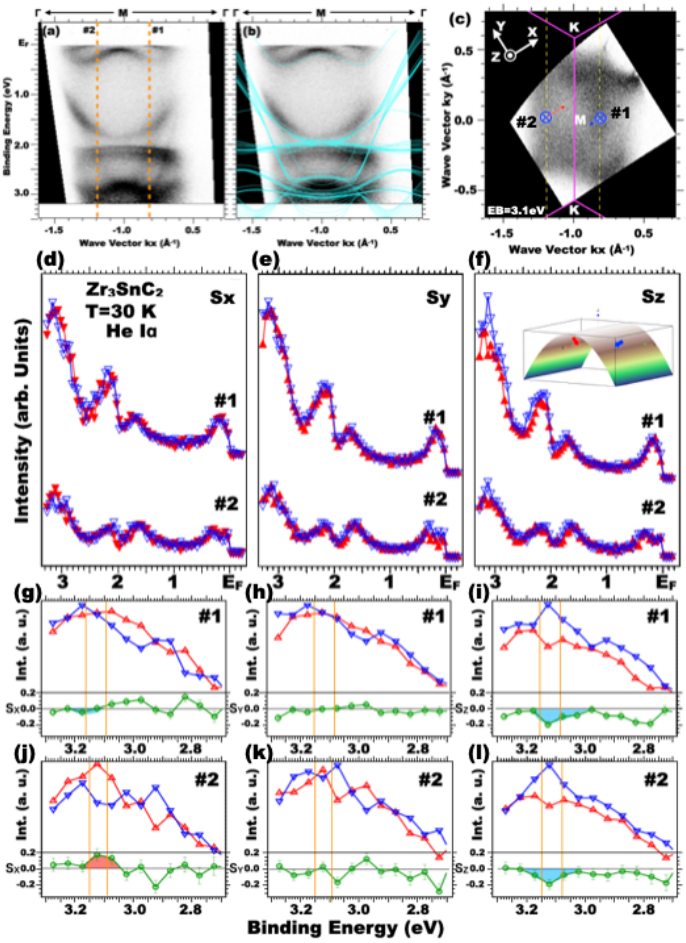

Fig. 1: (a) Band structure along the ΓM line of Zr_3SnC_2. (b) Same as (a) but compared with DFT calculation (light blue lines) of the Sn-terminated surface. (c) Constant energy ARPES image at 3.1 eV around the M point. The definition of the spin polarization directions (S_x, S_y and S_z) projected on the sample surface are indicated by white arrows, respectively. (d-f) SARPES spectra (S+:▲; S−:▽) at momentum cut#1 and #2 in Figs. 1(a) and (c) of Sx (a), Sy (b) and Sz (c), respectively. (g-l) Enlarged SARPES spectra around 3.1 eV. Spin-polarization is shown at the bottom of each panel.

eV, respectively. From the comparison with DFT calculation, it has been found that the electronic structure of Zr_3SnC_2 around the M point has been well reproduced by the Sn-terminated surface states, typically saddle-like dispersive feature just below the Fermi level.

While there is no clear sign of spin-polarization at the low binding energy side, we found that non-negligible spin-polarization seems to be observed around 3.1 eV. In Fig. 1(i) and (l), out-of-plane spin polarization (Sz) shows sizable Sz- sign at both cut#1 and #2. On the other hand, in-plane spin polarization Sx shows Sx+ sign at cut#2 (Fig. 1(j)). Furthermore, there is no clear sign of in-plane spin polarization along y (Fig. 1(h) and (k)). From the observed spin textures, we expect the possible existence of out-of-plane spin polarization at "bridge-like" band dispersion around 3.1 eV as shown in the inset of Fig. 1(f), though the symmetrically required antiparallel Sx- component has not been clearly observed. These results might suggest the effect of Dresselhaus spin-orbit coupling causing the out-of-plane spin texture [6] at the Sn-terminated surface of Zr_3SnC_2. To clarify the mechanisms of the formation of the observed spin-states and prove their existence, further ARPES study choosing surface termination as well as DFT calculation of spin-texture will be performed in our future work.

REFERENCES

[1] M. Barsoum, MAX phases (Wiley, Weinheim 2013).
[2] T. Ito *et al.*, Phys. Rev. B **96**, 195168 (2017).
[3] D. Pinek *et al.*, Phys. Rev. B **98**, 035120 (2018).
[4] D. Pinek *et al.,* Phys. Rev. B **102**, 075111 (2020).
[5] D. Pinek *et al.,* Phys. Rev. B **104**, 195118 (2021).
[6] L. L. Tao *et al*., Nature Commun. **9**, 2767 (2018).

HIGH-RESOLUTION TEMPERATURE DEPENDENT SPIN-RESOLVED PHOTOEMISSION SPECTROSCOPY OF HALF-METALLIC FERROMAGNET $La_{1-x}Sr_xMnO_3$

Takayoshi YOKOYA[1], Noriyuki KATAOKA[1], Takanori WAKITA[1], Hirokazu FUJIWARA[2], Yuto FUKUSHIMA[2], Kaishu KAWAGUCHI[2], Hiroaki TANAKA, Ryo MORI[2], Ayumi HARASAWA[2], Takeshi KONDO[2], Hiroshi KUMIGASHIRA[2], Yuji MURAOKA[3]

[1]*Research Institute for Interdisciplinary Science, Okayama University*

[2]*Institute for Solid State Physics, The University of Tokyo*

[3]*Institute of Multidisciplinary Research for Advanced Materials, Tohoku University*

Half metallic ferromagnets have a unique spin dependent electronic structure near the Fermi level (E_F), where only one of the spin states crosses E_F and the other has an energy gap across E_F [1]. The unique electronic structure gives rise to many-body effects different from other systems. Theoretically, the electronic states induced by many-body effects in half metals has been proposed as non quasiparticle (NQP) states [2]. The experimental verification for NQP states was made recently for a half metallic ferromagnet CrO_2 by using high-resolution (HR) spin-resolved photoemission spectroscopy (SRPES) [3]. In the present research, we have performed HRSRPES of another half metallic ferromagnet $La_{1-x}Sr_xMnO_3$ to experimentally explore the characteristics and universality of NQP states. $La_{1-x}Sr_xMnO_3$ is one of the famous perovskite materials, exhibiting colossal magnet resistance around Sr concentration x of 0.3.

Homoepitaxial films of $La_{1-x}Sr_xMnO_3$ were grown on the atomically-flat (001) surface of Nb-doped $SrTiO_3$ substrates using a laser MBE method. Laser-based HRSRPES experiments were performed at the Institute for Solid State Physics, The University of Tokyo [4]. The *p*-polarized light with $h\nu$ = 6.994 eV was used to excite the photoelectrons. Photoelectrons were analyzed with a combination of a ScientaOmicron DA30L analyzer and a very-low-energy-electron-diffraction (VLEED) type spin detector. During the measurement, the instrumental energy resolution was set to 30 meV to compensate small electron counts and the base pressure was kept below 1×10^{-8} Pa. Calibration of the Fermi edge (E_F) for the samples was achieved using a gold reference. The data were taken at T = 20, 50, 90, 110, 135, 195 and 300 K. The sample was annealed at 400 K under oxygen atmosphere prior to the experiment. We magnetized the $La_{1-x}Sr_xMnO_3$(001) sample along the magnetic easy axis ([110] direction) by bringing the sample close to a magnet. The approximate magnitude of the magnetic field at the sample position was 700 Oe.

Figure 1 shows the temperature dependent HRSRPES data. At 20 K, the spectrum of the majority spin states shows a Fermi edge, while that of the minority spin states shows negligible intensity near E_F. Accordingly, the polarization is nearly 100% near E_F, providing spectroscopic evidence for half metallicity of the sample at 20 K. In increasing temperature, the spectra of the majority and minority spin states, as well as the polarization, do not show drastic changes till

195 K. At 300 K, the spectral shapes of the majority and minority spin states become similar and the polarization reduces substantially. These results are consistent with the previous study [5]. However, we found that the temperature dependent polarization is different from the previous study. In the present study, temperature dependent polarization keeps similar values till 195K ($T/T_C \sim 0.56$, where T_C is a Curie temperature.), while that reduces at a much low temperature in the previous study. We attribute the difference to the difference in the bulk sensitivity of the present study. The steep reduction of polarization at E_F, which is expected from the growth of NQP, was not observed clearly within the experimental accuracy.

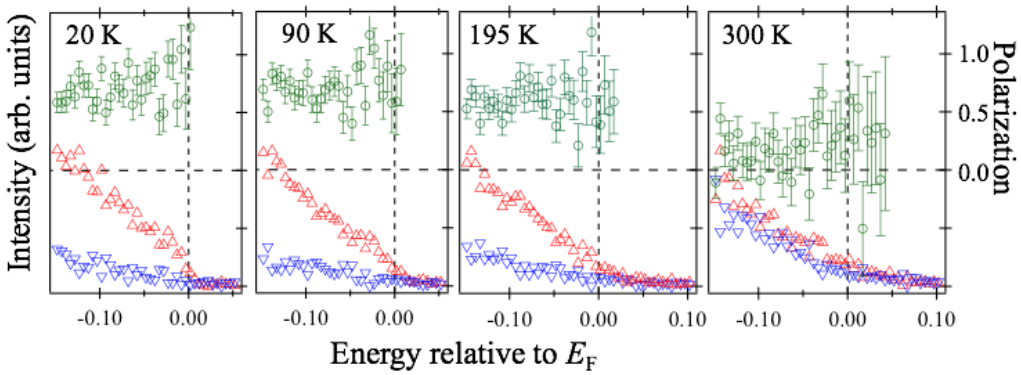

Fig. 1. Temperature dependent HRSRPES spectra and polarizations of $La_{1-x}Sr_xMnO_3$. The red triangles, bule triangles, and green circles show the majority spin spectrum, the minority spin spectrum, and polarization, respectively.

ACKNOWLEDGEMENT

This work was partially supported by JSPS KAKENHI Grand Numbers (JP20H0185313) from MEXT.

REFERENCES

[1] M.I. Katsnelson *et al.*, Rev. Mod. Phys. **80**, 315-378 (2008).
[2] V.Y. Irkhin and M.I. Katsnelson, Usp. Fiz. Nauk **164**, 705 (1994).
[3] H. Fujiwara *et al.*, Phys. Rev. Lett. **121**, 257201 (2018).
[4] K. Yaji *et al.*, Rev. Sci. Instrum. **87**, 053111 (2016).
[5] J.-H. Park *et al.*, Nature **392**, 794-796 (1998).

LIGHT POLARIZATION DEPENDENCE OF LOW-ENERGY ANGLE-RESOLVED PHOTOEMISSION SPECTROSCOPY OF A TRANSITION METAL DICHALCOGENIDE

Hiroaki Tanaka
The Institute for Solid State Physics, The University of Tokyo

Angle-resolved photoemission spectroscopy (ARPES) has been utilized to observe the band dispersion of crystals experimentally [1]. In ARPES measurements, X-ray or vacuum ultraviolet (VUV) light is irradiated on the crystal surface, and emitted photoelectrons are analyzed. The energy and momentum conservation laws determine the relationship between the Bloch wavevector and the binding energy, in other words, the band dispersion of solids.

As well as the band dispersion determined by ARPES, the photoemission intensity gives deeper insight into the electronic structure of solids because it is determined by the matrix element between the initial states (wave functions of the ground state) and the final states (approximated to plane waves). For example, the light polarization dependence of ARPES spectra has revealed orbital contributions of valence bands in the iron-based superconductor FeSe [2, 3]. Our study aims to quantitatively discuss the photoemission intensity distribution by combining the high-resolution ARPES and the photoemission intensity calculations based on the first-principles calculations.

We used the laser-based ARPES setup constructed at the Institute for Solid State Physics, the Univ. of Tokyo [4]. The photon energy was 7 eV, and the light polarization varied from $\theta = 0°$ (*s*-polarization) to $\theta = 180°$, where $\theta = 90°$ is the *p*-polarization. The measurement temperature was around 60 K, and the energy resolution was 13 meV.

We measured the photoemission spectra of the transition metal dichalcogenide 1*T*-TiS_2 [Fig. 1(a)]. TiS_2 is a simple one-layered material, so we don't need to consider the termination surface dependence. No structure transition, such as the charge density wave phase, has been reported. Therefore, TiS_2 is suitable for quantitatively analyzing the photoemission intensity by experiments and numerical simulations. The band dispersion of 1*T*-TiS_2 has two hole bands near the Γ point [Fig. 1(b)]. Since these bands have only weak k_z dispersion, as described by slightly thick slab band dispersion, we can expect that they can be observed whatever photon energy is used.

Figures 1(c) and 1(d) summarize our ARPES measurements. When we used *s*-polarized light, the heavy hole band [blue curves in Fig. 1(c)] strongly contributed to the photoemission intensity. On the other hand, when *p*-polarized light was used, the light hole band [red curves in Fig. 1(d)] was dominant. This difference reflects the orbital selectivity of the photoemission process and its dependence on incident light polarization.

We investigated the light polarization dependence by changing the angle θ with a 10° step. Since the λ/2 waveplate installed in the laser-ARPES setup can be mechanically controlled, we could measure the polarization dependence automatically using a Python program. Figure 1(d) shows the result. As discussed above, the peak position in the *p*-polarized light measurements is about 50 meV lower than in the *s*-polarized case. More important is that the polarization dependence of the peak position exhibits a smooth curve. When we consider the bulk band dispersion comprising heavy and light hole bands, one of two peaks or both peaks should appear. However, we observed that the spectrum peak could appear between two hole bands, even though the VUV-ARPES using 7 eV laser is considered relatively bulk sensitive due to the long inelastic mean free path [5]. This result clearly shows that the surface electronic structure should be considered to discuss the polarization dependence of ARPES spectra.

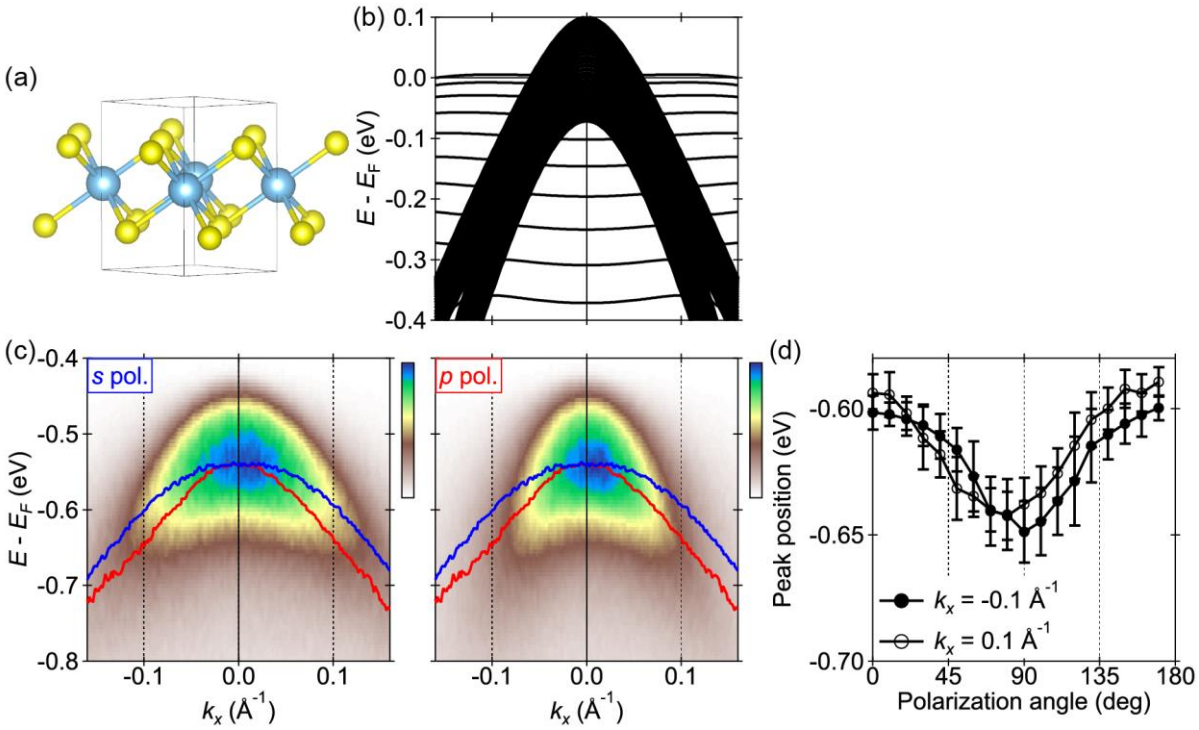

Figure 1: ARPES measurements of 1*T*-TiS_2. (a) Crystal structure. (b) Calculated slab band dispersion along the ΓK (k_x) direction. (c) Experimental band dispersion taken by *s*- and *p*-polarized light. The blue and red curves represent peak positions extracted from energy distribution curves in *s*- and *p*-polarization measurements. (d) Light polarization dependence of the peak position at k_x = -0.1 Å^{-1} and 0.1 Å^{-1}.

In summary, we investigated the polarization dependence of ARPES spectra using the transition metal dichalcogenide 1*T*-TiS_2 and a high-resolution VUV-ARPES machine equipped with a 7 eV laser. We observed that the peak position of the hole bands oscillated by changing the light polarization. Such a continuous change cannot be explained by the bulk band dispersion of 1*T*-TiS_2, so we will need to employ a slab system and detailed photoemission intensity calculations to reproduce the results theoretically.

REFERENCES

[1] J. A. Sobota *et al.*, Rev. Mod. Phys. **93**, 025006 (2021).
[2] M. Ti *et al.*, Phys. Rev. X **9**, 041049 (2019).
[3] R. P. Day *et al.*, npj Quantum Materials **4**, 54 (2019).
[4] K. Yaji *et al.*, Rev. Sci. Instrum. **87**, 053111 (2016).
[5] M. P. Seah and W. A. Dench, Surf. Interf. Anal. **1**, 2 (1979).

SURFACE STATE SPIN POLARIZATION MEASUREMENT OF Co DOPED LaFeAsO

Soonsang Huh[1], Yuto Fukushima[1], Kaishu Kawaguchi[1], Ayumi Harasawa[1], Felix Anger[2], Wurmehl Sabine[2], Bernd Büchner[2, 3], and Takeshi Kondo[1]

1. The Institute for Solid State Physics (ISSP), The University of Tokyo, Kashiwa, Chiba 277-8581, Japan

2. Leibniz Institute for Solid State and Materials Research, IFW-Dresden, 01069, Dresden, Germany

3. Institute of Solid State Physics, TU Dresden, 01069, Dresden, Germany

The discovery of the superconductivity in F-doped LaFeAsO has opened new era for iron-based superconductors and brought renew interest in high T_C superconductivity research [1]. Extensive and intensive studies have shown that the Oxypnictide system, so called 1111 crystal structure system, exhibits relatively high Tc than other systems. Up to now, $SmFeAsO_{1-x}$ (T_C ~ 55 K) has been observed with the highest Tc in bulk single crystal at ambient pressure among iron-based superconductors [2]. For this reason, understanding the mechanism that why high Tc favor in this crystal structure become one of the main issues in the research field.

In this regard, several angle-resolved photoemission spectroscopy (ARPES) experiments were conducted to understand the electronic structure, which is believed to provide important clues to the high T_C mechanism. However, the 1111 system shows a polarized cleaved surface arising from both Lanthanide Oxides layer and Iron Pnictogen layer, resulting in a complex electronic structure. For example, [LaO]+ layer and [FeAs]- layer exists in LaFeAsO. This leads to coexistence of surface and bulk electronic state. Although there are several studies reporting surface and bulk state [3, 4], still it is not clearly defined.

In this study, ARPES measurement were performed on 6% Co-doped LaFeAsO single crystal which is synthesized by solid state crystal growth technique [5]. Figures 1 (a) and (b) show Fermi surface taken at 10 K with photon energy of 40 eV and 7 eV, respectively. Fermi surface area of 7 eV data corresponds to red dashed box in Fig. 1 (a). Two large circular pockets are observed in both data. High symmetry cut along Γ – M direction is shown in Fig. 1 (c). Two electron band like dispersion is

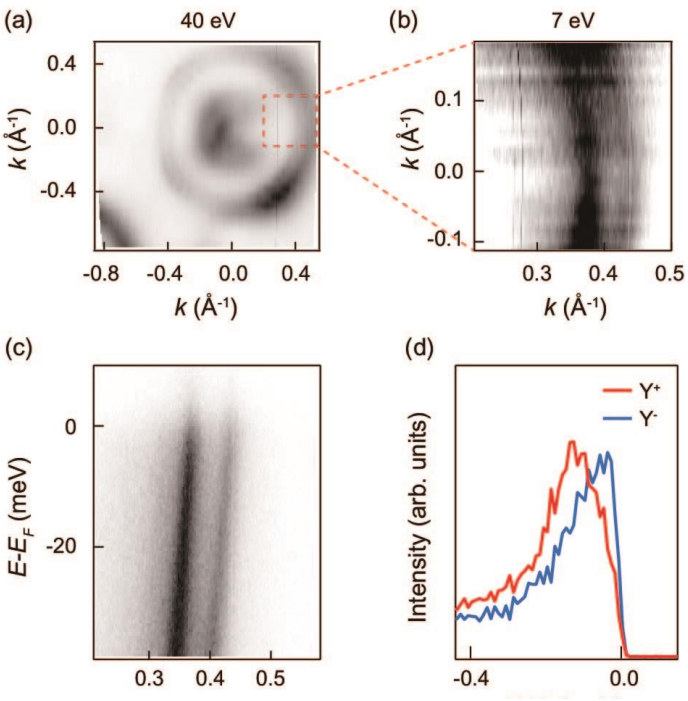

[Figure 1] Fermi surface taken by (a) 40 eV and (b) 7 eV. (c) High symmetry cut data taken along Γ – M direction. (d) Spin resolved energy distribution curve. Red and blue line indicates Y^+ and Y^- spin direction measurement result, respectively.

observed around k = 0.4 $Å^{-1}$. According to previous calculations, the observed bands are expected to be the surface state. We tested the spin polarization of the this observed surface states. Surprisingly, opposite spin polarization is observed between the two bands. Spin polarization is likely due to the presence of inversion symmetry breaking in this surface state. However, the cause of this spin polarization needs to be elucidated through further experimental/theoretical studies.

REFERENCES

[1] Y. Kamihara, T. Watanabe, M. Hirano, and H. Hosono, J. Am. Chem. Soc. **130**, 3296 (2008).
[2] Z.-A. Ren *et al*., Chin. Phys. Lett. **25**, 2215 (2008)
[3] L. X. Yang *et al.,* Phys. Rev. B **82**, 104519 (2010).
[4] P. Zhang *et al.,* Phys. Rev. B **94**, 104517 (2016).
[5] R. Kappenberger *et al.,* J. Cryst. Growth **483**, 9 (2018).

THICKNESS DEPENDENCE OF SPIN-POLARIZED BAND STRUCTURE IN TOPOLOGICAL INSULATOR Bi_2Te_3 THIN FILMS

Kaishu Kawaguchi[1], Ryo Mori[1], Yuto Fukushima[1], Hiroaki Tanaka[1], Shinichiro Hatta[2], Ayumi Harasawa[1], Tetsuya Aruga[2], Takeshi Kondo[1]

[1] *ISSP, The University of Tokyo*

[2] *Graduate School of Science, Kyoto University*

INTRODUCTION

Topological insulators, with their surface state exhibiting spin-polarized electronic states on the surface, hold promising applications in spintronics and quantum information, and so on. In this context, employing thin films to enhance surface effects is a key approach. Under this situation, interference effects occur between the electronic states present at the surface and interface [1]. And additionally, energy splits in band dispersion also occur originating from the substrate effects [1,2]. In particular, substrate effects, when viewed from a macroscopic perspective, can be considered as a kind of the Rashba effect resulting from broken inversion asymmetry from the interface between thin films and substrate, called structure inversion asymmetry (SIA) [2]. This offers exciting prospects of merging different physical properties through junctions with superconductors [3] and so on. However, these SIA largely depend on the substrate type and controlling them can be challenging due to the varying origins and quantitative differences of potential modulation. Therefore, it is crucial to reveal the more microscopic origins of SIA, details about the potential structure and its origins that were previously unclear. For this purpose, we have extensively investigated the thickness and substrate dependency of the energy splitting structure in the thin films of the topological insulator Bi_2Te_3, to explore how potential modulation can be controlled.

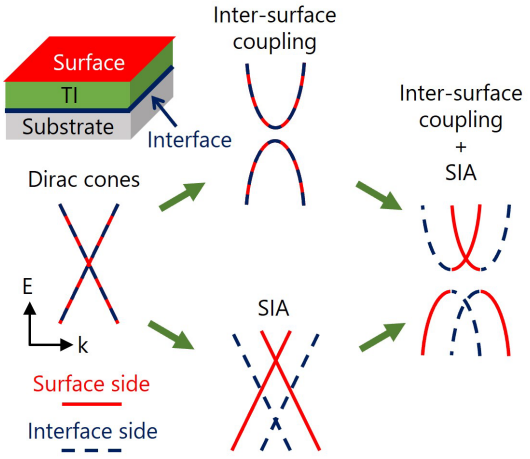

Fig. 1 : Band-dispersive depiction of energy-splitting structures originating from the hybridization of topological surface and interface states and SIA in topological insulator thin films.

METHODS

A challenge in this research lies in the fact that each energy-split band dispersion is localized at the surface and interface. Therefore, it is difficult to identify the interface side in Angle-Resolved Photoemission Spectroscopy (ARPES) due to the decay of photoelectron intensity within the thin film. This complication, along with band broadening, can lead to obscured energy splitting, making observation impossible—a phenomenon reported in previous studies that calls for a solution. In this study, by using spin-resolved ARPES (SARPES) technics, we aimed to clearly separate the energy splitting structure based on the difference in spin polarization direction derived from the reversed helicity of the surface and interface.

For this study, considering the importance of insulating films in applications, experiments were conducted using a CaF_2/Si(111) substrate prepared by depositing a CaF_2 thin film on a *p*-type Si(111) substrate. Bi2Te3 ultra-thin films were prepared in ultra-high vacuum using a Bi_2Te_3 deposition source [4]. The SARPES apparatus combines a Very Low Energy Electron Diffraction (VLEED) spin detector and a 7-eV laser to form a high-efficiency, high-resolution system [5] capable of decomposing even fine spin-split structures for efficient observation.

RESULTS AND DISCUSSION

Figure 2 shows the thickness dependency of the Bi_2Te_3 thin film made on the CaF_2/Si(111) substrate. A clear band structure can be observed, indicating high-quality thin film. Also, it is evident that a gap is formed at the Dirac point for less than 4 QL, aligning with previous research. Although the ARPES image does not reveal any energy-split behaviour, successful observation of the splitting structure was achieved by conducting spin-resolved measurements (Fig. 3). Furthermore, upon investigating the thickness dependency, an energy inversion of the spin-splitting structure was observed from 1 to 3 QL. Such an inversion phenomenon has never been observed in previous studies, making our research a first in this regard. Also, as the film thickness increases, a shift of the band to higher energy was noticed.

As possible origins of the energy split at the surface and interface, crystal structure distortion and peculiar charge transfer are considered. About structure distortion, it is especially noticeable when the film is thin [6]. On the other hand, if the charge is polarized towards the Bi_2Te_3 side, the effect becomes significant when the film is thick. Therefore, it is believed that this inversion phenomenon of spin-splitting depending on the thickness arose due to the competition between these two effects. To understand these origins in more detail, it will be necessary to examine the doping dependence and to verify it through calculations.

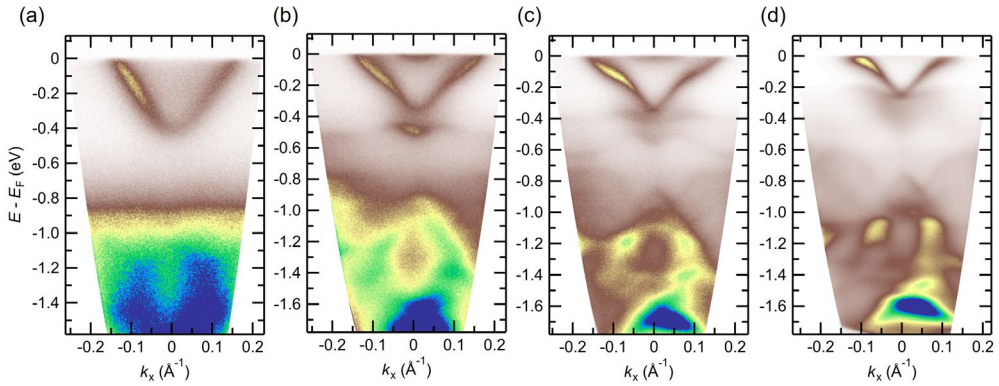

Fig. 2 : ARPES results of the thickness dependence of Bi_2Te_3 thin films, for thicknesses of (a) 1 QL, (b) 2 QL, (c) 3 QL, and (d) 8 QL.

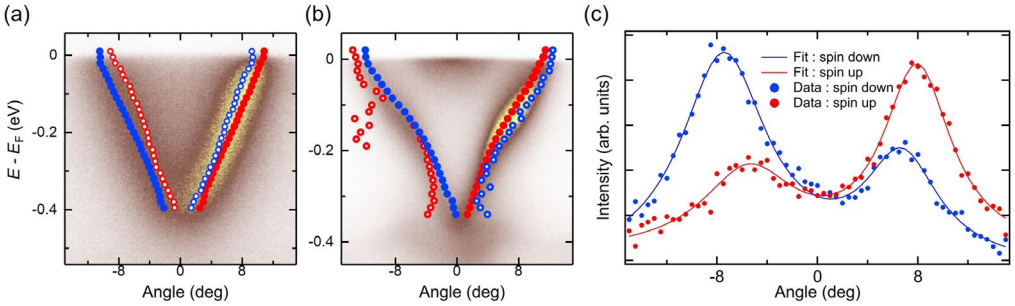

Fig. 3 : (a) 1 QL and (b) 3 QL, the peak positions obtained by fitting each spin-resolved ADC (angular distribution curve) spectrum are plotted on the ARPES image. The filling points indicate the spin up (red) and down (blue) peak positions for higher intensities and opaque points for lower intensities. (c) is ADC fitting result of (a) at E - E_F = -0.15 eV.

REFERENCES

[1] H. Zhang *et al.*, Nat. Phys. **5**, 438 (2009).
[2] Y. Zhang *et al.*, Nat. Phys. **6**, 584–588 (2010).
[3] H. Yi *et al.*, Nat. Mater. **21**, 1366–1372 (2022).
[4] S. Hatta *et al.*, Sci. Rep. **11**, 5742 (2021).
[5] K. Yaji *et al.*, Rev. Sci. Instrum. **87**, 053111 (2016).
[6] G. Landolt *et al.*, Phys. Rev. Lett. **112**, 057601 (2014).

QUANTUM CONFINED SURFACE STATES FORMED IN A HEXAGONAL CORRAL IN SELF-ASSEMBLED HYDROGEN-BONDED ORGANIC FRAMEWORKS

Kaname Kanai[1], Rena Moue[1], Hiroto Yamazaki[1], Kozo Mukai[2], Kaishu Kawaguchi[2], Yuto Fukushima[2], Fumihiko Ozaki[2], Ryo Mori[2], Takeshi Kondo[2], Ayumi Harasawa[2], Shik Shin[2], Jun Yoshinobu[2]

Faculty of Science and Technology Tokyo University of Science[1], The Institute for Solid State Physics, The University of Tokyo[2]

The ability to control and modify the electronic properties of material surfaces is essential for the realization of next-generation devices involving electron and spin transfer at the interface between material surfaces and electrodes. In the field of surface science, the properties of many surface states and techniques for the modification of these surface states have been pursued. In particular, the Shockley state (SS), which is a pseudo-two-dimensional free electronic surface state on the (111) surface of an fcc-metal, is sensitive to various molecular adsorptions and has been the subject of many studies. However, SS is easily and quickly dissipated by irregularly adsorbed molecules. Meanwhile, for regularly arranged molecules on the surface, SS survives, and in some cases, its properties are significantly modified[1]. This indicates that the sensitivity of SS to adsorbates originates from a situation in which spatially spread pseudo-free electrons in two dimensions are easily scattered by the periodic potentials newly created parallel to the surface by the adsorbed molecular array. In such a situation, electron waves scattered by adsorbates regularly arranged to form void spaces, referred to as corrals, are expected to create standing waves inside the corrals.

In recent years, several studies have mentioned that molecules with a macrocyclic structure, superstructures made by adsorbing molecules on their surfaces and metal clusters, can create standing waves of electrons and have demonstrated quantum confinement in these structures. However, the formation of such quantum confined surface states (QCSSs) associated with molecular adsorption is mostly caused by accidentally self-assembled superstructures, and neither the corral size nor its shape is easily tunable. In this study, we propose another approach that is relatively robust to self-assembly imperfections, namely quantum confinement based on hydrogen-bonded organic frameworks (HOFs).

Carbon nitride molecule, melem (2,5,8-triamino-tri-s-triazine) has three-fold symmetry. Melem forms HOFs with characteristic structures by forming multiple hydrogen bonds between adjacent molecules in the crystal or on the surface. In general, many carbon nitride compounds that use hydrogen bonding as one of their cohesive forces have large voids in their crystal structures, which is also true for HOFs formed on the surface (SHOF). The SHOF is expected to form a graphite-like structure with a long-range order rather than a localized structure. Under these conditions, the SHOFs formed on the fcc-metal (111) surface are expected to produce identical confinement potentials in the corral created in their structures, resulting in the formation of a two-dimensional network of nearly identical QCSSs.

In this study, SHOFs were formed on Au(111) by melem, and their electronic structures were investigated by angle-resolved photoemission spectroscopy (ARPES). The presence of slightly distorted hexagonal corrals in the SHOF of melem with a honeycomb (HC) structure is expected to lead to quantum confinement of SSs of Au(111). Meanwhile, the confinement potential is created as a result of the slight displacement of the Au(111) surface atoms in the surface vertical direction, and the magnitude of the potential formed is small.

The SS of clean Au(111) observed by ARPES (Figure 1a) shows parabolic band dispersion as a quasi-two-dimensional free-electron system. The SS band exhibits a large Rashba splitting characteristic of Au(111). This large splitting is because the SS of Au(111) has a strongly asymmetric wave function near the outermost nuclei of the Au atoms. The effective

mass of the SS electron was estimated to be m^* = (0.274 ± 0.020) m_e. the coveragees of the melem layers at 1 and 2 Å correspond to the coverages of the submonolayers, and the melem layer has a HC structure. The band mapping results of Melem(1 Å)/Au(111) (Figure 1b) clearly show that the SS band shape of Au(111) is different from that of pristine Au(111). ARPES band mapping showed no Rashba splitting and a single broad weak energy band. In contrast, a localized state with a narrow dispersion width, which does not exist in pristine Au(111), is newly formed at approximately 0.40 and 0.47 eV. Since the highest occupied molecular orbital of the melem appears below a binding energy of 2 eV, these localized states are not derived from the melem itself.

To examine the detailed band dispersion of this localized state, curve fitting was performed for each energy distribution curve, and the results are shown by black dashed lines in Figure 1b. This result also shows that the dispersion width is extremely narrow compared with that of the SS. In contrast, this level was slightly curved, indicating slight dispersion. The band mapping results of Melem(2 Å)/Au(111) by ARPES intensity (Figure 1c) were very similar to those of Melem(1 Å)/Au(111), with a localized state observed near the bottom of the SS. In contrast, the fitting analysis shows that the dispersion widths of the two localized states are slightly smaller than those of Melem(1 Å)/Au(111), indicating a more localized nature. The discrete states present in Melem(1 Å)/Au(111) and Melem(2 Å)/Au(111) suddenly disappeared in both the ARPES (Figure 1d) of Melem(3 Å)/Au(111). From the results of LEED experiments, when the coverage of the melem layer reached 3 Å, a monolayer was formed in which the closed-packed structure was dominant. This abrupt change in the surface electronic structure strongly suggests that the localized states originates from the HC structure and that this is the QCSSs in the corral of the HC structure. Melem(3 Å)/Au(111), where the closed-packed structure is dominant, does not have a corral similar to the HC structure, which can be interpreted as the disappearance of the localized states observed in the HC structure because quantum confinement of the surface electrons does not occur.

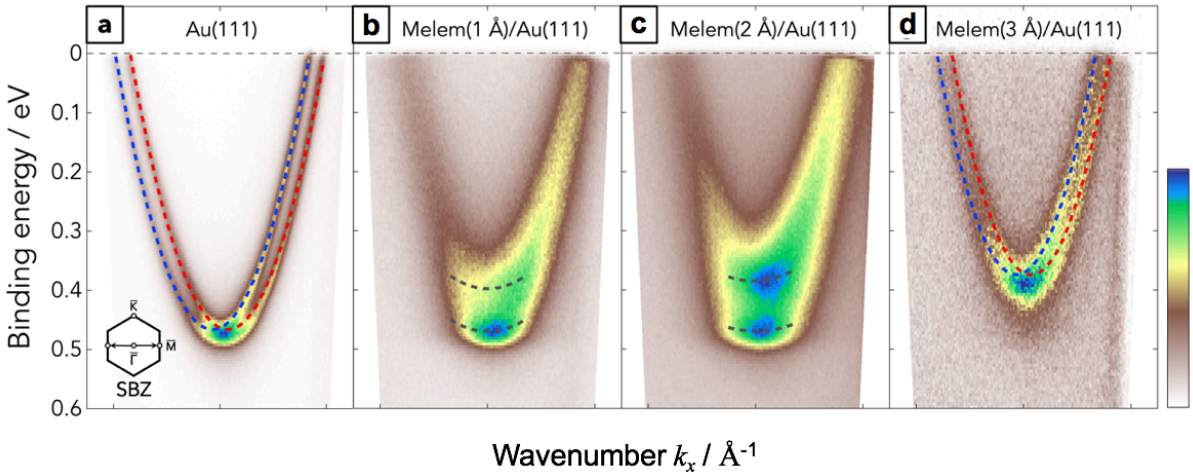

Figure 1. Band mapping around the Γ point (k_x = 0 Å^{-1}) of a) clean Au(111), b) melem(1 Å)/Au(111), c) melem(2 Å)/Au(111), and d) melem(3 Å)/Au(111) by angle-resolved photoemission spectroscopy (ARPES).

REFERENCE

[1] R. Moue *et al.*, *Adv. Mater. Inter.*, **2022**, 2201102 (2022).

STUDY ON SPIN STRUCTURE OF THE SURFACE STATE IN TYPE-II WEYL SEMIMETAL $NbIrTe_4$

Soonsang Huh[1], Soohyun Cho[2], Wei Xia[3, 4], Soonsang Huh[1], Yuto Fukushima[1], Ayumi Harasawa[1], Takeshi Kondo[1, 5], Yanfeng Guo[3, 4] and Dawei Shen[2]*

1. *Institute for Solid State Physics, University of Tokyo, Kashiwa 277-8581, Japan*
2. *National Synchrotron Radiation Laboratory, University of Science and Technology of China, Hefei 230029, China*
3. *School of Physical Science and Technology, Shanghai Tech University, 201210, Shanghai, China*
4. *Shanghai Tech Laboratory for Topological Physics, Shanghai Tech University, 201210, Shanghai, China*
5. *Trans-scale Quantum Science Institute, University of Tokyo, Tokyo 113-0033, Japan.*

The topological Weyl semimetals (TWS) originate from their unusual bulk electronic structure and have the nondegenerate bands crossing in a single point of **k** space, so-called the Weyl point. This can be realized in the quantum materials where either time-reversal or inversion symmetry, or both, is broken [1-3]. The symmetry tends to produce copies of Weyl points and separate the Weyl nodes with different non-zero Chern number in the Brillouin zone. On the boundary, topological edge states exist at edges of 2D planes and disappear at edges of other planes in which the separation points between two types of planes are Weyl points [1]. Therefore, the Fermi surface of the TWS simply consist of only two such points and show an opened line that connect each pair of Weyl nodes with opposite chirality, which is called a Fermi arc [1-3]. Moreover, in $Mo_xW_{1-x}Te_2$ compound, another type of the TWS has been discovered with called type-II TWS whose Weyl nodes are highly anisotropic and tilted, breaking the Lorentz symmetry [1-5]. Given the feature of the band touching at the Weyl node, the Fermi surface at the Weyl nodes of the type-II WSM exhibit the electron and hole pockets [2-5]. This distinction feature of the band touching near the Weyl node may give a rise to marked differences in the thermodynamics and response to external magnetic field [2-5].

Recently, it has been reported that (Nb, Ta)$IrTe_4$ is a ternary TWS of type-II [3-5]. This compound crystallizes in a non-centrosymmetric orthorhombic lattice with space group $Pmn2_1$ (No. 31) and have van der Waals interaction within layers [3-5]. Figure 1a show the side and top view of the crystal structure in $NbIrTe_4$, which show that the Nb and Ir atoms are octahedrally coordinated by Te atoms. The structural symmetry and a stacking configuration of $NbIrTe_4$ is identical structure with the orthorhombic $1T_d$-MX_2 (M = Mo, W; X = S, Se, Te) as the first suggestion with the type-II WSM, but $NbIrTe_4$ has a unit cell doubled along **b** direction and the substitution from M atoms in $1T_d$-MX_2 to Nb and Ir atoms in $NbIrTe_4$ [3-5]. Because of the similarity in the crystal structure, $NbIrTe_4$ has the Nb-Ir chain as shown in the top view of Fig. 1a, which is similar with the Mo-Mo or W-W chain that can be related to the unusual electronic transport in $1T_d$-MX_2. The Nb-Ir chain is along the **a** and Γ to X direction in the crystal and Brillouin zone (BZ) coordinates in Figs. 1a and 1b, respectively. Figure 1b

shows the orthorhombic bulk BZ and projected surface BZ onto the (001) surface with the high symmetry points.

In this study, we investigate the electronic and spin structure of the surface state in $NbIrTe_4$ utilizing high-resolution angle- and spin- resolved photoemission spectroscopy. The low-energy photoemission spectra taken from the laser-based ARPES with 6.994 eV photons clearly describe the fine dispersion of the surface state near the Y point with the higher momentum resolution in Figs. 1 (c) and (d). In previous ARPES study in Refs. [5], $NbIrTe_4$ show the Weyl points between the Γ and Y points, and the Weyl nodes would be connected by the surface state along k_y direction in Fig. 1(c). In our band calculation, the surface state at Y point show the spin-polarization along the $+s_y$ or $-s_y$ direction, but we cannot obtain the opposite sign of the spin-resolved energy distribution curves (EDCs) between $-k_F$ and $+k_F$ as shown in Figs. 1(e) and (f). For the experiment failure to show the spin texture in the surface state, we speculate that there could be a possibility to be a photoelectron interference effects in the surface state [6].

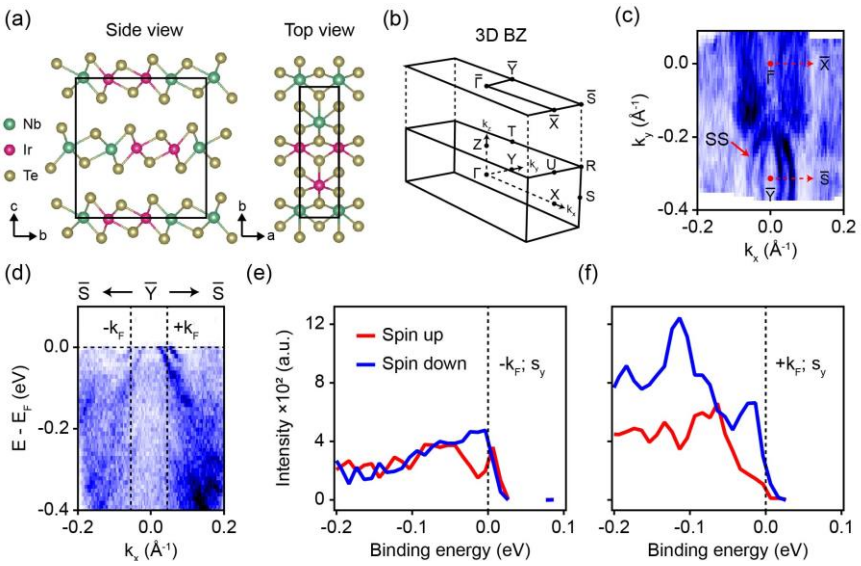

Figure 1. (a) The top and side view of the crystal structure of $NbIrTe_4$. (b) The orthorhombic bulk BZ and projected surface BZ onto the (001) surface with the high symmetry points. (c) Experimentally obtained Fermi surface at 6.994 eV and 15 K. (d) The ARPES spectra along the S-Y-S direction. The spin-resolved EDCs of the surface state at $-k_F$ (e) and $+k_F$ (f) as marked in **d**. The spin-resolved EDCs represent spin texture along the s_y direction.

REFERENCES

[1] C. Zhang *et al*., Annu. Rev. Mater. Res. **2020**, 50:131-153.
[2] A. A. Soluyanov *et al*., Nature **2015**, 527 495.
[3] Ilya Belopolski *et al*., Nat. Commun. **2017**, 8 942.
[4] E. Haubold *et al*., Phys. Rev. B **2017**, 95 241108(R).
[5] S. A. Ekahana *et al*., Phys. Rev. B **2020**, 102 085126.
[6] Z.-H. Zhu *et al*., Phys. Rev. Lett. **2014**, 112 076802.

6. Staff

Director: HARADA Yoshihisa, Professor
MATSUDA Iwao, Professor
KIMURA Takashi, Associate Professor
KONDO Takeshi, Associate Professor
HORIO Masafumi, Research Associate
KIUCHI Hisao, Research Associate
TAKEO Yoko, Research Associate
MORI Ryo, Research Associate (2022.7~)
HARASAWA Ayumi, Senior Technical Specialist
SHIBUYA Takashi, Technical Specialist
KUDO Hirofumi, Technical Specialist

Project Academic Specialist:
FUKUSHIMA Akiko
KOSEGAWA Yuka
ARAKI Mihoko (~2023.3)

Secretary:
AIHARA Yumiko
YOSHIZAWA Motoko
TSUTSUMI Yumiko (~2023.3)
IKEDA Kuniko (~2023.3)
TERAMOTO Tomoka (~2022.5)

Project Researcher:
OHDAIRA Takeshi
ZHANG Wenxiong
KURAHASHI Naoya(~2022.11)
KITAKATA Emi
Al Samarai Mustafa
LIU Daobin
NIIBE Masahito
TATSUTA Kazuo (~2022.9)
ANDO Hiroshi (~2022.12)

Graduate Student:
UGALINO Ralph John
SATO Yusuke
TSUJIKAWA Yuki
YANG Tianqi
SUMI Toshihide
WADA Tetsuya
LI Hao
ZHANG Xiaoni
ZHAO Haochong
FURUYA Noboru (~2023.3)
SAKURAI Kai
SENOO Tomoaki (~2023.3)
YIN Heming
TOMIYORI Yusuke
HUA Yangyang
YOSHINAGA Kyota
YAMAGUCHI Kazuki
MIYAMOTO Masashige
GUAN Yanze
SU Xingyu